NASA TECHNICAL NOTE

NASA TN D-7420

NASA TN D-7420

FLIGHT INVESTIGATION OF A STRUCTURAL MODE CONTROL SYSTEM FOR THE XB-70 AIRCRAFT

by

Wilton P. Lock, Eldon E. Kordes, and James M. McKay

Flight Research Center
Edwards, Calif. 93523

and

John H. Wykes

North American Rockwell Corporation
Los Angeles, Calif. 90009

NATIONAL AERONAUTICS AND SPACE ADMINISTRATION • WASHINGTON, D. C. • OCTOBER 1973

1. Report No.	2. Government Accession No.	3. Recipient's Catalog No.
NASA TN D-7420		

4. Title and Subtitle	5. Report Date
FLIGHT INVESTIGATION OF A STRUCTURAL MODE CONTROL SYSTEM FOR THE XB-70 AIRCRAFT	October 1973
	6. Performing Organization Code
7. Author(s)	8. Performing Organization Report No.
Wilton P. Lock, Eldon E. Kordes, James M. McKay (Flight Research Center), and John H. Wykes (North American Rockwell Corporation)	H-732
	10. Work Unit No.
9. Performing Organization Name and Address	743-36-22-00
NASA Flight Research Center P.O. Box 273 Edwards, California 93523	11. Contract or Grant No.
	13. Type of Report and Period Covered
12. Sponsoring Agency Name and Address	Technical Note
National Aeronautics and Space Administration Washington, D.C. 20546	14. Sponsoring Agency Code

15. Supplementary Notes

16. Abstract

A flight investigation of a structural mode control system termed identical location of accelerometer and force (ILAF) was conducted on the XB-70-1 airplane. During the first flight tests, the ILAF system encountered localized structural vibration problems requiring a revision of the compensating network. After modification, successful structural mode control that did not adversely affect the rigid body dynamics was demonstrated.

The ILAF system was generally more effective in supersonic than subsonic flight, because the conditions for which the system was designed were more nearly satisfied at supersonic speeds. The results of a turbulence encounter at a Mach number of 1.20 and an altitude of 9754 meters (32,000 feet) indicated that the ILAF system was effective in reducing the vehicle's response at this flight condition.

An analytical study showed that the addition of a small canard to the modal suppression system would greatly improve the automatic control of the higher frequency symmetric modes.

17. Key Words (Suggested by Author(s))	18. Distribution Statement
Structural mode control Elastic mode control Control systems	Unclassified - Unlimited

19. Security Classif. (of this report)	20. Security Classif. (of this page)	21. No. of Pages	22. Price*
Unclassified	Unclassified	82	Domestic, $3.75 Foreign, $6.25

* For sale by the National Technical Information Service, Springfield, Virginia 22151

FLIGHT INVESTIGATION OF A STRUCTURAL MODE CONTROL SYSTEM FOR THE XB-70 AIRCRAFT

Wilton P. Lock, Eldon E. Kordes, and James M. McKay
Flight Research Center

and

John H. Wykes
North American Rockwell Corporation

INTRODUCTION

Structural flexibility must be considered in the design of large, high performance aircraft. Aeroelastic deformation affects not only basic flight characteristics such as performance, controllability, handling, and ride qualities; it also increases structural loads and fatigue. The problems associated with flexible aircraft are not new; however, the technology required to control structural dynamics behavior was first developed for the inherently aerodynamically unstable launch vehicles. The success of the launch vehicle systems prompted the development of similar systems for aircraft, including systems for the control of structural mode response (ref. 1).

Two flight-test programs sponsored by the United States Government were initiated to achieve elastic mode control in large, flexible aircraft. The first program, which was conducted by the Boeing Company and Honeywell, Inc., was devoted to the development of a load alleviation and mode stabilization (LAMS) system for the B-52 airplane. Extensive analytical and simulator studies were used to define the details of the system and also to demonstrate the system's potential (ref. 2).

The second program, which used the XB-70 airplane, was undertaken to develop an elastic mode control system called identical location of accelerometer and force (ILAF). The concept on which it is based was first developed in the analytical study reported in reference 3. The design of the ILAF control system is described in reference 4. Reference 5 discusses the analytical design and briefly evaluates the first flight-test results.

The ILAF system flight-test program was conducted to investigate the ILAF system concept rather than to develop an optimum operational system. To flight test the ILAF system under well-controlled conditions, the aerodynamic shaker system described in reference 6 was used. The shaker system was capable of exciting the first four symmetric structural modes.

This paper describes the integration of the ILAF system with the XB-70's control system and presents test results obtained in flight at subsonic and supersonic airspeeds. This report also includes the performance calculated for a number of altitudes and Mach numbers that are representative of the flight condition.

SYMBOLS

Physical quantities in this report are given in the International System of Units (SI) and parenthetically in U.S. Customary Units. The measurements were taken in Customary Units. Factors relating the two systems are presented in reference 7.

f forcing frequency

g acceleration due to gravity

g_i structural mode damping (structural plus aerodynamic)

h_p pressure altitude

$i = \sqrt{-1}$

$K_I = 0.11$

$K_{(\ )}$ control system gain associated with subscripted parameter

l distance from flight augmentation control system accelerometer to vehicle center of gravity

M Mach number

n_z normal load factor

q pitch rate about Y-axis

s Laplace operator

Δ increment

δ control surface deflection

δ_t wingtip deflection

$\dot{\delta}$ rate of control surface deflection

δ_{sv} shaker-vane deflection; positive deflection produces positive lift force

$\eta_{(\ )}$ generalized coordinate; subscript indicates mode

σ root mean square value

$\sigma_i = 57.3 \frac{d\omega}{d\phi}$, real part of root of the characteristic equation as in $s + \sigma_i \pm \omega_i$

Φ power spectral density

ϕ phase angle

ϕ_i i^{th} normalized mode shape

ϕ_i' slope of i^{th} normalized mode

ω forcing frequency

ω_i natural frequency of i^{th} mode

Subscripts:

c command

e all elevons except inboard

P pilot's station

w_g gust velocity

$\dot{\theta}$ pitch rate

1 inboard elevon

2,3,4,5,6 individual elevon panels outboard of inboard panel

A dot over a quantity denotes the time derivative of that quantity.

ABBREVIATIONS

BP butt plane

CADS central air data system

FACS flight augmentation control system

FS fuselage station

HS canard horizontal station

ILAF identical location of accelerometer and force

LAMS load alleviation and mode stabilization

TEST APPARATUS

Airplane

The XB-70 airplane (fig. 1) is a large, delta-winged, multiengine jet airplane designed by North American Rockwell Corporation for supersonic cruise at a Mach number of 3.0 and altitudes above 21,336 meters (70,000 feet). Two airplanes, designated XB-70-1 and XB-70-2, were built. This investigation was conducted using the XB-70-1. The general configuration and overall dimensions of the XB-70-1 are shown in figure 2. The basic design incorporates a thin, low-aspect-ratio wing with a leading edge swept back 65.57°, folding tips, twin vertical stabilizers, and movable canards with trailing-edge flaps. The XB-70-1 was manufactured with the wings mounted at a dihedral angle of zero.

Stability Augmentation System

The flight-test data reported herein were obtained with the stability augmentation system, called the flight augmentation control system (FACS), engaged. A brief description of this system is given below. A more detailed description is given in reference 4 along with the system's frequency response characteristics.

The FACS is a conventional command augmentation system designed to improve handling qualities by operating simultaneously with the pilot's manual control system. A block diagram of the pitch augmentation system is shown as the unshaded blocks in figure 3. Pilot commands for pitch control are processed through two paths to the elevon actuation system. The first path is purely mechanical. Pilot commands are transmitted to the master cylinder, which outputs through linkage to the elevon actuators to produce the desired control surface motion without force feedback to the controls. In the second path, pilot commands actuate a transducer that provides electrical signals that are in turn electrically summed with signals from two aircraft response sensors (a gyro and an accelerometer). The combined signal is filtered to reduce the transmission of high frequency signals to the servo. The signal is then gain scheduled according to altitude and Mach number information provided from the central air data system (CADS). Finally, the signal positions the pitch servo, which sums mechanically with the pilot commands from the first path to drive the inboard elevon panel. The motion of the inboard panel commands the motion of all the outboard panels (fig. 2) as described below.

Redundancy was accomplished by dualizing the electronics from the sensors to the servo. Other safety provisions were incorporated to provide self-monitoring and to control servo centering rates upon disengagement.

The FACS controls only the elevons in the pitch mode. The elevons for each wing are divided into six segments to prevent control surface binding under aerodynamic loading. With the wingtips in the 0° position, all five outboard panels are slaved to the inboard panel. In the 25° and 65° wingtip positions, the two outermost panels are disengaged and centered, and the three remaining outboard panels are slaved to the inboard panel.

ILAF Structural Mode Control System

The ILAF system was first developed under a U.S. Air Force study contract using early XB-70 design information to develop an analytical model (ref. 3). The objective of the study was to design a simple, stable system to maintain system stability and to provide damping to the structural modes. The system was to operate over a wide range of altitude and Mach number conditions and vehicle weights. The principle on which the ILAF system is based is explained in reference 3, and a more detailed description of the design and a performance analysis are given in reference 4. Briefly stated, the design synthesis locates the structural motion sensor (accelerometer) as close as possible to the force generator (elevon).

Design limitations.– Several constraints were imposed on the ILAF system. It was to control only the first four airplane symmetric structural modes (those less than 8 hertz). It was to utilize the existing pitch FACS, but no modification was to be made to the FACS that would affect the basic handling qualities of the airplane. A further requirement was that the pitch FACS was to be in operation before the ILAF system could be engaged in flight, and, to preclude instability problems (ref. 4), it was to be impossible to engage the ILAF system on the ground.

The ILAF system was mechanized as a dual channel system to make it compatible with the existing pitch FACS and to make it possible to utilize the existing failure protection circuitry.

Description.– The shaded blocks in figure 3 show the ILAF system components incorporated into the pitch augmentation system. A primary structural motion sensing accelerometer was located in each wing near the number 2 elevon panel hinge line, and a secondary accelerometer was located near the airplane's center of gravity. Together, the three accelerometers provided the ILAF system input signals (ref. 4). The signals from the two wing accelerometers were halved and then summed to eliminate whole-vehicle roll motion and antisymmetric modes. The signal from the accelerometer near the center of gravity was subtracted from this signal to eliminate vehicle rigid body plunge motion.

The combined signal from the accelerometers was passed through a notch filter network to a manually adjusted gain control knob in the cockpit. The notch filter was designed to attenuate the signal associated with elevon natural frequencies at approximately 20 hertz. From the gain control, the signal passed through the compensation network into the pitch augmentation system electronics. The ILAF system compensation shaping, shown in figure 4, was a lead-lag network designed to improve the damping for the third mode (ref. 4).

To protect the pitch servo from large amplitude high frequency commands generated with the ILAF system, an electronic limiter was added to the pitch electronics that reduced the servo authority from $\pm 7.5^\circ$ to $\pm 7.0^\circ$.

The ILAF system electronics were blended into the FACS electronics just in front of the pitch augmentation gain, K_{h_p} (fig. 3), which is an automatic function of the CADS.

To prevent possible instability of the ILAF system on the ground, a switch was installed in the landing gear system that prevented the ILAF system from being operated unless the landing gear was fully retracted.

Vibration Excitation System

Movable aerodynamic vanes trapezoidal in planform and 0.19 square meter (2 square feet) in area were mounted on each side of the forward fuselage in front of the pilot's station (ref. 6). The location of the shaker-vane system relative to the cockpit is shown in figure 5. The vanes constituted an excitation system capable of producing a controlled, oscillatory motion in the XB-70 over the frequency range from 1.4 to 8.0 hertz. The system was installed to determine the dynamic response of the airplane in flight. The shaker-vane system, operational procedure, and safety features are described in detail in reference 6.

INSTRUMENTATION AND RECORDING

The performance of the ILAF system as a structural mode damper was evaluated primarily with sensors already installed in the airplane, as shown in figure 6. The only sensors added to the airplane were the wing and fuselage accelerometers required for the operation of the ILAF system.

The sensors used for the evaluation of the ILAF system are listed in table 1 along with their ranges and locations on the aircraft. The natural frequencies of these sensors were such that their responses were essentially flat up to frequencies commensurate with those being measured.

The flight data used to evaluate system performance were recorded on magnetic tape by either analog or digital techniques, depending upon the parameter and its frequency response requirements. The magnetic tape generated within the airborne system was processed by a ground station computer to convert the data to engineering units (ref. 6).

A data acquisition system previously installed on the XB-70 (ref. 8) made it possible to evaluate the ILAF system during turbulence encounters. This data acquisition package consisted of a gust boom installed at the nose of the airplane and the sensors associated with it. The data obtained were used to correct for airplane motion at the nose. The procedure used to reduce the turbulence data is discussed in reference 8.

The analog and digital data acquisition systems are described in references 9 and 10.

FLIGHT CONDITIONS

The flight conditions for the ILAF system evaluation tests were generally representative of the XB-70's flight envelope (fig. 7). The airplane weights, the center of gravity locations, and other flight-test conditions are given in table 2.

TEST PROCEDURE

The tests of the ILAF system were performed in wings-level, 1g, trimmed flight at several airspeeds. The system was not operated during deliberate maneuvers, and during the open-loop ILAF system evaluation the system was not operated in turbulence.

Open-Loop Tests

The first tests were performed by increasing the ILAF system gain in the open-loop mode without shaker-vane input and observing airplane response. The performance of the ILAF system was then evaluated by setting shaker-vane input at a constant amplitude and measuring aircraft response and control system motion with and without the ILAF system operating. Shaker-vane amplitude was set, and the frequency was slowly increased to approach and excite each symmetrical mode up to 8 hertz. The system was mechanized so that a relay was intentionally opened between the output of the ILAF system electronics and the input to the pitch FACS electronics, allowing the ILAF system from the accelerometers through the shaping and compensation network to be monitored during flight without disturbing the airplane. The frequency sweeps were repeated at higher levels of shaker-vane amplitude.

Closed-Loop Tests

Closed-loop tests were performed in the same manner, but with the interconnecting relay closed. The tests were started with a low value of ILAF system gain and zero shaker-vane input and continued by increasing the gain while overall system performance and aircraft response were observed. Then the shaker-vane system was used to excite the structural modes with and without the ILAF system operating.

The ILAF system was further tested during encounters with turbulence; the response of the airplane was measured with and without the ILAF system engaged.

Structural damping information was obtained for each mode with and without the ILAF system engaged. Because of fuel consumption and the associated change in airplane mass, it was necessary to reestablish the mode being investigated. Once excited, the modal frequency was allowed to stabilize. The shaker-vane system was then shut down abruptly, and data were recorded until telemetry indicated that the responses were completely damped out.

During all the ILAF system evaluation tests, modal frequencies and amplitudes were monitored by a test engineer on the ground, who used telemetered data on airplane response and system operation. The signal from the nose ramp accelerometer at fuselage station 7.43 meters (292.5 inches) was used to observe airplane structural response. The parameters telemetered for ground monitoring of the ILAF system and aircraft structural integrity were monitored on strip charts.

DATA ANALYSIS

Detailed response calculations were made for the XB-70 airplane and reported in references 3 to 5. However, the conditions analyzed were specific design conditions not readily obtainable in flight. To more readily compare analytical results with the response of the airplane during these tests, calculations were made for the weight, altitude, and Mach number conditions of the actual tests. These conditions are shown in table 2 for Mach numbers of 0.87, 0.86, and 1.59. The analysis used the updated mass and stiffness data given in reference 6 for the basic airplane and for the airplane with FACS engaged. The analysis of airplane response with the ILAF system engaged is described in appendix A.

RESULTS AND DISCUSSION

System Stability

Original ILAF system.– Initially it was planned to evaluate the ILAF system stability during climbout at a high subsonic speed and in a heavyweight condition. During this initial stability evaluation, a limit cycle occurred at a low ILAF system gain. The first indication of a limit cycle was a large amplitude oscillation observed in the pitch servo. The telemetry data indicated that the oscillation occurred at 26 hertz. Additional flight tests for system stability in a supersonic, mediumweight flight condition and a high subsonic, lightweight flight condition confirmed the presence of a limit cycle. During one of the three ILAF system stability evaluation flights, a failed wing accelerometer allowed the system loop gain to approximately double before the limit cycle appeared. However, at the later two test conditions the dominant frequency in the pitch servo occurred at 12 hertz.

Figure 8 illustrates the various frequencies and amplitudes measured during the ILAF system stability tests with and without the ILAF system operating. Data are presented for fuselage acceleration, wing acceleration, inboard elevon deflection, and pitch servo deflection. The plots are composed of data from frequency analysis and time histories from the three closed-loop stability tests. The frequency analysis identified the peak responses, and the time history data aided in determining the magnitude of the response.

The data in figure 8 show that the predominant frequency on the pitch servo is 12 hertz with a smaller peak at 26 hertz with the ILAF system engaged. On the other hand, the inboard elevons responded to the 12-hertz signal, but there were no noticeable elevon deflections at 26 hertz. The fuselage accelerometer, which was located in the nosewheel well, indicated only a 12-hertz response, whereas the wing accelerometer did not respond appreciably to frequencies below 20 hertz.

A series of ground vibration tests was conducted to verify the source of the 12- and 26-hertz vibrations and to determine any other significant mode of vibration. One test consisted of oscillating the pitch servo at various frequencies and amplitudes, forcing the elevon surfaces to move and excite the vehicle structure. The fuselage accelerometer revealed a number of significant modes above 10 hertz. The wing accelerometer also sensed large amplitude response from 10 hertz to over 32 hertz. Both accelerometers reflected an elevon mode contribution near 20 hertz which had been noted in previous ground tests.

The mounting arrangement of the ILAF system wing accelerometers was also checked for effects on frequency response. Figure 9 shows the results of the tests. The ice and water mentioned in the figure were used to provide adequate cooling for the accelerometers for the duration of each flight. These test results showed that the mounting arrangement made no contribution to the 26-hertz oscillation, but they did indicate poorly damped modes near 29 hertz and 38 hertz for the accelerometer with mount.

The limit cycle instability measured from flight tests is shown schematically in figure 10. The two dominant frequencies are 12 hertz and 26 hertz for the fuselage and wing accelerometers, respectively. The 26-hertz oscillation was measured on the pitch servo; however, associated elevon motion was not noticeable. A hydromechanical coupling must, therefore, have existed between the servo and accelerometers, causing a sustained oscillation between them as shown in the figure. Airplane response decreased with increasing frequency near 26 hertz, but at 26 hertz the gain of the accelerometer and ILAF system shaping network increased.

(See fig. 4.) The amplitude of the servo is also decreased at this frequency because of servo rate limiting. This combination of factors allowed a high gain closed-loop signal transmission which caused the limit cycle near 26 hertz. The attenuation of the overall system, however, was great enough to eliminate any limit cycles above 26 hertz.

The 12-hertz oscillation is shown schematically in figure 10 as a mechanical coupling mode between the elevons and the ILAF system fuselage accelerometer. The ground test indicated that the relative response of the fuselage accelerometer was increasing with increasing frequency in the 10- to 16-hertz range, and that the relative gain through the ILAF system shaping network (fig. 5) was decreasing with increasing frequency for the same range. However, the gain magnitude was still greater than unity at these frequencies. The pitch servo was capable of driving the elevons at 12 hertz, reinforcing the signal until the limit cycle existed. Relocating the ILAF system fuselage accelerometer to a less sensitive fuselage location could have alleviated this problem; however, this was not possible within the scope of the program. Instead, the compensating shaping network was revised.

Revised system.– To prevent further limit cycle response and to obtain benefit from using the ILAF system, the shaping network was revised, even to the extent that the performance of the ILAF system was impaired. Acceptable system performance in the third mode, along with eliminating the limit cycle problems beyond 8 hertz, would have required the mechanization of the desired shaping network shown in figure 11 to provide phase angle lead near 5 hertz. Several nonlinear filtering techniques were considered, but, again, this task was not within the scope of the program. The revised shaping network shown in figure 11 was a compromise between potential performance, simplicity, reliability, and modification time. Phase characteristics were discarded in favor of satisfactory amplitude ratio, partly because electrical noise became a problem with increased phase lead. In addition, as indicated in figure 11, although attenuating the ILAF system signal in frequencies of 12 and 26 hertz would have eliminated the limit cycle problem, the phase lag associated with a 5-hertz lead might have adversely affected system performance at the third mode frequency.

After the modification of the shaping network was completed, the ILAF system was flight tested for stability margins at each of the three flight conditions previously investigated. ILAF system gain was increased to a value of 6 (0.043 radian per g) before any high frequency oscillations were detected for the heavyweight condition at $M = 0.87$. A maximum gain of 10 (0.185 radian per g) was attained for the meduimweight condition at $M = 1.59$, and a maximum gain of 10 (0.143 radian per g) was also attained for the lightweight condition at $M = 0.86$.

Although the original ILAF system shaping network was developed from an early analytical model of the XB-70 airplane, this shaping network revealed problems that can be encountered during flight test that would be difficult to predict, even with the best design information.

Performance With Shaker-Vane Excitation

To evaluate the performance of the ILAF system, a baseline was established for comparison purposes. The airplane, which was normally operated with the FACS on, is referred to as the basic vehicle, or just FACS, and the vehicle with the ILAF system operating is referred to as FACS + ILAF.

shows that the frequency at which the structural modes occurred was higher for the lighter vehicle weight. The data also indicate that after the airplane response had approached a particular mode, only a small change in frequency was necessary to cause the mode to peak. The abruptness of the peak indicates that the total damping of these modes was low at both subsonic and supersonic flight conditions. Even though the shaker-vane frequency sweeps were begun at frequencies higher than the basic airplane short period dynamics, successful structural mode control was demonstrated without adversely affecting the rigid body dynamics.

The elevon motion measured during the operation of the ILAF system at the mediumweight condition at $M = 1.59$ is presented in figure 16. The data show that the inboard elevon amplitudes were greater at the second-third mode frequency than at the first mode frequency, even though the second-third airplane mode was not damped effectively. This loss of effectiveness at the higher frequency was due primarily to the phase lag in the shaping network and to the position of the node lines, as discussed previously.

A comparison of figures 13 and 16 along with figures 12 and 15 indicates that although the inboard elevon has approximately the same amplitude for the first mode, the ILAF system was more effective in damping the first structural mode at the $M = 1.59$ flight condition. The phase lag measured at the first structural mode between the inboard elevon and the normal acceleration at the pilot's station for the lightweight condition at $M = 0.86$ (fig. 13) was approximately $-60°$ for an ILAF system gain of 6 (0.086 radian per g), as compared with approximately $-45°$ for an ILAF system gain of 4 (0.072 radian per g) for the mediumweight condition at $M = 1.59$ (fig. 16). Because of the FACS gain change with altitude, the overall ILAF system gain was approximately 0.014 radian per g higher at the lightweight flight condition at $M = 0.86$.

The phase relationship between the inboard elevons and the normal acceleration at the pilot's station was also compared for the second-third mode frequency. Phase lag was found to be $-205°$ for the mediumweight condition at $M = 1.59$ and $-155°$ for the lightweight condition at $M = 0.86$. Although the inboard elevons responded to the ILAF system commands, phase lag was such that the ILAF system signal reinforced the shaker-vane input and caused higher acceleration response throughout the vehicle.

M = 2.38, mediumweight condition.– The acceleration response at the pilot's station for a mediumweight flight condition at $M = 2.38$ is shown in figure 17 for the first mode. The effect on the aircraft's response of varying the ILAF system gain is shown in the figure. The peak vehicle response with FACS only was established by extrapolating the test results at the previous flight conditions. The FACS-only peak response occurred at 2.34 hertz. Peak response was also established with the ILAF system engaged, for gain settings of 4 (0.099 radian per g), 6 (0.149 radian per g), 8 (0.199 radian per g), and 10 (0.248 radian per g). Although the resonance frequency shifted with ILAF system gain, so that the 2.34-hertz data did not correspond to the peak response, the data show that there was a reduction in response with increased system gain.

The performance of the ILAF system was expected to be better at the supersonic than at the subsonic flight conditions; the aerodynamic forces generated by control surface deflection in supersonic flight are concentrated at the control surfaces, so the conditions for which the ILAF system was designed are more nearly satisfied (ref. 5).

M = 0.87, heavyweight condition.– It was believed that the elevon deflection was so small ($\pm 0.6°$) that the nonlinear characteristics added sufficient phase lag to the system to cause the elevons to produce vehicle accelerations instead of structural damping. To

evaluate the ILAF system under conditions of larger elevon deflection, either an increase in system gain or a larger shaker-vane input was required. The decision made was to keep the gain constant and increase the shaker-vane amplitude for the next series of tests. The first structural mode was the only mode evaluated during these tests, and the results of several frequency sweeps with and without the ILAF system are shown in figure 18 for a heavy-weight condition at $M = 0.87$. A reference sweep with FACS only was first obtained for a shaker-vane input of ±4°, followed by a frequency sweep with the ILAF system engaged for the same shaker-vane input. The other curve shown is for a shaker-vane amplitude of ±6°, also with the ILAF system engaged. The figure shows that a small reduction in peak amplitude occurred when the larger shaker-vane amplitude was used; however, the data with the ILAF system engaged indicated peaks somewhat higher than the FACS-only data. The phase angles between the inboard elevon and the vertical acceleration at the pilot's station for the two frequency sweeps with the ILAF system engaged are not appreciably different.

Performance With High Surface Rates and ILAF System Gains

Elevon surface rate limiting was investigated, but it was not considered to present a problem for operation at the first mode because higher surface rates had been measured for operation at the second-third mode. The peak elevon displacements corresponding to peak vehicle response for the first and second-third modes for all test conditions are summarized in figure 19 as a function of elevon surface rates. The figure indicates that all measurements obtained during the first mode tests fall along a straight line with a slope of 0.048 degree per degree per second. As noted in the figure, the solid symbols represent the test conditions where the ILAF system reduced the vehicle response. The data obtained from the supersonic test conditions indicated that successful mode damping was obtained with the ILAF system with elevon surface displacements greater than ±0.52°, whereas the data at subsonic test conditions for the first mode indicated that a minimum elevon deflection of ±0.66° was necessary for the ILAF system to improve the structural response.

The maximum inboard elevon deflection measured at peak vehicle response is shown in figure 20 as a function of ILAF system gain. The data were obtained for the first mode only, and with the exception of two data points the data were for high subsonic flight. For the subsonic flight condition, the data appear to follow a pattern according to shaker-vane amplitude. The subsonic data indicate that positive damping was not necessarily achieved by increasing the ILAF system gain alone, but rather that it also depended upon vane excitation amplitude. The data show that for vane amplitudes of ±4° and for several ILAF system gain values between 0.04 and 0.095 radian per g, positive damping did not result. However, at a vane amplitude of ±8°, positive damping could be achieved with an ILAF system gain setting of 0.06 radian per g.

The percentage of change in vehicle acceleration at the pilot's station is shown in figure 21 as a function of ILAF system gain for the first structural mode. The data presented are for both the subsonic and supersonic test conditions. The subsonic data for a shaker-vane input of ±4° indicate that increasing the ILAF system gain only was not enough to provide adequate damping for the first structural mode.

Performance With Turbulence Excitation

The results of a turbulence encounter with the shaker system off at $M = 1.20$ and $h_p = 9754$ meters (32,000 feet) are shown in figure 22. The ILAF system was engaged for

approximately 15 seconds. The data are presented in power spectral density format showing the vehicle's response at the pilot's station with and without the ILAF system operating. Turbulence intensity was measured by means of a gust boom installed on the airplane (ref. 8) and was found to be different for the time periods when the ILAF system was and was not operating; therefore, the data were normalized to a root mean square gust input of 0.30 meter per second (1 foot per second). These data show that the ILAF system was effective in reducing the vehicle's response. The pilots also reported a noticeable reduction in the airplane's response with the ILAF system operating. The peak responses associated with the aircraft structural modes do not show in these data because of the filter bandwidth that had to be used to give good statistical accuracy with the short sample time.

In figure 23 the average number of zero crossings is shown as a function of the incremental vertical acceleration at the pilot's station for the turbulence encounter. The data show that accelerations larger than 0.03*g* were reduced with the ILAF system engaged.

Improving the Performance of the ILAF System

Because of the degraded performance of the ILAF system after the revision of the shaping network, a study was made of methods for improving the system's capability. Since the shaker-vane exciter proved to be an effective means of forcing the aircraft modal response, the shaker-vane system was evaluated as a mode damper in conjunction with the ILAF system (appendix B). The calculated results show that with a simple modification the shaker vane would be effective in damping the higher modes and would aid the ILAF system in damping the first mode. The flight program on the XB-70 was completed without installing this system for evaluation.

CONCLUDING REMARKS

A flight investigation of a structural mode control system termed identical location of accelerometer and force (ILAF) was conducted on the XB-70 airplane. The ILAF system encountered localized structural vibration problems requiring a revision of the compensating shaping network. However, successful structural mode control was obtained without adversely affecting the rigid body dynamics. Although the ILAF system was developed with information from an early analytical model of the XB-70 airplane, flight tests of the modified shaping network and associated filter revealed problems that can be encountered during flight that would be difficult to predict, even with the best design information.

In general, the ILAF system was more effective at supersonic than subsonic flight conditions because the aerodynamic forces generated by control surface deflections in supersonic flight are concentrated at the control surfaces; thus the conditions for which the ILAF system was designed were more nearly satisfied. The ILAF system reduced the response of the first symmetric mode when elevon deflections were greater than $\pm 0.66^\circ$ in subsonic flight and greater than $\pm 0.52^\circ$ in supersonic flight.

The results of a turbulence encounter at a Mach number of 1.20 and an altitude of 9754 meters (32,000 feet) indicated that the ILAF system reduced vehicle response at this flight condition.

The results of an analytical study showed that the addition of a small canard to the modal suppression system would greatly improve the automatic control of the high frequency symmetric modes.

Flight Research Center,
National Aeronautics and Space Administration,
Edwards, Calif., August 1, 1973.

APPENDIX A

THEORETICAL ANALYSIS OF THE XB-70 ILAF SYSTEM

The design of the ILAF system was based on early estimates of the XB-70 airplane's mass and its structural and aerodynamic characteristics (refs. 3 to 5). Therefore discrepancies appeared when vehicle response characteristics obtained in flight (ref. 5) were compared with analytical responses based on these early estimates. Because of these discrepancies, a study using the XB-70 airplane was initiated to determine just how well the response characteristics of a flexible airplane could be predicted. The results of the new analysis, with a detailed accounting of the updated mass, structural, and aerodynamic data, are given in reference 6. The results show the response of the vehicle with and without FACS operating. The data presented herein attempt to reconcile the analytical and the flight-measured ILAF system performance.

Flight Conditions

Three specific flight conditions were selected for which analyses using updated data were made. The conditions, which were representative of the flights during which the ILAF system was operated, are the heavyweight, $M = 0.87$; lightweight, $M = 0.86$; and mediumweight, $M = 1.59$ conditions shown in table 2.

ILAF System Nonlinear Characteristics

During the flight tests of the ILAF system on the XB-70, it became apparent that the system's nonlinear characteristics were largely responsible for the lack of agreement between the analytical and flight-measured system performance. Figures 24 and 25, both for the first mode, illustrate this problem. They show the same basic trend; that is, the ILAF system did not improve performance at the subsonic flight condition for the low shaker-vane amplitudes at which most of the flight-test data were obtained ($\delta_{sv} = \pm 4°$). However, some improvement is shown at $M = 1.59$ (fig. 26). The data show that had larger shaker-vane inputs been used to obtain responses with the ILAF system operating, the predicted performance improvements at subsonic Mach numbers for the first mode would have been obtained.

Analytical Description of Elevon System

The analytical model for the FACS was described in reference 6 using two sets of transfer functions. The first set described the motion of the inboard elevon, the second set the motion of the remaining three elevon segments.

The analytical model for the ILAF system is described herein in a similar way using servo tables. The development is general, but the specific numerical data used in the examples are for the mediumweight, $M = 1.59$ case. Table 3 shows the numerical data for this case. Tables 4 and 5 show similar data for the heavyweight, $M = 0.87$ and lightweight, $M = 0.86$

cases, respectively.

The inboard elevon deflection is given by the expression:

$$\delta_1 = (\text{ILAF system gain adjust})\, K_{h_p} \left(\frac{\delta_1}{\Delta n_{z_{\text{ILAF}}}} \right) \left(K_{\text{ILAF}} \frac{\Delta l}{g} s\, q - \sum K_{\text{ILAF}} \frac{\Delta \phi_i}{g} s^2\, \eta_i \right)$$

With $K_{\text{ILAF}} = 1.0$ and $K_{h_p} = 0.62$, and expanding as a function of independent variables, the expression becomes:

$$\delta_1 = -\frac{K_I}{g} [\, (ST\text{-}1)\, \Delta l q + (ST\text{-}2)\, \Delta \phi_1 \eta_1 + (ST\text{-}2)\, \Delta \phi_2 \eta_2 + (ST\text{-}2)\, \Delta \phi_3 \eta_3 + (ST\text{-}2)\, \Delta \phi_4 \eta_4 + (ST\text{-}2)\, \Delta \phi_5 \eta_5 \,]$$

where

$K_I = 0.11$ radian per g

$\Delta l, \Delta \phi_i$ differences in data at the ILAF system wing accelerometers and the accelerometer at the center of gravity (table 6)

$ST\text{-}1, ST\text{-}2$ servo tables in table 3

The expression for outboard elevon deflection with the addition of the lag between the inboard elevon and the outboard elevons can be written:

$$\delta_{2\text{-}4} = (\text{ILAF system gain adjust})\, K_{h_p} \left(\frac{\delta_1}{\Delta n_{z_{\text{ILAF}}}} \right) \left(\frac{\delta_{2\text{-}4}}{\delta_1} \right) \left(K_{\text{ILAF}} \frac{\Delta l}{g} s\, q - \sum K_{\text{ILAF}} \frac{\Delta \phi_i}{g} s^2\, \eta_i \right)$$

$$\delta_{2\text{-}4} = -\frac{K_I}{g} [\, (ST\text{-}3)\, \Delta l q + (ST\text{-}4)\, \Delta \phi_1 \eta_1 + (ST\text{-}4)\, \Delta \phi_2 \eta_2 + (ST\text{-}4)\, \Delta \phi_3 \eta_3 + (ST\text{-}4)\, \Delta \phi_4 \eta_4 + (ST\text{-}4)\, \Delta \phi_5 \eta_5 \,]$$

where

$ST\text{-}3, ST\text{-}4$ servo tables in table 3

The K_{ILAF} term used in the numerical example above should not be confused with the value of the pilot control panel ILAF system gain select (ref. 4). The value $K_{\text{ILAF}} = 1.0$ as used herein is a computer control system gain input that, when combined with K_{h_p}, yields an overall ILAF system gain, K_I, equal to 0.11 radian per g.

Elevon Response Analyses

It remains to explain and qualify the elevon frequency response data $\frac{\delta_1}{\Delta n_{z_{\text{ILAF}}}}$ and $\frac{\delta_{2\text{-}4}}{\delta_1}$.

Because of the mechanics of obtaining frequency response with the ILAF system engaged using a digital program, there was no automatic way to coordinate the magnitude of the elevon response with the amplitude characteristics of the nonlinear system dynamics. Because of this, an iterative scheme was used. If the elevon amplitudes were not in agreement with those assumed for the system dynamics, a new estimate was used and the elevon response was recalculated. This procedure was used to obtain the results herein. However, completely converged solutions were not obtained in all cases because of the computer time required.

Figure 27(a) presents the frequency response from the ILAF system's blended accelerometer signal through the inboard elevon deflection. The solid curves are constructed from data presented in reference 4. The solid-line curves are not curves of constant δ_1, as they are in reference 4, but rather are curves passed through various magnitudes of δ_1 at the indicated frequencies. The magnitudes of δ_1 used in constructing these curves are taken from flight-test results and were used to start the previously mentioned iterative process. The dashed curves are the calculated results that best represent what was measured in flight. Only amplitude data could be obtained from flight records with accuracy. The curves showing the phase characteristics (fig. 27(b)) were based on the estimates made in the iterative procedure that produced the best agreement between the measured and computed amplitude characteristics.

Table 7 compares flight-test data and analytical data at several points in the control system as well as at the pilot's station. These flight-test data reflect the dashed-line data of figure 27. Since the dashed-line data produce the best analytical agreement with flight-test data, and the solid-line data are based on ground vibration test measurements, it can be inferred that flight aerodynamic loads or other unidentified influences had changed the system's frequency response characteristics.

Vertical Acceleration Responses

Vertical acceleration responses were calculated for various locations on the airplane. Flight-test measurements were made at these locations, and data measured with the FACS only operating are compared with the predicted response in reference 6, where the better agreement obtained from the refined analyses is shown. Hence, only results using the refined analysis are used herein, and the airplane with FACS on is used as the basic vehicle since the aircraft normally operated with the FACS engaged. The ILAF system evaluations were made from this base configuration, and the calculated results are shown for the pilot's station in figure 28 for the heavyweight condition, $M = 0.87$, in figure 29 for the lightweight condition, $M = 0.86$, and in figure 30 for the mediumweight condition, $M = 1.59$.

Control Surface Responses

The calculated frequency responses of elevon action due to ILAF system operation per unit of shaker-vane input are shown in figures 31 to 33 for the three flight cases studied. As explained, the FACS servo drives the inboard elevon and the motion of the inboard elevon activates the remaining elevon panels (panels 2 to 4 for the flight cases analyzed with the wingtips deflected). Because of this arrangement, it was desirable to determine separately the inboard and outboard elevon motions in the analyses with the ILAF system engaged. This was easy to do analytically, but it could not be done with data from the actual airplane.

The elevon deflection data presented can be used to obtain elevon rate information by using the relationship $\dot{\delta} = \omega\delta$ for sinusoidal oscillations.

Structural Mode Damping

For a lightly damped dynamic system, the calculated damping (structural plus aerodynamic) can be obtained from the dynamic system characteristic determinant in the form of phase angle as a function of forcing frequency (ref. 6). Using this technique requires knowledge of the mode natural frequency, ω_i, and the phase angle slope with frequency, $\frac{d\phi}{d\omega}$, at that natural frequency. The damping calculated for the vehicle with and without the ILAF system operating is presented in table 8.

APPENDIX B

DESIGN OF A STRUCTURAL MODE CONTROL SYSTEM FOR THE XB-70 AIRPLANE USING A SMALL AUXILIARY CONTROL SURFACE

The results of this study and studies reported in reference 4 show that the XB-70 elevon ILAF system has significant potential as a means of damping the first and second structural modes. However, it has less potential as a means of damping the third structural mode. This is because a third mode node line (the locus of zero displacement) runs between the elevons, rendering the elevons relatively less efficient for generating generalized forces for third mode control. Further, flight-test results show that the elevon ILAF system is ineffective in damping even the first structural mode when elevon amplitudes are less than $\pm 0.66^\circ$. Several other factors associated with the use of the elevon surfaces are discussed in reference 4.

When ways to improve the ILAF system's performance were examined, it became apparent that a more effective structural mode control system might be implemented with a relatively small modification to the XB-70 system. Specifically, it appeared that the shaker-vane system, which was utilized to excite the XB-70 airplane during the elevon ILAF system evaluation, could be converted to perform the structural mode control function. Previous studies have shown that a small aerodynamic control surface located at the nose of a flexible vehicle is effective in damping the lower frequency modes. An inspection of the lower frequency mode shapes showed that the existing shaker-vane location was well placed to add damping to the third mode (which could not be controlled adequately with only the elevon ILAF system) as well as to augment the elevon ILAF system in damping the first and second modes.

Shaker-Vane Characteristics

The shaker-vane system, which is described in reference 6, is capable of continuous operation in the frequency range from 1.4 to 8.0 hertz. The vane amplitudes are variable from 0° to 12° on either side of a preselected vane trim position (no load condition).

Laboratory tests were conducted to define the shaker-vane steady-state inputs to excite the symmetric structural modes of the airplane. The specific actuation transfer function was not available from laboratory tests, however, and flight-test data were used to make estimates of the actuation system's dynamics. The transfer function for the linear range of the actuator was estimated to be $60/(s + 60)$, and this estimate was used in all the design analyses.

Structural Mode Control System Design

The conversion of the shaker-vane system to a structural mode control system required installing an accelerometer in the vicinity of the shaker vane (as required by the ILAF system technique), subtracting the existing FACS accelerometer signal from the signal of the accelerometer, shaping the net signal, and then feeding it back through the actuation system. The

primary objective of the design was the augmentation of the elevon ILAF control system; however, the shaker-vane ILAF system and the elevon ILAF systems were designed to operate independently of one another within their own limitations.

To minimize the effort of installing the shaker-vane ILAF system, existing components in the FACS and the original shaker-vane system were used in the design study. Figure 34 shows a block diagram of the shaker-vane ILAF system that was designed. The accelerometer to be installed near the shaker vane was the required ILAF system primary sensor, while measurements from a second sensor (a FACS accelerometer was used to maximize use of existing equipment) were used to cancel all the rigid body plunge and some of the rigid body pitching acceleration signals. The reason for canceling the rigid body signals in the shaker-vane ILAF system signals was to avoid amplitude saturation, which is a possibility with such a small control surface. It is possible that rigid body signals alone could command all the available surface authority of the small shaker vane, leaving nothing for the structural mode signals to command. For example, at a gain of 0.25 radian per g, a rigid body signal amplitude of $0.5g$ would command all of the 12° available in the shaker-vane system. To avoid such amplitude saturation the ILAF system and FACS accelerometer signals were combined and shaped before commanding the shaker-vane actuator. The shaping networks were limited to use of the spare components already existing within the FACS equipment to minimize the need for wiring, cooling, packaging, and so forth. Manual engagement and selection of input frequency and amplitude, automatic disengagement, and fail-safety features of the original shaker-vane system were retained and incorporated in the shaker-vane ILAF system. The primary ILAF system accelerometer and the gain selector were the only new components.

Two shaping networks, shown in figure 35 and designated shaping 1 and 2, were evaluated for the shaker-vane ILAF system. Shaping 1 was a simple first order lag or $5/(s + 5)$ and was selected to provide a lag of approximately 90° at the frequencies of the structural modes to be controlled. However, a first order lag was unsatisfactory for the proposed shaker-vane system because the large attenuation at the mode frequencies required a very high gain. The FACS equipment initially restricted the maximum gain (occurring at $f = 0$ hertz) to be within 0.3 radian per g. This restriction, together with the attenuation characteristics of a first order lag, meant that gains available at the third mode frequencies would be limited to within 0.05 radian per g, which is too low to be effective at some flight conditions. Shaping 2 was selected as $1600/(s + 40)^2$ and alleviated the 0.05-radian-per-g gain limitation by increasing the gain at mode frequencies to 0.2 radian per g while providing approximately the same phase lags at the third mode frequencies. However, shaping 2 phase lags could be too small at the first mode frequencies, too high at fourth-fifth mode frequencies, or both. Thus the shaker-vane ILAF system could adversely affect the pilot station acceleration at these frequencies.

Performance and Stability Characteristics

A typical estimate of the performance of the shaker-vane ILAF system is shown in figure 36 for supersonic and subsonic flight conditions as a function of shaker-vane forcing frequency.

Most of the performance estimates were restricted to a maximum gain of 0.3 radian per g, although a few higher gains were investigated to determine whether any modification of the existing equipment was necessary. Estimated performance with shaping 1 (fig. 36) was unsatisfactory

because of shaping attenuation at the third mode frequencies. The estimated performance with shaping 2 was promising enough to be considered for installation in the XB-70 airplane for flight-test evaluation. However, the two lag time constants were designed to allow modifications to be made prior to each flight. Investigation of the air vehicle and shaping phase variations with frequency indicate that the estimated performance with shaping 1 and 2 would be significantly better if it were not for some adverse phase effects at frequencies slightly away from the peak response frequencies which apparently shift these peaks. Because of these shifts in response peaks (usually in the direction of higher frequency), the vehicle response at some specific frequencies with the ILAF system engaged are worse than without the ILAF system.

The stability analyses corresponding to the performance data in figure 36 are shown in figure 37. The stability analysis technique, which is not a conventional one, is described in detail in reference 4. In effect, a continuously decreasing phase angle with increasing frequency is considered to denote a stable system, and a mode that shows a reverse trend is unstable. As these figures demonstrate, the systems investigated were stable.

As indicated in figure 38, the shaker vane as being used here has a dual function—to excite and also to provide damping to the structural modes. Figure 38 also shows required shaker-vane ILAF system deflections as functions of ILAF system gain and pilot-selected shaker-vane excitation input. Because shaker-vane excitation input and shaker-vane ILAF system feedback signals are subtracted before actually commanding a net shaker-vane motion, required deflections and rates decrease with increasing ILAF system gain. Therefore, no saturation problems are expected to occur if phase estimates are correct. When possible, previous flight-test data were examined for phase characteristics and compared with estimates of the analytical model used to represent the air vehicle in an attempt to anticipate phasing problems, and none were uncovered.

Most of the estimated performance data were obtained by using the shaker vane as the input because of on-demand availability and repeatability advantages over gust inputs for data for comparison with analytical data. However, some analytical data with gust as the input were obtained to estimate potential saturation problems. Figures 39 and 40 show typical performance and required shaker-vane rates and deflections, respectively, for random gust inputs. These estimates indicate that good performance can be expected up to a root mean square gust magnitude of 1.22 meters per second (4 feet per second). Possible adverse effects can occur when root mean square gust magnitudes exceed 1.52 meters per second (5 feet per second) because of shaker-vane rate saturation. This area was considered worthy of further investigation prior to flight-test evaluation.

Although this study showed the shaker-vane ILAF system to be effective in reducing the modal response, the XB-70 airplane was taken off flight status before the system could be installed and tested.

REFERENCES

1. Garrick, I. E.: Perspectives in Aeroelasticity. Israel J. Technology, vol. 10, no. 1–2, 1972, pp. 1–22.

2. Burris, P. M.; and Bender, M. A.: Aircraft Load Alleviation and Mode Stabilization (LAMS). AFFDL-TR-68-158, Air Force Flight Dynamics Lab., Wright-Patterson AFB, Apr. 1969.

3. Wykes, John H.; and Mori, Alva S.: An Analysis of Flexible Aircraft Structural Mode Control. AFFDL-TR-65-190, Part I, Air Force Flight Dynamics Lab., Wright-Patterson AFB, June 1966.

4. Wykes, John H.; Nardi, Louis U.; and Mori, Alva S.: XB-70 Structural Mode Control System Design and Performance Analyses. NASA CR-1557, 1970.

5. Wykes, John H.; and Kordes, Eldon E.: Analytical Design and Flight Tests of a Modal Suppression System on the XB-70 Airplane. Part 1: Design Analysis. Part 2: Flight Tests. Aeroelastic Effects From a Flight Mechanics Standpoint, AGARD Conf. Proc. No. 46, Mar. 1970, pp. 23-1 – 23-18.

6. McKay, James M.; Kordes, Eldon E.; and Wykes, John H.: Flight Investigation of XB-70 Structural Response to Oscillatory Aerodynamic Shaker Excitation and Correlation With Analytical Results. NASA TN D-7227, 1973.

7. Mechtly, E. A.: The International System of Units–Physical Constants and Conversion Factors. NASA SP-7012, 1969.

8. Wilson, Ronald J.; Love, Betty J.; and Larson, Richard R.: Evaluation of Effects of High-Altitude Turbulence Encounters on the XB-70 Airplane. NASA TN D-6457, 1971.

9. Edwards, E. L.: A Data Processing Facility for the XB-70 Flight Test Program. Flight Test Instrumentation, AGARD Conf. Proc. No. 32, 1967, pp. 243–258.

10. Ince, D. B.: Application Experience With the B-70 Flight Test Data System. Aerospace Instrumentation. Vol. 4–Proceedings of the Fourth International Aerospace Symposium, College of Aeronautics, Cranfield, Eng., March 21–24, 1966, M. A. Perry, ed., Pergamon Press, Ltd., 1967, pp. 195–208.

TABLE I. INSTRUMENTATION CHARACTERISTICS

Parameter	Transducer		System resolution	Accuracy, percent full range	Sample rate, sample/sec	Location		
	Type	Range				Fuselage station, m (in.)	Butt plane, m (in.)	Waterplane, m (in.)
Airplane basic data–								
True velocity	Airplane electrical system	66 to 1632 knots	±1.702 knots	[a] 0.1	40			
Angle of pitch at center of gravity	Attitude gyro	10.45° to 35.3°	±0.049°	2.0	40	41.58 (1637.0)		
Rate of pitch at center of gravity	Rate gyro	±5.33 deg/sec	±0.0116 deg/sec	2.0	40	35.54 (1399.0)		
Rate of yaw at center of gravity	Rate gyro	±5.7 deg/sec	±0.0124 deg/sec	2.0	20	35.66 (1404.0)	0.406 (16.0)	-1.626 (-64.0)
Rate of roll at center of gravity	Rate gyro	±21.66 deg/sec	±0.047 deg/sec	2.0	20	35.66 (1404.0)	0.406 (16.0)	1.626 (-64.0)
Right elevon position at inboard actuator	Position transmitter	±30.0°	±0.0652°	1.2	20			
Right outboard elevon position	Position transmitter	±30.0°	±0.0652°	1.2	20			
Left elevon position at inboard actuator	Position transmitter	±30.0°	±0.0652°	1.2	20			
Left outboard elevon position	Position transmitter	±30.0°	±0.0652°	1.2	20			
Pitch axis acceleration, FACS output	Airplane electrical system	1g to 3g	±0.00436g	2.5				
Pitch rate gyro, FACS output	Airplane electrical system	±10 deg/sec	±0.0217 deg/sec	2.5				
Roll rate gyro, FACS output	Airplane electrical system	±60 deg/sec	±0.1304 deg/sec	2.5				
Pitch differential servo displacement, FACS output	Airplane electrical system	±15	±0.0326	2.5	20			
Nose-boom angle of attack (low response)	Angle of attack and sideslip sensor	10° to 30°	0.0435	0.1	40	2.308 (91.875)	0.152 (6.0)	0.508 (20.0)
Total outside air temperature: Low range	Temperature sensing probe	218° K to 433° K (-67° F to 320° F)	0.234° K (0.042° F)	1.2	4			
High range	Temperature sensing probe	422° K to 650° K (300° F to 711° F)	0.248° K (0.045° F)	1.2	4			
Nose-boom total pressure	Absolute pressure transducer	0 to 206.843 N/m² (0 to 30 psia)	224.8 N/m² (0.0326 psia)	0.05	20			
Nose-boom static pressure	Absolute pressure transducer	0 to 110.316 N/m² (0 to 16 psia)	119.9 N/m² (0.0174 psia)	0.05	20			
Altitude: Coarse	Airplane subsystem	304.8 to 30,480 m (1000 to 100,000 ft)	33.5 m (109.8 ft)	2.0	40			
Fine	Airplane subsystem	1524 m/revolution (5000 ft/revolution)	1.66 m/revolution (5.43 ft/revolution)	2.0	40			
Airspeed: Coarse	Airplane subsystem	50 to 800 knots	0.815 knots	2.0	40			
Fine	Airplane subsystem	70 knots/revolution	0.076 knots/revolution	2.0	40			
Mach number: Coarse	Airplane subsystem	0.5 to 3.2 Mach number	0.0029 Mach number	2.0	40			
Fine	Airplane subsystem	0.3 Mach number/revolution	0.00033 Mach number/revolution	2.0	40			

[a] 0.1 Mach number.

TABLE 1. INSTRUMENTATION CHARACTERISTICS Concluded

Parameter	Transducer		System resolution	Accuracy, percent full range	Sample rate, sample sec	Location		
	Type	Range				Fuselage station, m (in.)	Butt plane, m (in.)	Waterplane, m (in.)
Vertical airplane response								
Normal acceleration at nose	Accelerometer	±2.84g	±0.0062g	2.0	40	4.947 (194.75)		
Normal acceleration at nose ramp	Accelerometer	±3.0g	±0.0065g	2.5	40	7.43 (292.50)		
Normal acceleration at pilot station	Accelerometer	±3.0g	±0.0065g	2.0	40	11.125 (438.00)	0.305 (12.0)	0.914 (36.0)
Normal acceleration at nosewheel well	Accelerometer	±3.0g	±0.0065g	2.0	40	32.61 (1284.00)		
Normal acceleration at center of gravity	Accelerometer	±1.37g	±0.00298g	2.0	40	37.72 (1485.0)	0.279 (11.0)	-1.803 (-71.0)
Normal acceleration at left wing	Accelerometer	±5.88g	±0.01275g	2.0	40	46.23 (1820.0)	9.53 (375.0)	
Normal acceleration at right wing	Accelerometer	±6.40g	±0.014g	2.0	40	46.23 (1820.0)	9.53 (375.0)	
Normal acceleration at left wing	Accelerometer	±6.44g	±0.014g	2.0	40	55.17 (2172.0)	9.53 (375.0)	
Normal acceleration at right wing	Accelerometer	±6.81g	±0.0148g	2.0	40	55.17 (2172.0)	9.53 (375.0)	
Normal acceleration at left wing	Accelerometer	±9.24g	±0.021g	2.0	40	55.88 (2200.0)	13.21 (520.0)	
Normal acceleration at mixer bay	Accelerometer	1.2g to 3.2g	±0.0048g	2.0	40	51.70 (2035.5)		
ILAF system parameters [a]								
Normal acceleration at left wing, ILAF system output	Accelerometer	1g to 3.0g	0.00436	2.5	40	56.18 (2212.0)	7.11 (280.0)	
Normal acceleration at right wing, ILAF system output	Accelerometer	1g to 3.0g	0.00436	2.5	40	56.18 (2212.0)	7.11 (280.0)	
Normal acceleration at center of gravity, ILAF system output	Accelerometer	1g to 3.0g	0.00436	2.5	40	41.99 (1653.0)		
ILAF system computer output:								
Channel 1	Airplane electrical system	±6 V		2.5				
Channel 2	Airplane electrical system	±6 V		2.5				
ILAF system notch filter output signal, channel 1	Airplane electrical system	±20 V		2.5				
ILAF system lead input signal, channel 1	Airplane electrical system	±20 V		2.5				
Vertical component of true gust velocity –								
Normal acceleration at nose	Accelerometer	±2.84g	±0.0062g	2.0	40	4.947 (194.75)		
Nose-boom angle of attack (high response)	Angle of attack and sideslip sensor	0° to 8.0°	±0.008°	.8	40	2.308 (91.875)	0.152 (6.0)	0.508 (20.0)
Angle of pitch at airplane nose	Attitude gyro	±4.24°	±0.009°	5.0	40	4.947 (194.75)		
Rate of pitch at airplane nose	Airplane electrical system	±5.0 deg sec	±0.0109 deg sec	2.0	40	7.487 (294.75)		
Nose-boom vertical bending	Bonded strain gage	±153,752,925 N m² (±22,300 psi)	±334,245.5 N m² (±48.48 psi)	2.5	40	3.251 (128.00)		

[a] Dual analog and digital recording. Analog recording system natural frequency had flat response up to 30 hertz.

TABLE 2. – FLIGHT-TEST CONDITIONS

Mach number	Altitude, m (ft)	Weight, kg (lb)	True velocity, knots	Dynamic pressure, N/m^2 (lb/ft^2)	Wingtip position, deg	Location of center of gravity, m (in.)
0.87	7,620 (25,000)	195,680 (431,400) Heavy	521	19,727 (412)	25	FS 40.3 (1585.4)
0.86	7,620 (25,000)	147,417 (325,000) Light	515	19,248 (402)	25	FS 40.6 (1598.1)
1.59	11,918 (39,100)	172,184 (379,600) Medium	909	34,522 (721)	65	FS 40.3 (1586.8)
2.38	18,898 (62,000)	163,974 (361,500) Medium	1365	25,999 (543)	65	FS 40.5 (1594.8)

TABLE 3. - COMPUTER PRINTOUT OF SERVO TABLE DATA FOR THE ILAF SYSTEM

[Mediumweight, M = 1.59, h_p = 11,918 m (39,100 ft), δ_t = 65°, K_I = 0.11 rad/g]

(a) Inboard elevon

Frequency, rad/sec	Real, rad/sec	Imaginary, rad/sec
	ST-1	
0.19999999E 0C	0.0	C.19999999E 00
0.59999996E 0C	C.0	C.59999996E 00
0.10000000E 01	0.0	C.10000000E 01
0.20000000E 01	C.73999995E CC	C.18599997E 01
0.60000000E 01	0.35999994E C1	C.47999992E 01
0.10000000E 02	C.86999998E C1	C.23999996E 01
0.20000000E 02	C.10599999E 02	-C.60000000E 01
0.30000000E 02	C.45000000E C1	-C.11700000E 02
0.40000000E 02	-C.31999998E C1	-C.10799999E 02
0.50000000E 02	-C.75000000E C1	-C.60000000E 01
0.60000000E 02	-C.65999994E C1	C.17999992E 01
0.70000000E C2	-C.33599997E C1	C.46899996E 01
0.80000000E C2	C.13599997E C1	C.42399998E 01
0.90000000E C2	C.25199995E C1	C.26099997E 01
0.10000000E 03	0.20999994E C1	C.59999996E 00
	ST-2	
0.19999999E CC	0.39999999E-C1	C.C
0.59999996E 0C	0.35999995E CC	C.C
0.10000000E 01	C.10000000E C1	C.C
0.20000000E 01	0.37199993E C1	-C.14799995E 01
0.60000000E 01	0.28799988E C2	-C.21599991E 02
0.10000000E 02	C.24000000E C2	-C.87000000E 02
0.20000000E C2	-C.12000000E C3	-C.21200000E 03
0.30000000E 02	-C.35100000E C3	-C.13500000E 03
0.40000000E 02	-0.43200000E C3	C.12800000E 03
0.50000000E 02	-C.30000000E C3	C.37500000E 03
0.60000000E 02	C.10800000E C3	C.39600000E 03
0.70000000E 02	C.32700000E C3	C.23400000E 03
0.80000000E 02	C.34000000E C3	-C.11000000E 03
0.90000000E C2	C.23600000E C3	-C.22800000E 03
0.10000000E 03	C.60000000E C2	-C.21000000E 03

TABLE 3. - Concluded

(b) Outboard elevon

Frequency, rad/sec	Real, rad/sec	Imaginary, rad/sec
ST-3		
0.19999999E 0C	0.0	C.19999999E 00
0.59999996E 0C	0.0	C.59999996E 00
0.10000000E C1	0.0	C.10000000E 01
0.20000000E 01	0.10199995E C1	C.17399998E 01
0.60000000E 01	C.47999992E C1	C.31199999E 01
0.10000000E 02	C.80000000E C1	-C.11999998E 01
0.20000000E 02	C.30000000E C1	-C.80000000E 01
0.30000000E 02	-0.32999992E C1	-C.65999994E 01
0.40000000E 02	-0.60000000E C1	-C.15999994E 01
0.50000000E 02	-C.40000000E C1	C.25000000E 01
0.60000000E 02	-C.35999995E CC	C.30000000E 01
0.70000000E 02	C.15400000E C1	C.16799994E 01
0.80000000E 02	0.15999994E C1	-C.31999999E 00
0.90000000E 02	C.10000000E C1	-C.10000000E 01
0.10000000E 03	C.19999999E CC	-C.79999995E 00
ST-4		
0.19999999E 0C	C.39999999E-C1	C.0
0.59999996E 0C	C.35999995E CC	C.0
0.10000000E C1	C.10000000E C1	C.0
0.20000000E C1	C.34799995E C1	-C.20400000E 01
0.60000000E C1	C.18599991E C2	-C.28799988E 02
0.10000000E C2	-C.12000000E C2	-C.80000000E 02
0.20000000E C2	-C.16000000E C3	-C.60000000E 02
0.30000000E 02	-C.19800000E C3	-C.99000000E 02
0.40000000E 02	-C.64000000E C2	C.24000000E 03
0.50000000E C2	C.12500000E C3	C.20000000E 03
0.60000000E 02	C.18000000E C3	C.21599991E 02
0.70000000E 02	C.11800000E C3	-C.10800000E 03
0.80000000E C2	-C.25599991E C2	-C.12800000E 03
0.90000000E C2	-C.90000000E C2	-C.90000000E 02
0.10000000E C3	-0.80000000E C2	-C.20000000E 02

TABLE 4. COMPUTER PRINTOUT OF SERVO TABLE DATA FOR THE ILAF SYSTEM

[Heavyweight, M = 0.87, h_p = 7620 m (25,000 ft), δ_t = 25°, K_I = 0.07 rad/g]

(a) Inboard elevon

Frequency, rad/sec	Real, rad/sec	Imaginary, rad/sec
ST-1		
0.19999999E 00	0.0	0.19999999E 00
0.59999996E 00	0.0	0.59999994E 00
0.10000000E 01	0.0	0.10000000E 01
0.20000000E 01	0.73999995E 00	0.18599997E 01
0.60000000E 01	0.35999994E 01	0.47999992E 01
0.10000000E 02	0.86999938E 01	0.23999996E 01
0.20000000E 02	0.10599999E 02	-0.60000009E 01
0.30000000E 02	0.45000000E 01	-0.11700000E 02
0.40000000E 02	-0.31999998E 01	-0.10799999E 02
0.50000000E 02	-0.75000000E 01	-0.60000000E 01
0.60000000E 02	-0.65999994E 01	0.17999992E 01
0.70000000E 02	-0.33599997E 01	0.46899994E 01
0.80000000E 02	0.13599997E 01	0.42399998E 01
0.90000000E 02	0.25199995E 01	0.26099997E 01
0.10000000E 03	0.20999994E 01	0.59999996E 00
ST-2		
0.19999999E 00	0.39999999E-01	0.0
0.59999996E 00	0.35999995E 00	0.0
0.10000000E 01	0.10000000E 01	0.0
0.20000000E 01	0.37199993E 01	-0.14799995E 01
0.60000000E 01	0.28799988E 02	-0.21599991E 02
0.10000000E 02	0.24000000E 02	-0.87000000E 02
0.20000000E 02	-0.12000000E 03	-0.21200000E 03
0.30000000E 02	-0.35100000E 03	-0.13500000E 03
0.40000000E 02	-0.43200000E 03	0.12800000E 03
0.50000000E 02	-0.30000000E 03	0.37500000E 03
0.60000000E 02	0.10800000E 03	0.39600000E 03
0.70000000E 02	0.32700000E 03	0.23400000E 03
0.80000000E 02	0.34000000E 03	-0.11000000E 03
0.90000000E 02	0.23600000E 03	-0.22800000E 03
0.10000000E 03	0.60000000E 02	-0.21000000E 03

TABLE 4. Concluded

(b) Outboard elevon

Frequency, rad/sec	Real, rad/sec	Imaginary, rad/sec
	ST-3	
0.19999999E 00	0.0	0.15999999E 00
0.59999996E 00	0.0	0.59999996E 00
0.10000000E 01	0.0	0.10000000E 01
0.20000000E 01	0.10199995E 01	0.17399998E 01
0.60000000E 01	0.47999992E 01	0.31199999E 01
0.10000000E 02	0.80000000E 01	-0.11999998E 01
0.20000000E 02	0.30000000E 01	-0.80000000E 01
0.30000000E 02	-0.32999992E 01	-0.65999994E 01
0.40000000E 02	-0.60000000E 01	-0.15999994E 01
0.50000000E 02	-0.40000000E 01	0.25000000E 01
0.60000000E 02	-0.35999995E 00	0.30000000E 01
0.70000000E 02	0.15400000E 01	0.16799994E 01
0.80000000E 02	0.15999994E 01	-0.31999999E 00
0.90000000E 02	0.10000000E 01	-0.10000000E 01
0.10000000E 03	0.19999999E 00	-0.79999995E 00
	ST-4	
0.19999999E 00	0.39999999E-01	0.0
0.59999996E 00	0.35999995E 00	0.0
0.10000000E 01	0.10000000E 01	0.0
0.20000000E 01	0.34799995E 01	-0.20400000E 01
0.60000000E 01	0.18599991E 02	-0.28799988E 02
0.10000000E 02	-0.12000000E 02	-0.80000000E 02
0.20000000E 02	-0.16000000E 03	-0.60000000E 02
0.30000000E 02	-0.19800000E 03	-0.99000000E 02
0.40000000E 02	-0.64000000E 02	0.24000000E 03
0.50000000E 02	0.12500000E 03	0.28000000E 03
0.60000000E 02	0.18000000E 03	0.21599991E 02
0.70000000E 02	0.11800000E 03	-0.10800000E 03
0.80000000E 02	-0.25599991E 02	-0.12800000E 03
0.90000000E 02	-0.90000000E 02	-0.90000000E 02
0.10000000E 03	-0.80000000E 02	-0.20000000E 02

TABLE 5. COMPUTER PRINTOUT OF SERVO TABLE DATA FOR THE ILAF SYSTEM

[Lightweight, M = 0.86, h_p = 7620 m (25,000 ft), δ_t = 25°, K_I = 0.07 rad/g]

(a) Inboard elevon

Frequency, rad/sec	Real, rad/sec	Imaginary, rad/sec
ST-1		
0.19999999E CC	C.0	C.19999999E 00
0.59999996E CC	C.0	C.59999996E 00
0.1CCCCCCCE C1	C.0	C.10000000E 01
0.2CCCCCCCF 01	C.73999995F CC	0.18599997E 01
0.6CCCCCCCE C1	C.35999994E 01	0.47999992E 01
0.1CCCCCCCE C2	C.86999998E C1	0.23999996E 01
C.2CCCCCCCF C2	C.1C599999F C2	-C.60000000E 01
0.3CCCCCCCE C2	C.45CCCCCCF C1	-C.11700000E 02
0.4CCCCCCCF C2	-C.31999998E C1	-C.10799999E 02
0.5CCCCCCCE C2	-C.75000000F 01	-C.60000000E 01
0.6CCCCCCCE C2	-C.65999994F C1	0.17999992E 01
0.7CCCCCCCF C2	-C.33599997F C1	0.46899996E 01
0.8CCCCCCCF C2	C.13599997E C1	0.42399998E 01
C.9CCCCCCCE C2	C.25199995E C1	0.26099997E 01
C.1CCCCCCCE C3	C.2C999994E C1	0.59999996E 00
ST-2		
0.19999999E CC	C.39999999E-C1	0.0
0.59999996E CC	C.35999995E CC	0.0
0.1CCCCCCCF C1	C.1C0CCCCF C1	0.0
0.2CCCCCCCF C1	C.37199993E C1	-C.14799995E 01
C.6CCCCCCCE 01	C.28799988E 02	-C.21599991E 02
0.1CCCCCCCE C2	C.24CCCCCCE C2	-C.87CCCCCE 02
0.2CCCCCCCF C2	-C.12CCCCCCE C3	-C.21200000E 03
0.3CCCCCCCE C2	-C.351CCCCCE 03	-0.13500000E 03
0.4CCCCCCCF C2	-C.432CCCCCE C3	0.12800000E 03
0.5CCCCCCCF C2	-C.30CCCCCCE C3	C.37500000E 03
C.6CCCCCCCF C2	C.1C8CCCCCF C3	0.39600000E 03
0.7CCCCCCCF C2	C.327CCCCCE C3	0.23400000E 03
0.8CCCCCCCE C2	C.34CCCCCCE C3	-C.11000000E 03
0.9CCCCCCCE C2	C.236CCCCCF C3	-C.22800000E 03
0.1CCCCCCCF C3	C.6CCCCCCCE C2	-C.21000000E 03

TABLE 5. – Concluded

(b) Outboard elevon

Frequency, rad/sec	Real, rad/sec	Imaginary, rad/sec
ST-3		
0.19999999E CC	C.0	0.19999999E 00
C.59999996E 0C	C.0	0.59999996E 00
0.10000000E C1	C.0	0.10000000E 01
0.20000000E 01	0.10199995E C1	C.17399998E 01
C.60000000E C1	C.47999992E 01	C.31199999E 01
0.10000000E C2	C.80C00000E 01	-0.11999998E 01
0.20000000E C2	C.30C00000E C1	-0.80000000E 01
0.30000000E C2	-C.32999992E C1	-0.65999994E 01
0.40000000E C2	-C.60C00000E C1	-0.15999994E 01
0.50000000E C2	-C.40C00000E C1	C.25000000E 01
0.60000000E 02	-0.35999995E CC	C.30000000E 01
C.70000000E C2	C.15400000E 01	C.16799994E 01
0.80000000E C2	C.15999994E C1	-0.31999999E 00
0.90000000E C2	C.10000000E C1	-C.10000000E 01
C.10000000E C3	C.19999999E CC	-0.79999995E 00
ST-4		
0.19999999E CC	C.39999999E-C1	0.0
0.59999996E CC	C.35999995E CC	C.0
0.10000000E C1	C.10000000E C1	0.0
0.20000000E C1	C.14399996E C1	-0.55199995E 01
0.60000000E C1	-C.10200000E C2	-0.47399994E 02
0.10000000E 02	-C.92000000E C2	-C.68C00000E 02
0.20000000E C2	-C.22000000E C3	0.10000000E 03
0.30000000E C2	-C.10000000E C3	C.29700000E 03
0.40000000E C2	C.17600000E C3	0.30400000E 03
0.50000000E 02	C.32500000E C3	0.75000000E 02
0.60000000E 02	C.20200000E C3	-0.15800000E 03
0.70000000E 02	C.10000000E 02	-0.22600000E 03
0.80000000E C2	-C.15300000E C3	-C.10200000E 03
0.90000000E C2	-C.18000000E C3	0.0
C.10000000E C3	-C.10000000E C3	0.60000000E 02

TABLE 6. – MODE SHAPE CHARACTERISTICS AT SELECTED LOCATIONS

[Mediumweight, M = 1.59, $\delta_t = 65°$]

Location	Mode	ϕ_i	ϕ_i'
Fuselage nose, FS 4.95 m (194.75 in.)	1	2.1200	
	2	0.1500	
	3	3.7300	
	4	0.0680	
	5	−0.8600	
Pilot station, FS 11.12 m (438 in.)	1	1.2500	
	2	0.0650	
	3	1.1000	
	4	0.2100	
	5	0.1500	
Nosewheel well, FS 32.61 m (1284 in.)	1	0.4200	0
	2	0.0250	0.00077
	3	−0.1900	0.02930
	4	0.0045	−0.00072
	5	−0.1100	0.00720
Near center of gravity, FS 37.72 m (1485 in.)	1	−0.3817	
	2	0.0037	
	3	0.2125	
	4	0.0068	
	5	−0.1529	
Wing accelerometer, FS 56.18 m (2212 in.)	1	0.6000	
	2	−0.0600	
	3	−0.9000	
	4	−0.0550	
	5	−0.4300	
Center of gravity, FS 41.99 m (1653 in.)	1	−0.2992	
	2	−0.0162	
	3	0.4240	
	4	0.0112	
	5	−0.1190	

TABLE 6. - MODE SHAPE CHARACTERISTICS AT SELECTED LOCATIONS

[Mediumweight, M = 1.59, $\delta_t = 65°$]

Location	Mode	ϕ_i	ϕ_i'
Fuselage nose, FS 4.95 m (194.75 in.)	1	2.1200	
	2	0.1500	
	3	3.7300	
	4	0.0680	
	5	0.8600	
Pilot station, FS 11.12 m (438 in.)	1	1.2500	
	2	0.0650	
	3	1.1000	
	4	0.2100	
	5	0.1500	
Nosewheel well, FS 32.61 m (1284 in.)	1	0.4200	0
	2	0.0250	0.00077
	3	0.1900	0.02930
	4	0.0045	0.00072
	5	0.1100	0.00720
Near center of gravity, FS 37.72 m (1485 in.)	1	−0.3817	
	2	0.0037	
	3	0.2125	
	4	0.0068	
	5	−0.1529	
Wing accelerometer, FS 56.18 m (2212 in.)	1	0.6000	
	2	−0.0600	
	3	−0.9000	
	4	−0.0550	
	5	−0.4300	
Center of gravity, FS 41.99 m (1653 in.)	1	−0.2992	
	2	−0.0162	
	3	0.4240	
	4	0.0112	
	5	−0.1190	

TABLE 7. – COMPARISON OF FLIGHT-MEASURED AND ANALYTICAL CONTROL SYSTEM PERFORMANCE WITH THE ILAF SYSTEM INPUT

Parameter	Heavyweight, M = 0.87, h_p = 7620 m (25,000 ft), δ_t = 25°				Lightweight, M = 0.86, h_p = 7620 m (25,000 ft), δ_t = 25°						Mediumweight, M = 1.59, h_p = 11,918 m (39,100 ft), δ_t = 65°			
	Mode 1, f = 2.4 Hz				Mode 1, f = 2.6 Hz				Mode 2,3, f = 5.6 Hz		Mode 1, f = 2.2 Hz		Mode 2,3, f = 5.0 Hz	
	δ_{sv} = ±4°		δ_{sv} = ±8°		δ_{sv} = ±4°		δ_{sv} = ±12°		δ_{sv} = ±4°		δ_{sv} = ±4°			
	Flight	Analytical	Flight	Analytical	Flight	Analytical	Flight	Analytical	Flight	Analytical	Flight	Analytical	Flight	Analytical
Pilot, n_z, g	±0.16	±0.095	±0.25	±0.19	±0.16	±0.098	±0.30	±0.29	±0.18	±0.17	±0.16	±0.156	±0.25	±0.304
FACS, n_z, g					±0.07	±0.033			±0.10	±0.06	±0.06	±0.056	±0.08	±0.039
ILAF system, wing, n_z, g					±0.10	±0.06				±0.123	±0.09	±0.085		±0.029
ILAF system, fuselage, n_z, g					±0.03	±0.025			±0.07	±0.016	±0.03	±0.042	±0.11	±0.065
ILAF system, Δn_z, g					±0.13	±0.085					±0.12	±0.127		
δ_1, deg	±0.25	±0.15	±0.48	±0.31	±0.50	±0.18	±0.82	±0.56	±0.35	±0.16	±0.46	±0.484	±0.60	±0.86
δ_2, deg		±0.11		±0.22	±0.40	±0.12		±0.36		±0.086	±0.42	±0.358	±0.36	±0.34

TABLE 8. – TOTAL CALCULATED MODE DAMPING

Mode	Heavyweight, M = 0.87		Lightweight, M = 0.86		Mediumweight, M = 1.59	
	[1] g_i	[2] σ_i	[1] g_i	[2] σ_i	[1] g_i	[2] σ_i
FACS						
1	0.193	1.365	0.174	1.365	0.103	0.763
2	0.159	1.910	0.178	2.210	0.090	1.145
3	0.052	0.810	0.049	0.885	0.049	0.820
4	0.068	1.435	0.083	1.910	– – –	– – –
FACS + ILAF						
1	0.277	2.050	0.184	1.510	0.237	1.810
2	0.188	2.290	0.150	1.910	0.098	1.270
3	0.075	1.192	0.058	1.060	0.037	0.630
4	0.068	1.430	0.075	1.740	– – –	– – –

[1] $g_i = \frac{2\sigma_i}{\omega_i}$.

[2] As in $s + \sigma_i \pm \omega_i$.

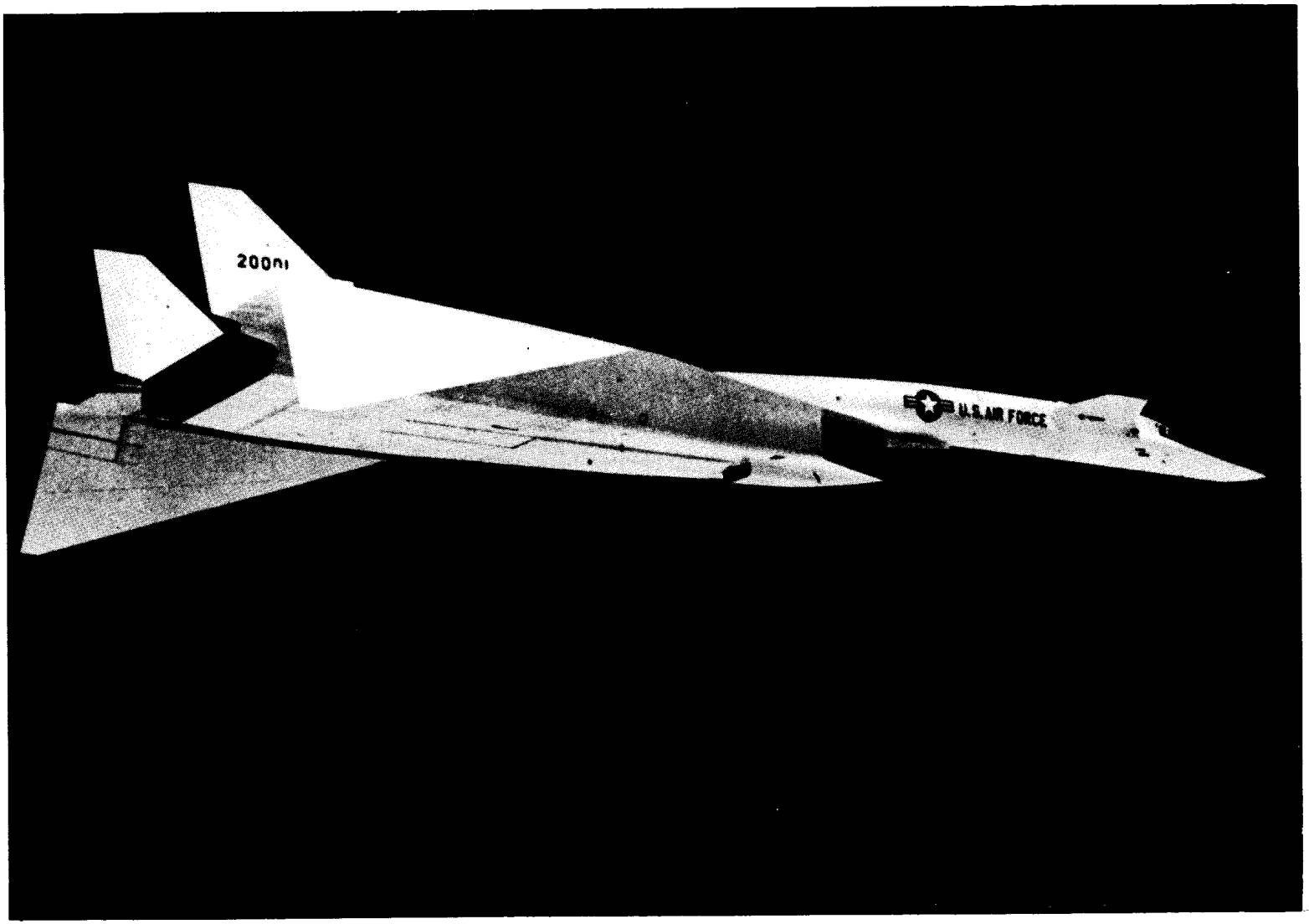

Figure 1. XB-70 airplane. Supersonic configuration; $\delta_t = 65^\circ$.

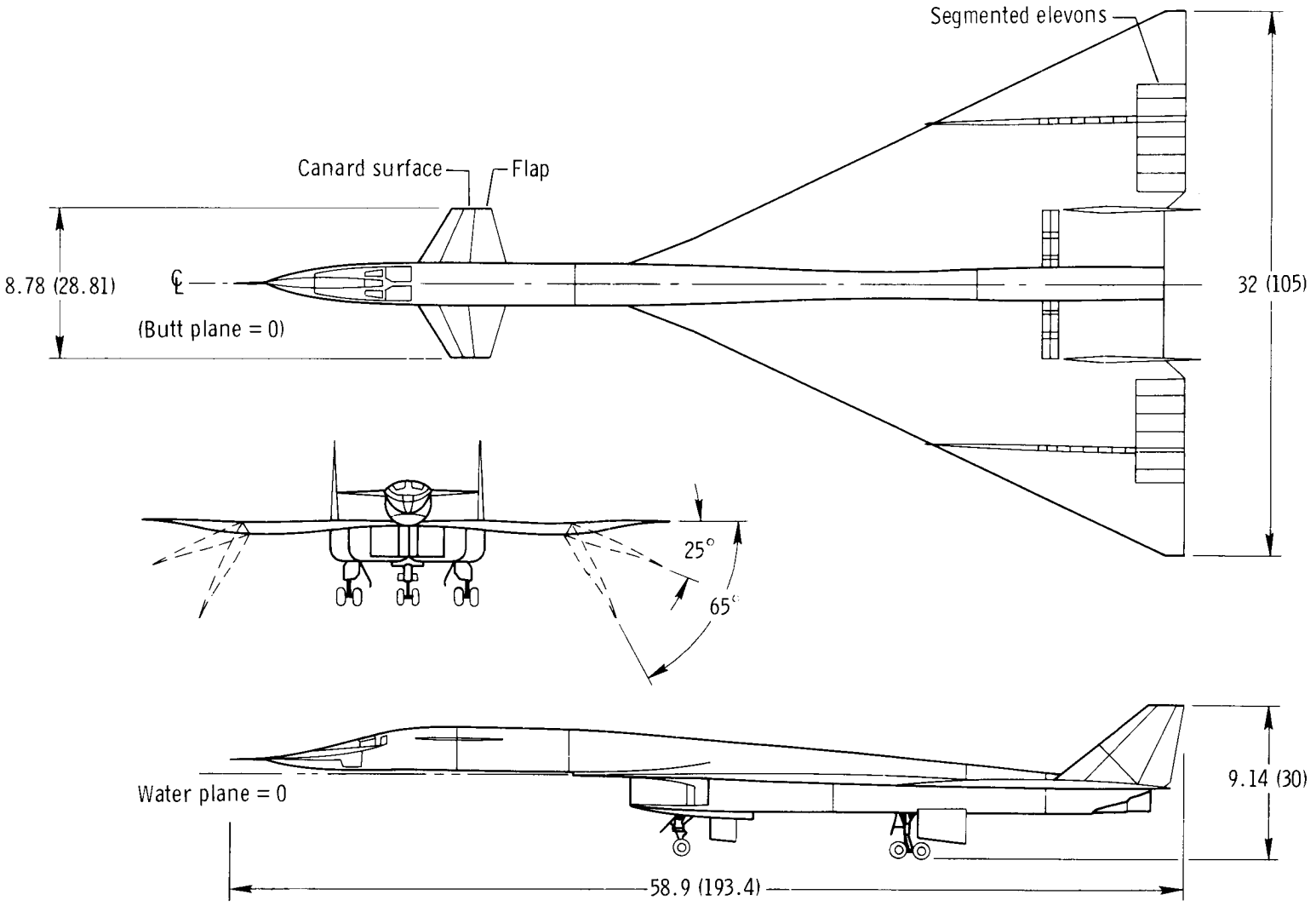

Figure 2. XB-70-1 airplane. Dimensions in meters (feet) except where otherwise noted.

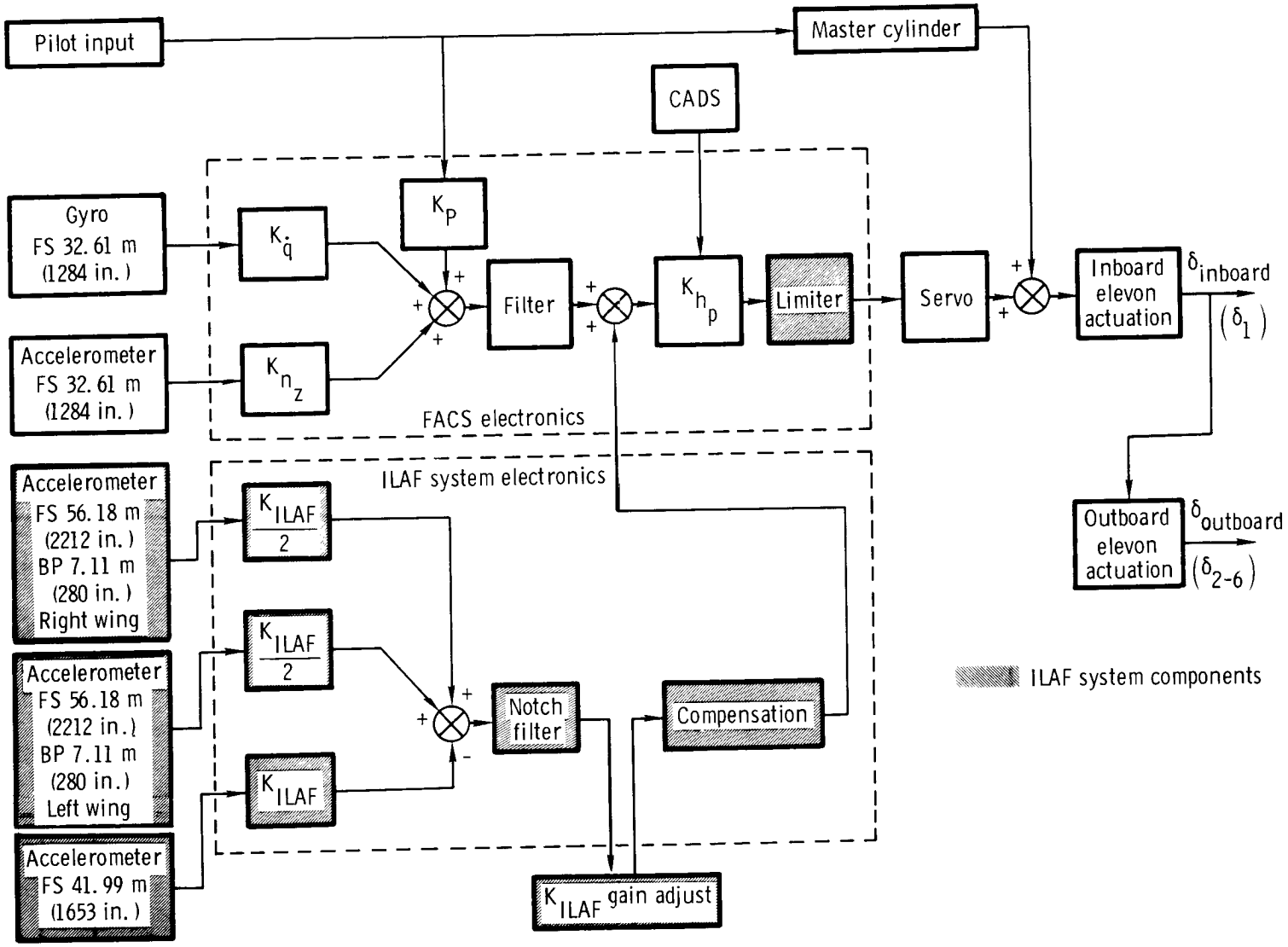

Figure 3. Integrated pitch FACS and ILAF system.

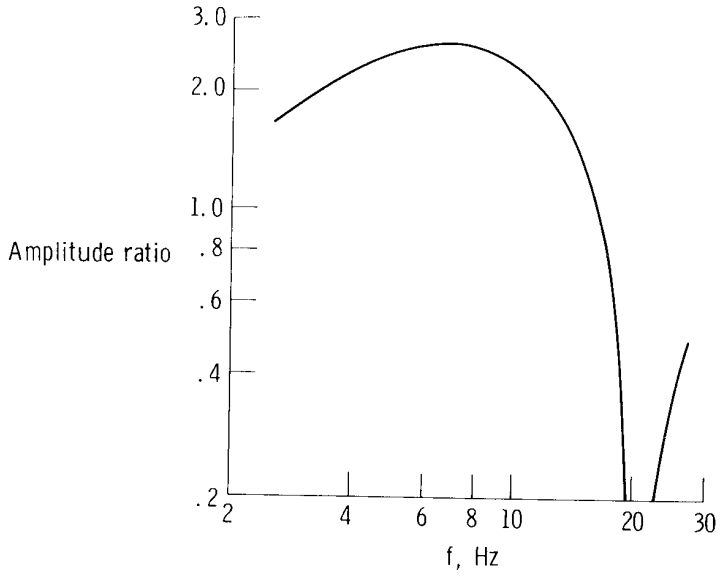

(a) Amplitude.

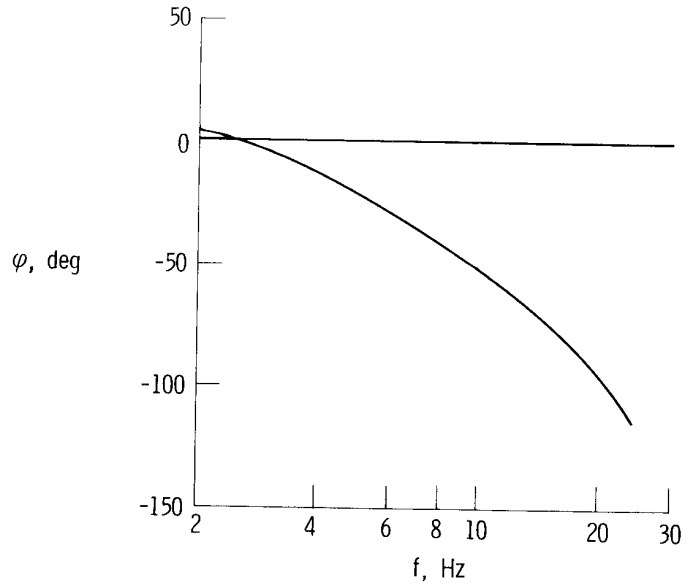

(b) Phase angle.

Figure 4. XB-70 ILAF system initial flight-test shaping network.

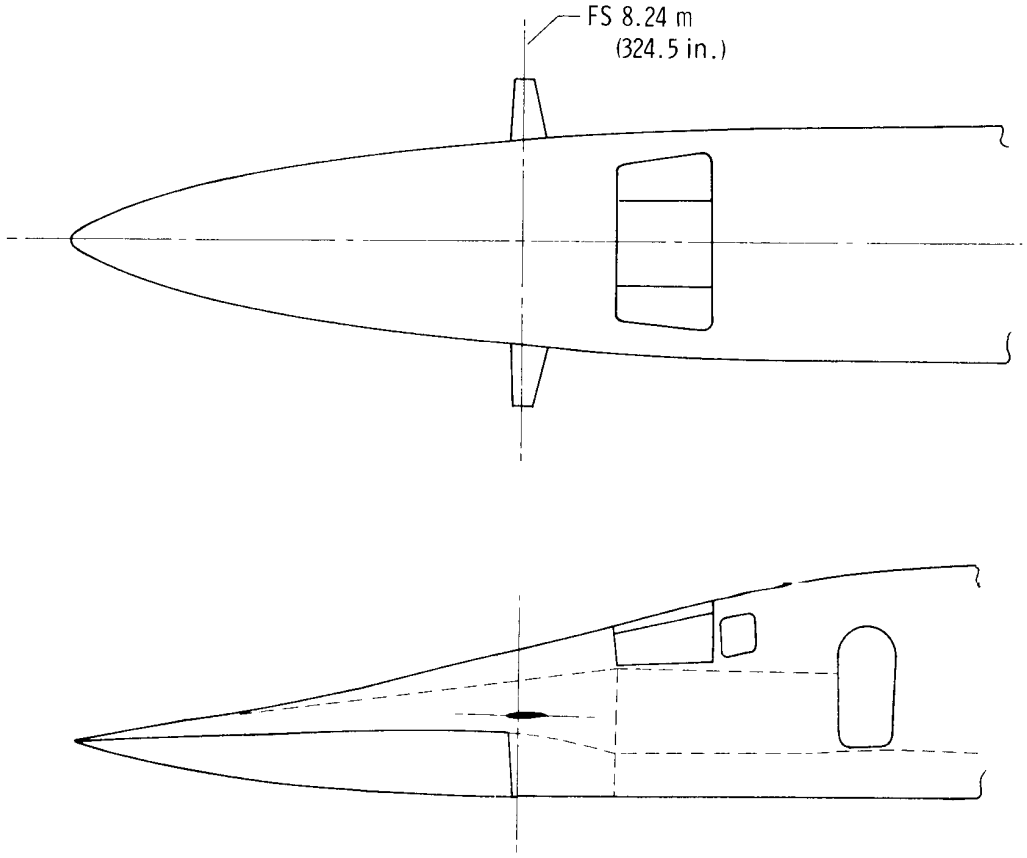

Figure 5. XB-70 shaker-vane location.

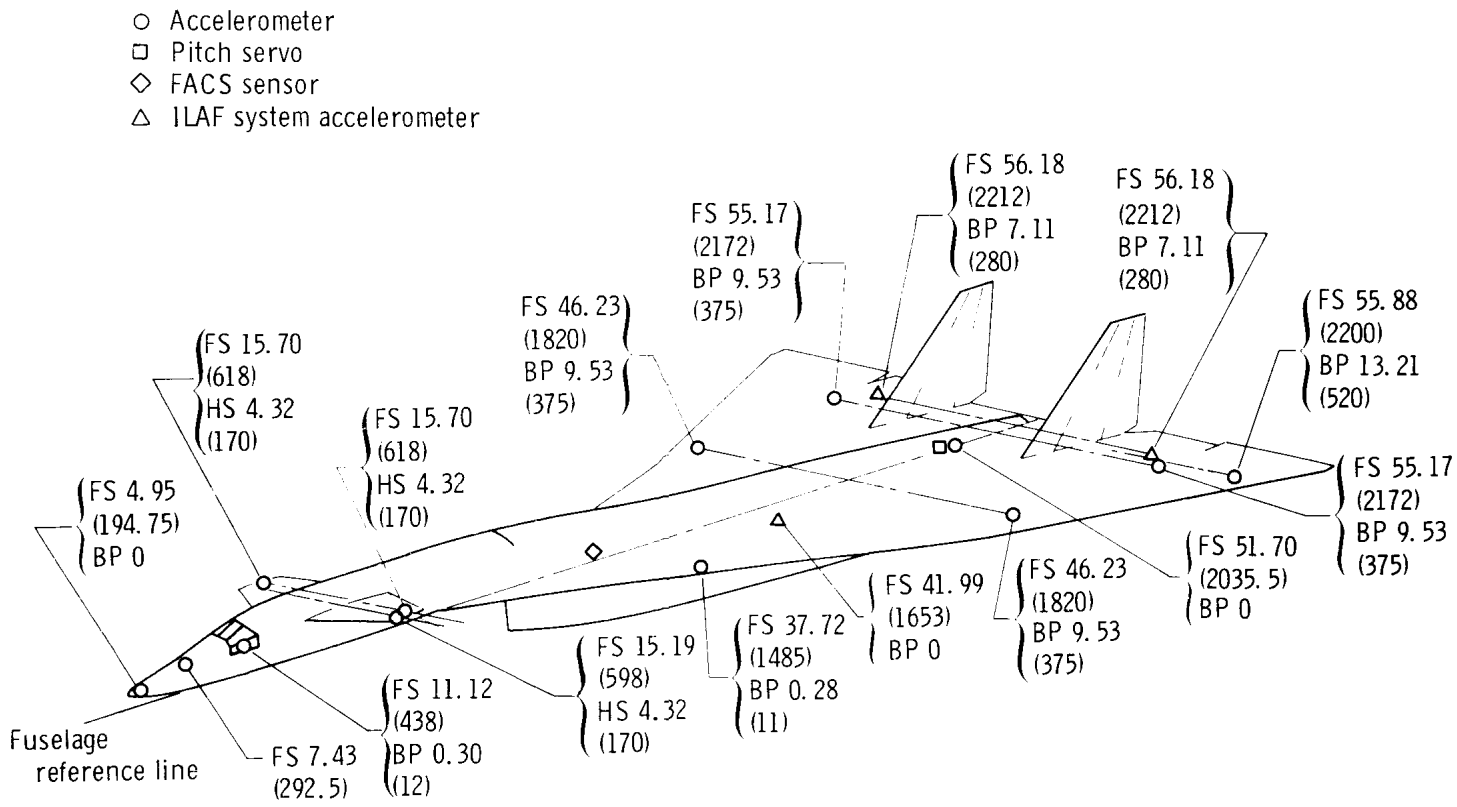

Figure 6. Location of the instrumentation used for evaluating the ILAF system. Dimensions in meters (inches).

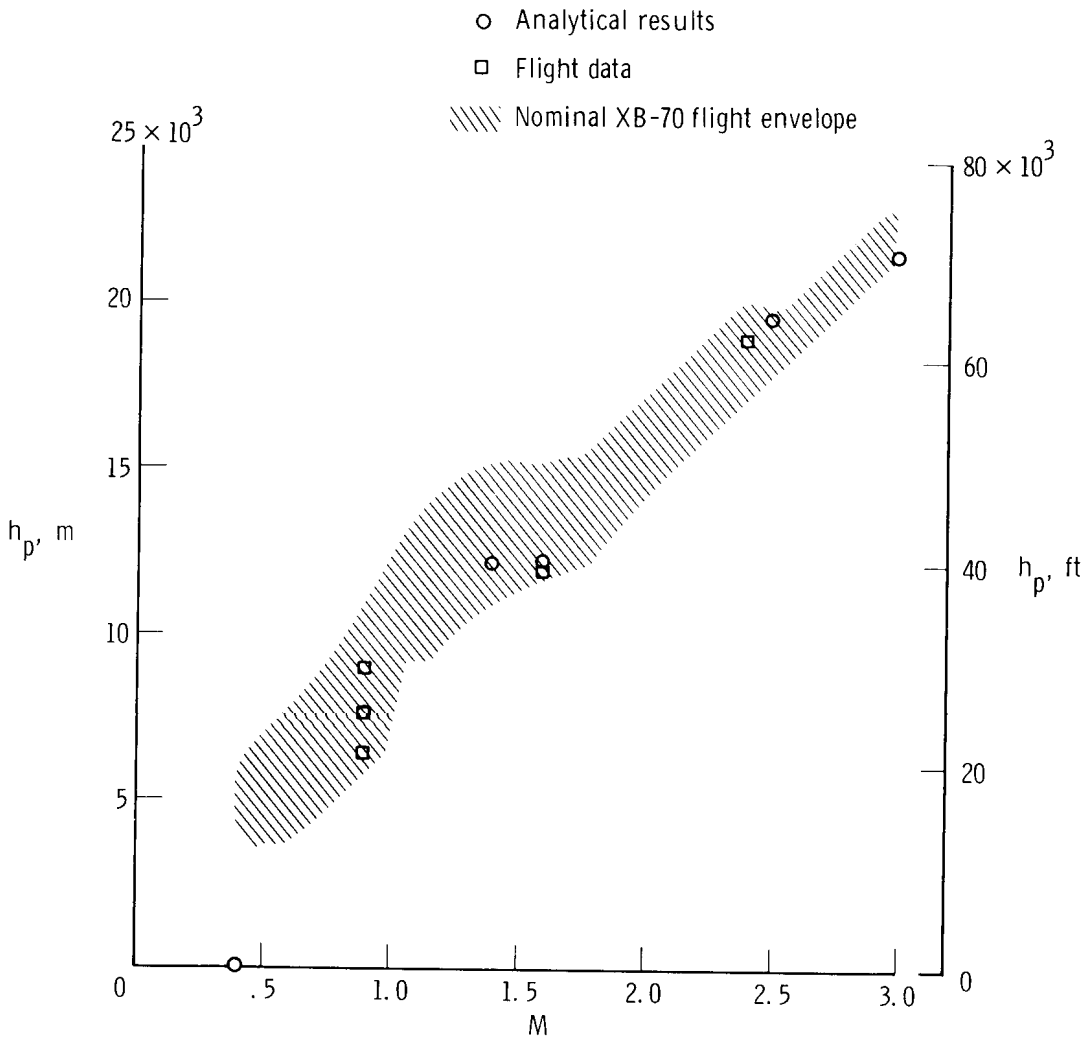

Figure 7. ILAF system flight-test envelope.

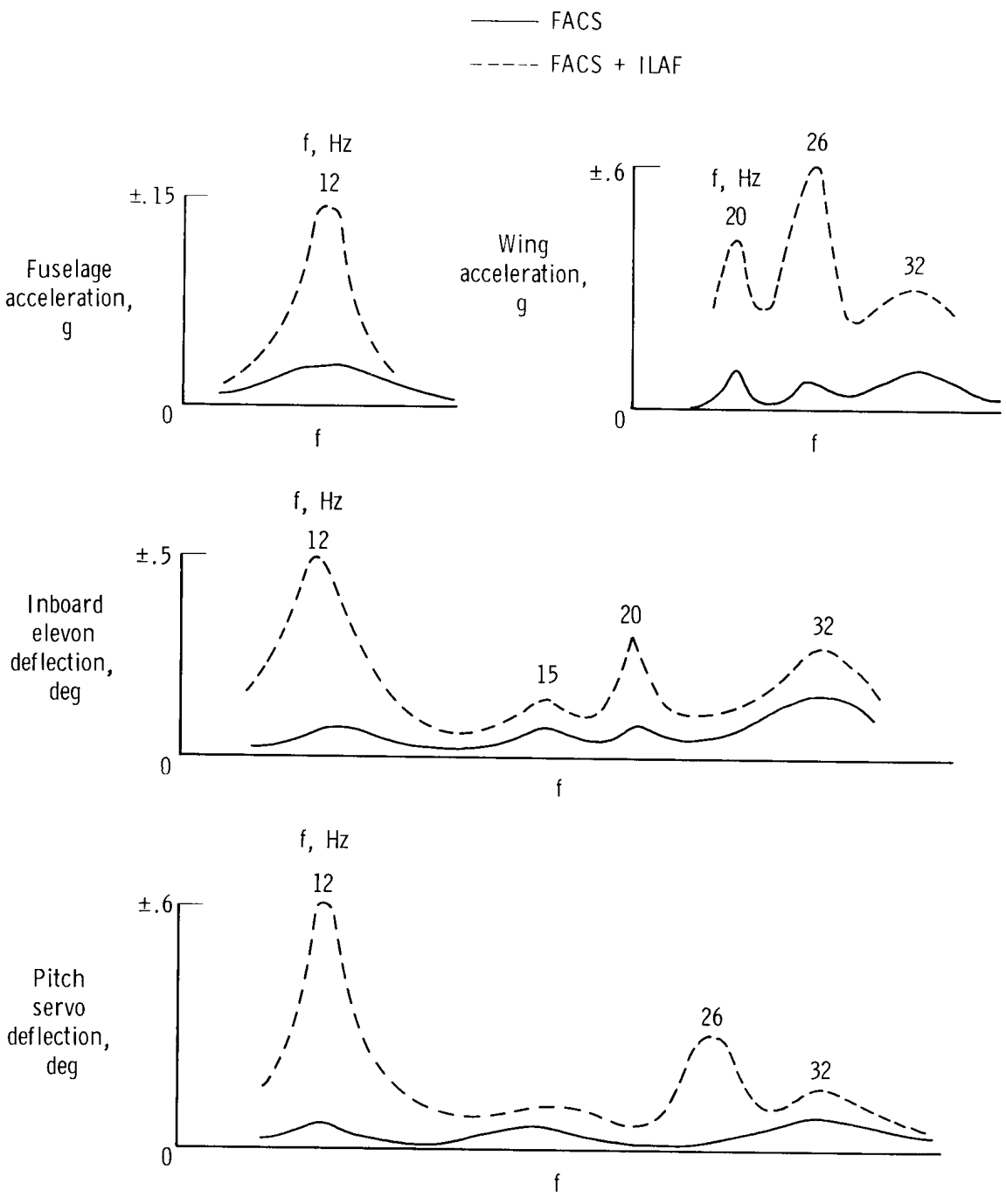

Figure 8. Limit cycle oscillations due to ILAF system operation from composite data for three flight conditions.

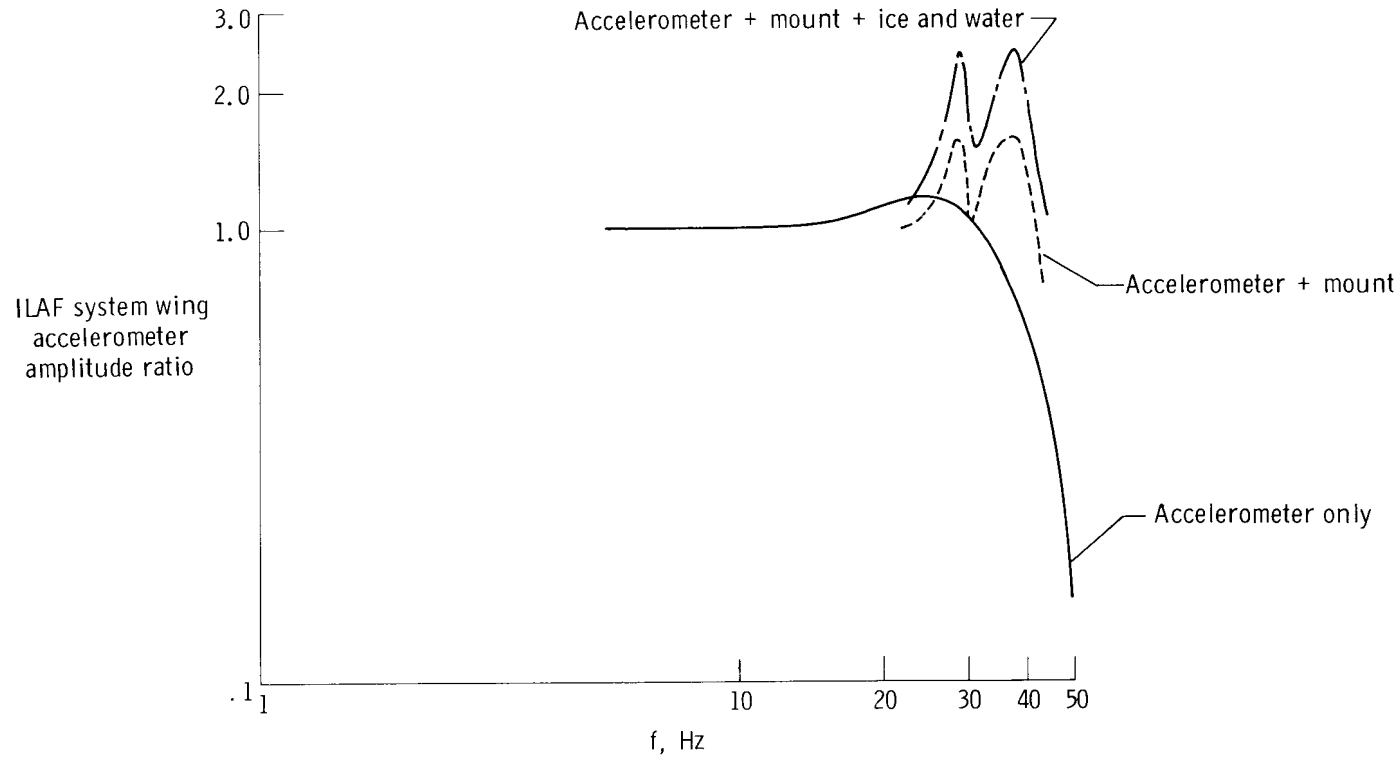

Figure 9. Frequency response of ILAF system shaping and wing accelerometer dynamics from ground vibration tests.

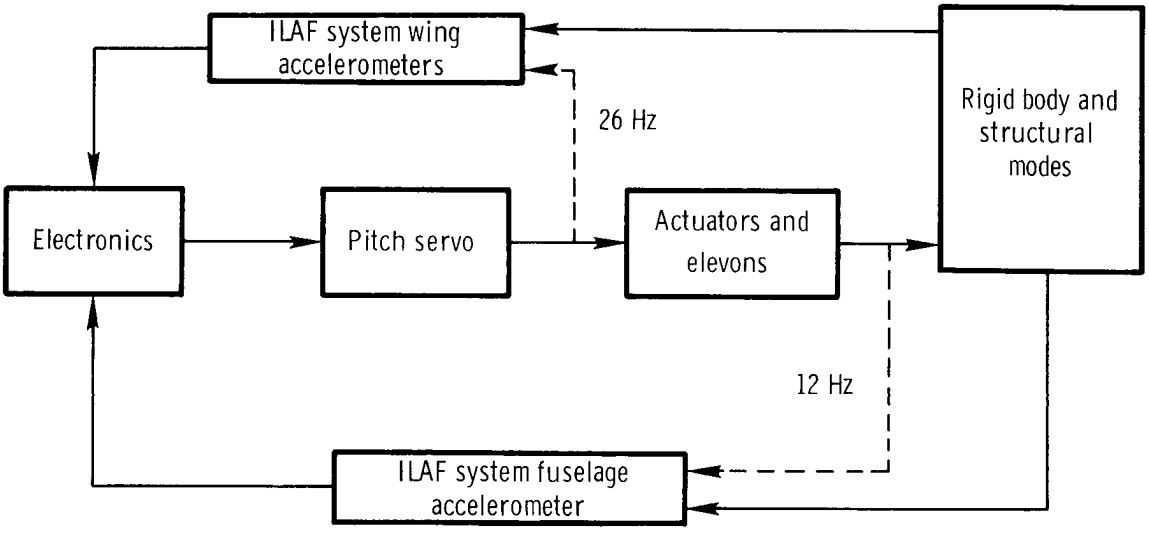

Figure 10. Deduced sources of limit cycle instabilities.

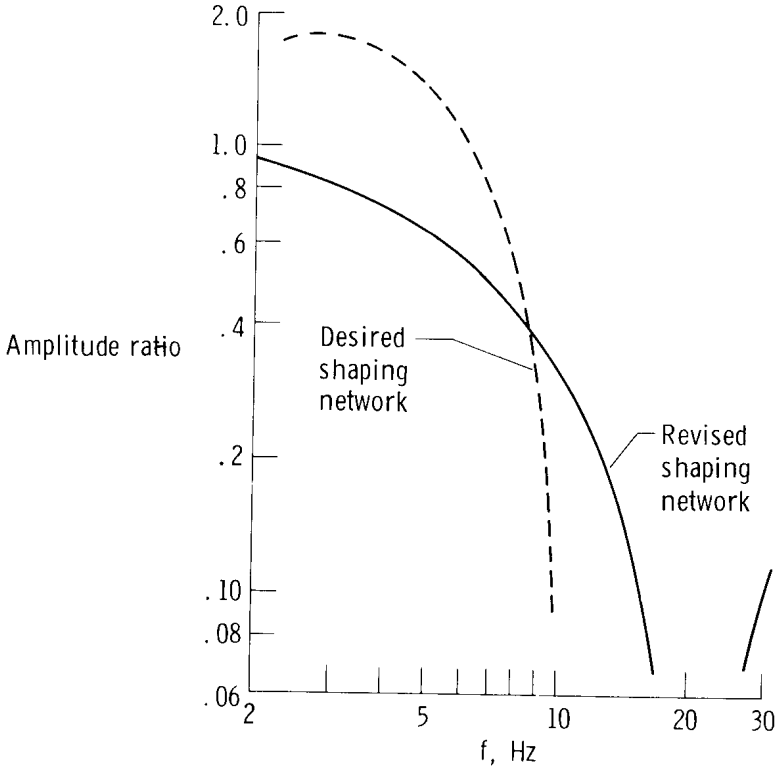

(a) Amplitude.

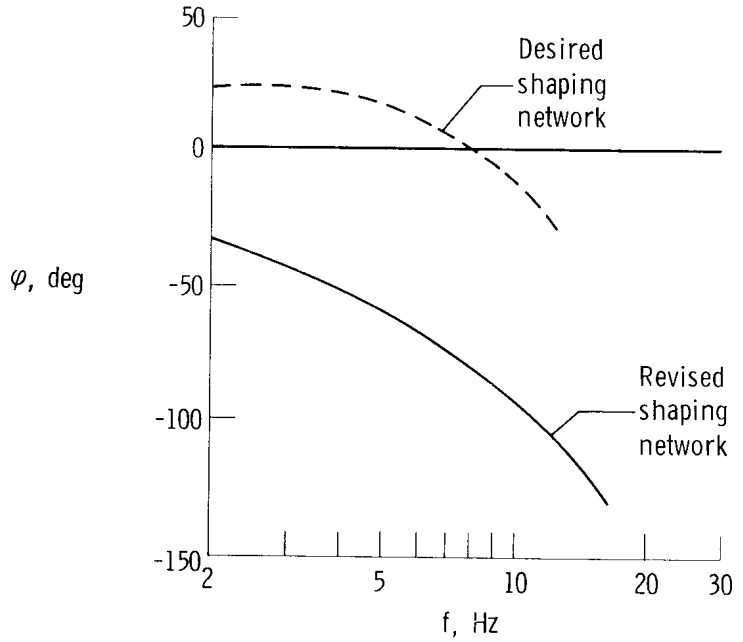

(b) Phase angle.

Figure 11. ILAF system shaping network.

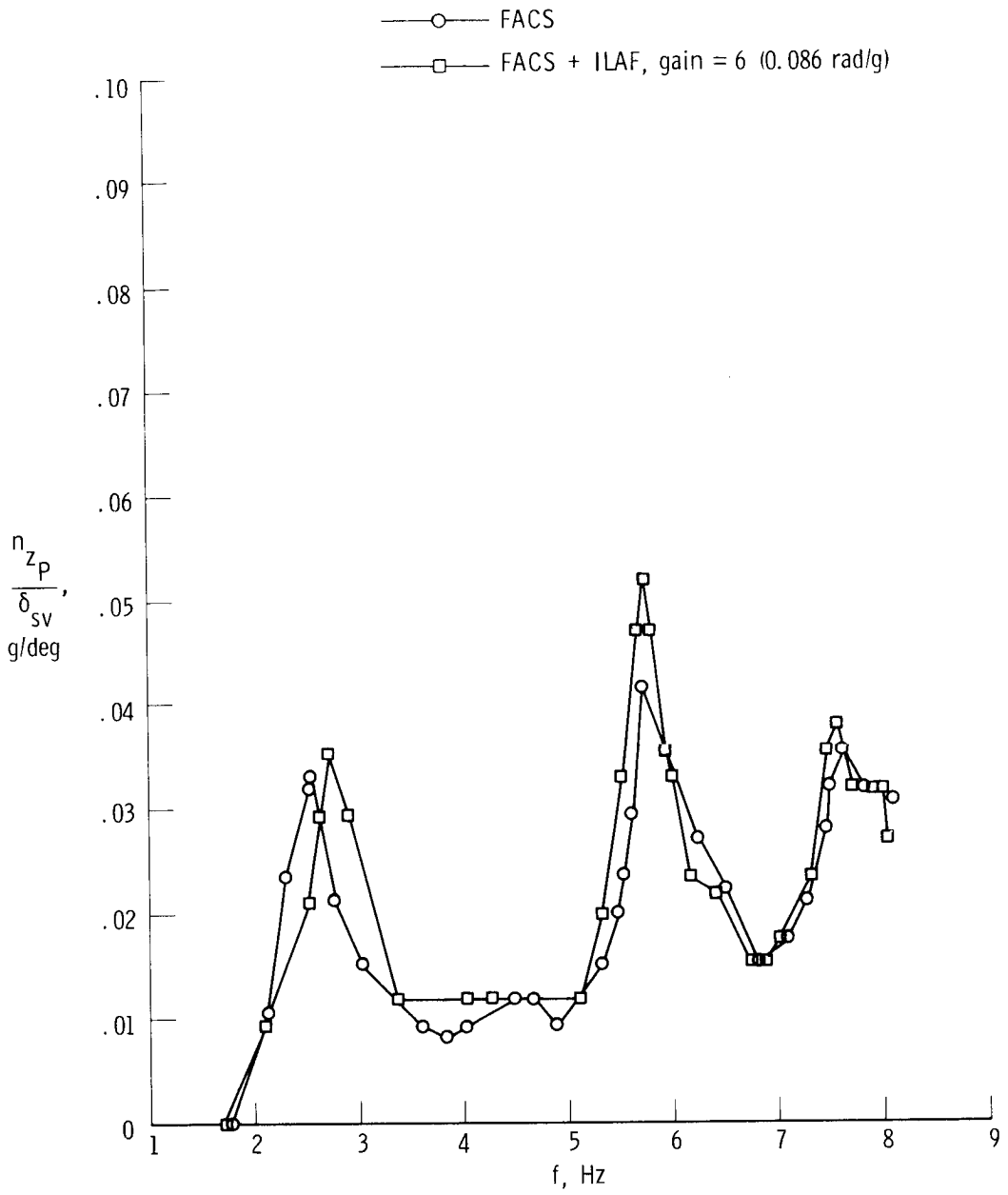

Figure 12. Flight-measured vertical acceleration response at the pilot's station with and without the ILAF system engaged. Lightweight, M = 0.86; h_p = 7620 m (25,000 ft); $\delta_t = 25°$.

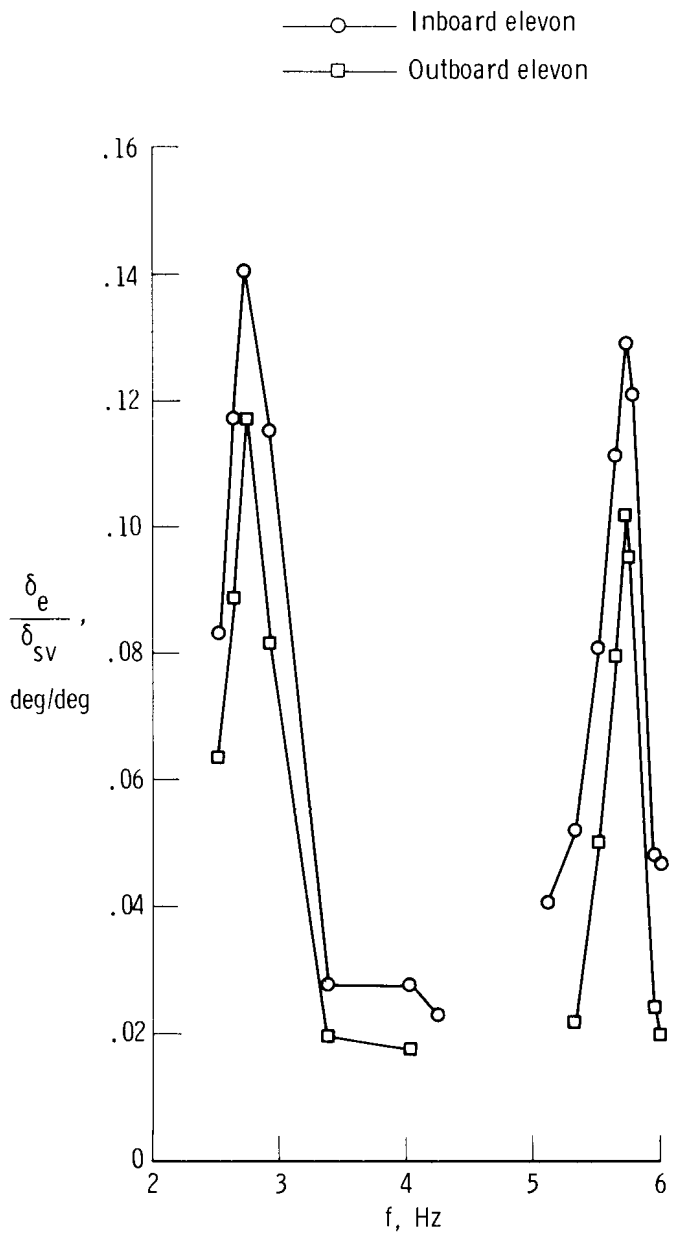

Figure 13. Elevon motion due to ILAF system operation. Lightweight, M = 0.86; h_p = 7620 m (25,000 ft); δ_t = 25°; ILAF system gain = 6 (0.086 rad/g).

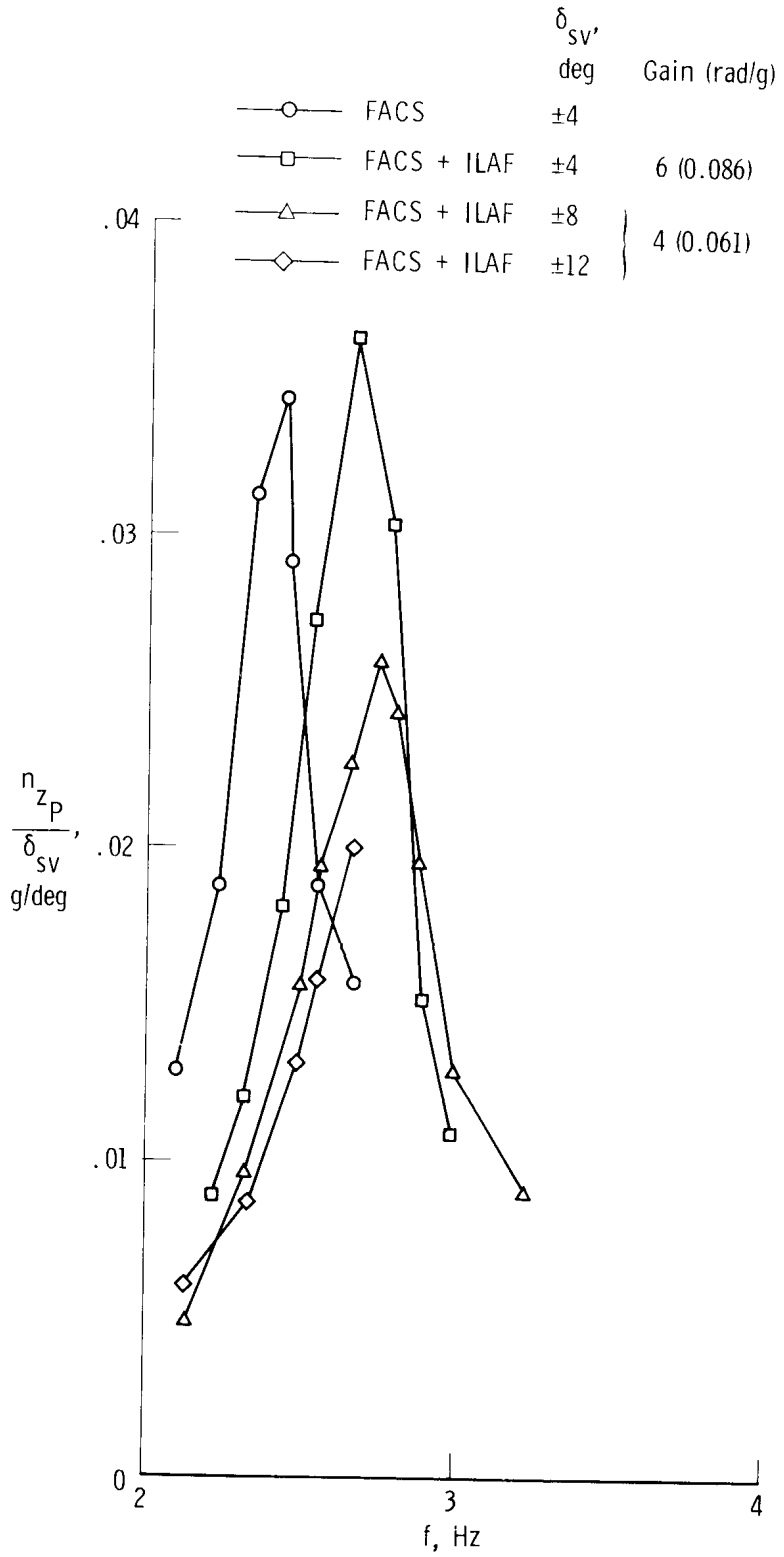

Figure 14. Flight-measured vertical acceleration response at the pilot's station with and without the ILAF system engaged. Lightweight, M = 0.86; h_p = 7620 m (25,000 ft); δ_t = 25°.

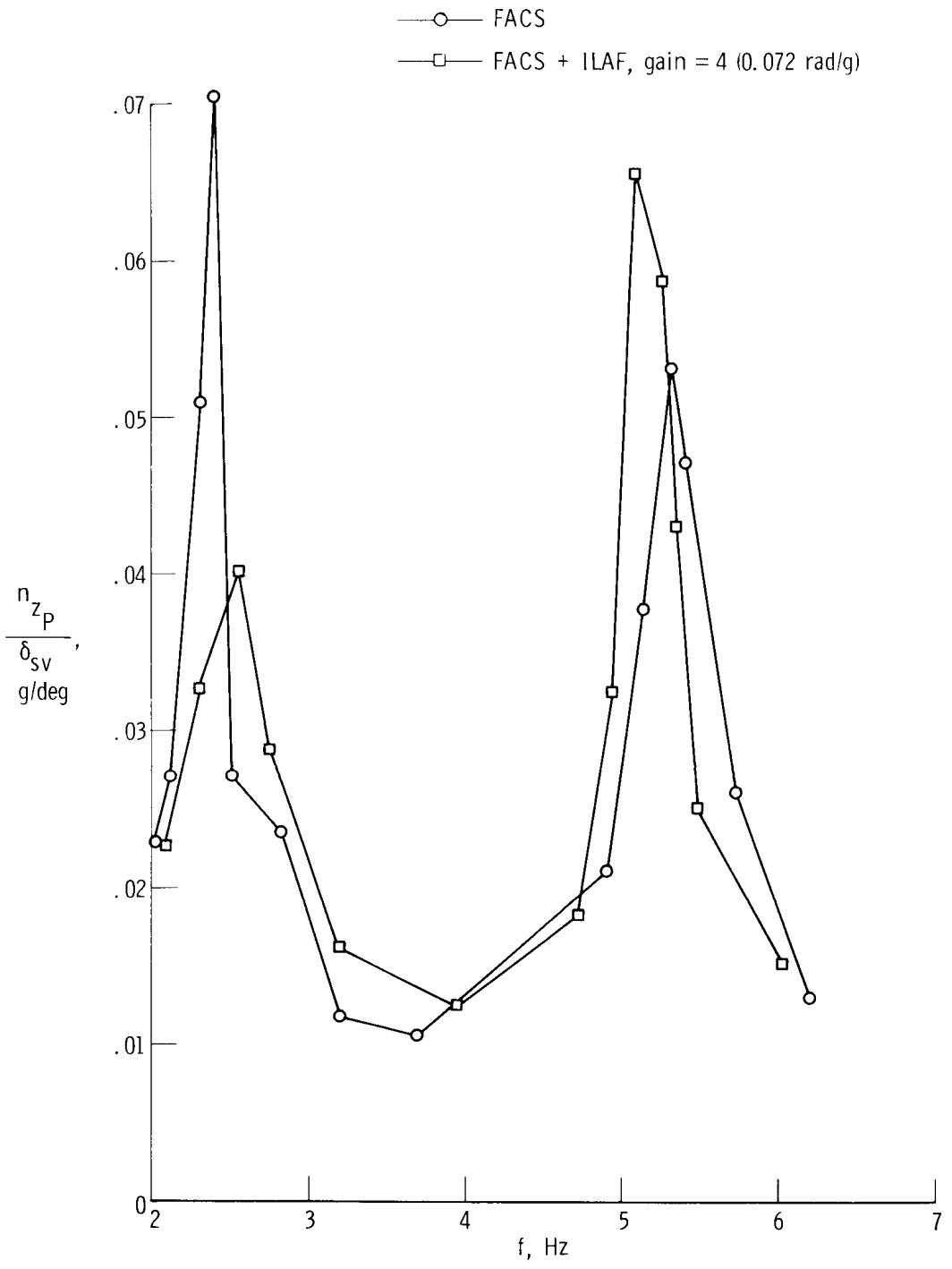

Figure 15. Flight-measured vertical acceleration response at the pilot's station with and without the ILAF system engaged. Mediumweight, M = 1.59; h_p = 11,918 m (39,100 ft); δ_t = 65°.

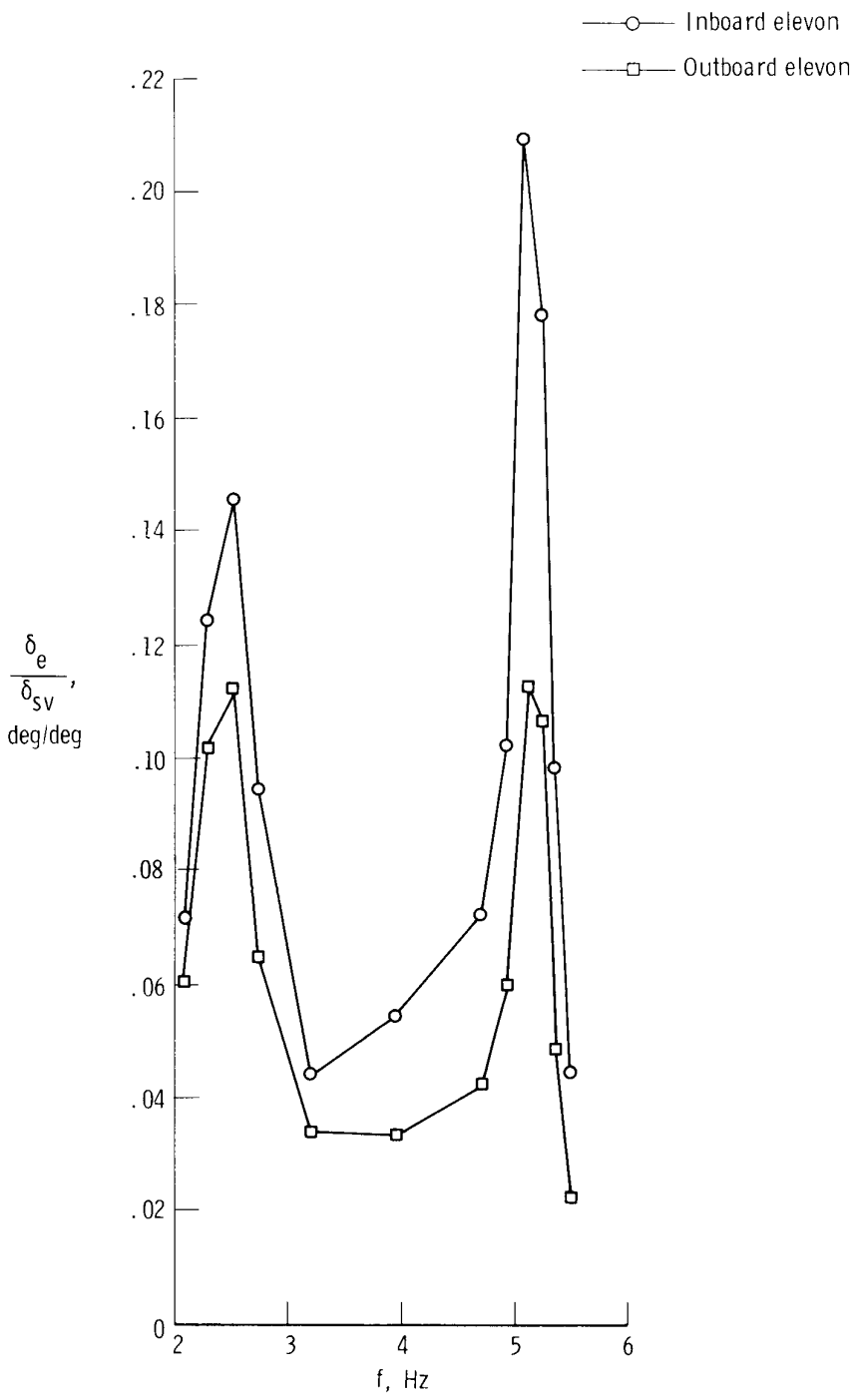

Figure 16. Elevon deflection due to ILAF system operation. Mediumweight, M = 1.59; h_p = 11,918 m (39,100 ft); δ_t = 65°; ILAF system gain = 4 (0.072 rad/g).

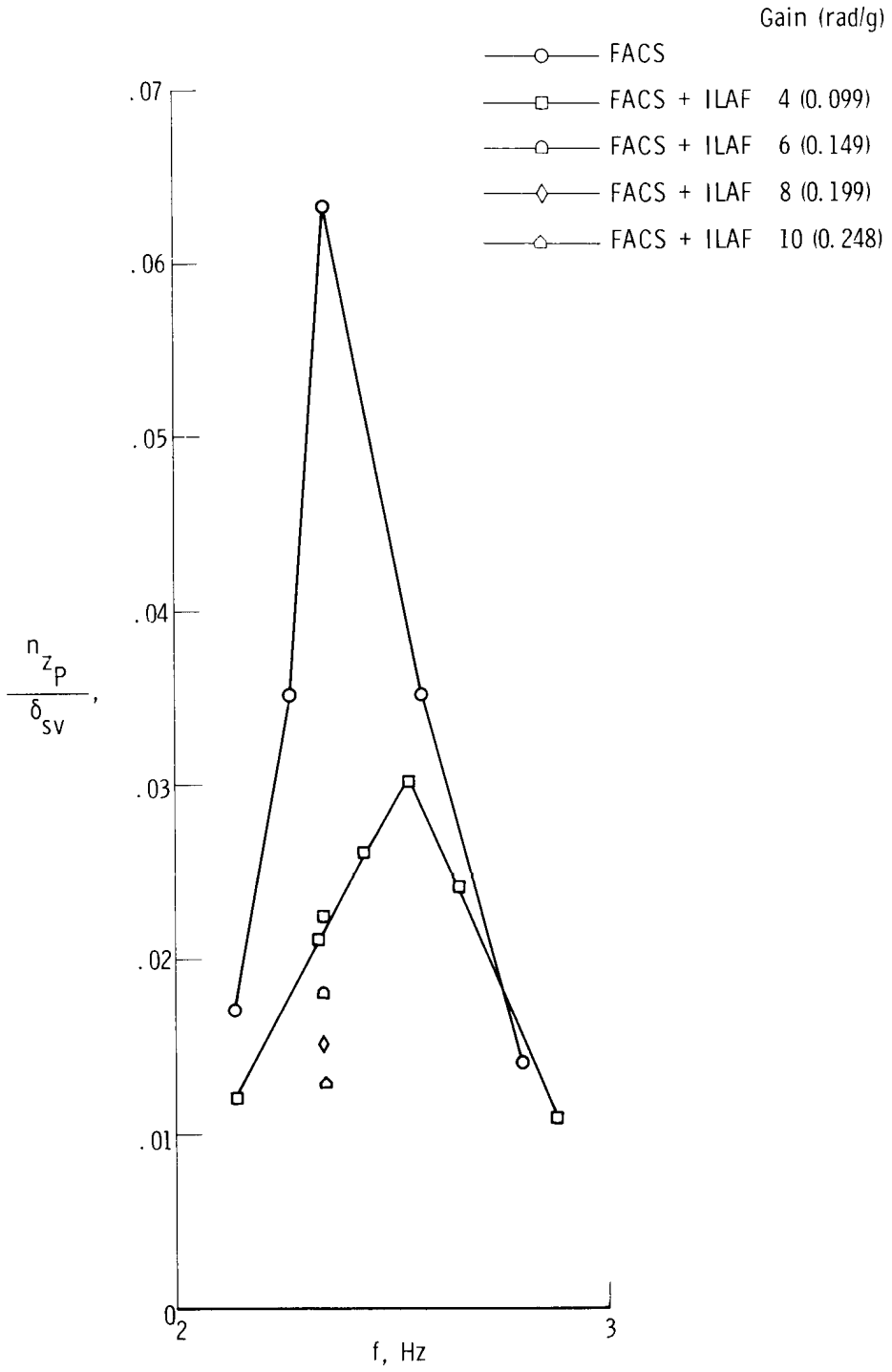

Figure 17. Flight-measured vertical acceleration response at the pilot's station with and without the ILAF system engaged. Mediumweight, M = 2.38; h_p = 18,898 m (62,000 ft); $\delta_t = 65^\circ$.

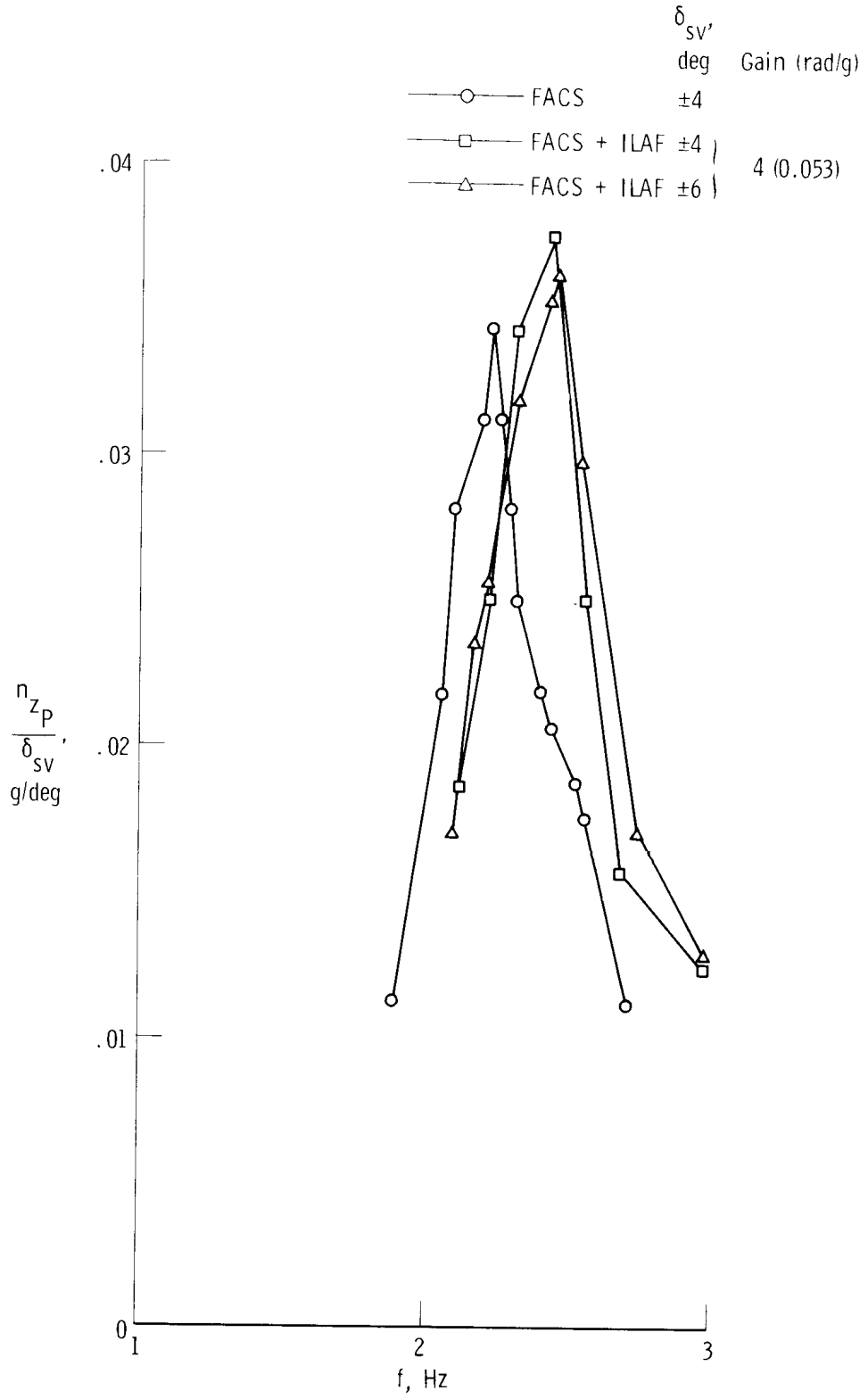

Figure 18. Flight-measured vertical acceleration response at the pilot's station with and without the ILAF system engaged. Heavyweight, M = 0.87; h_p = 6400 m (21,000 ft); $\delta_t = 25°$.

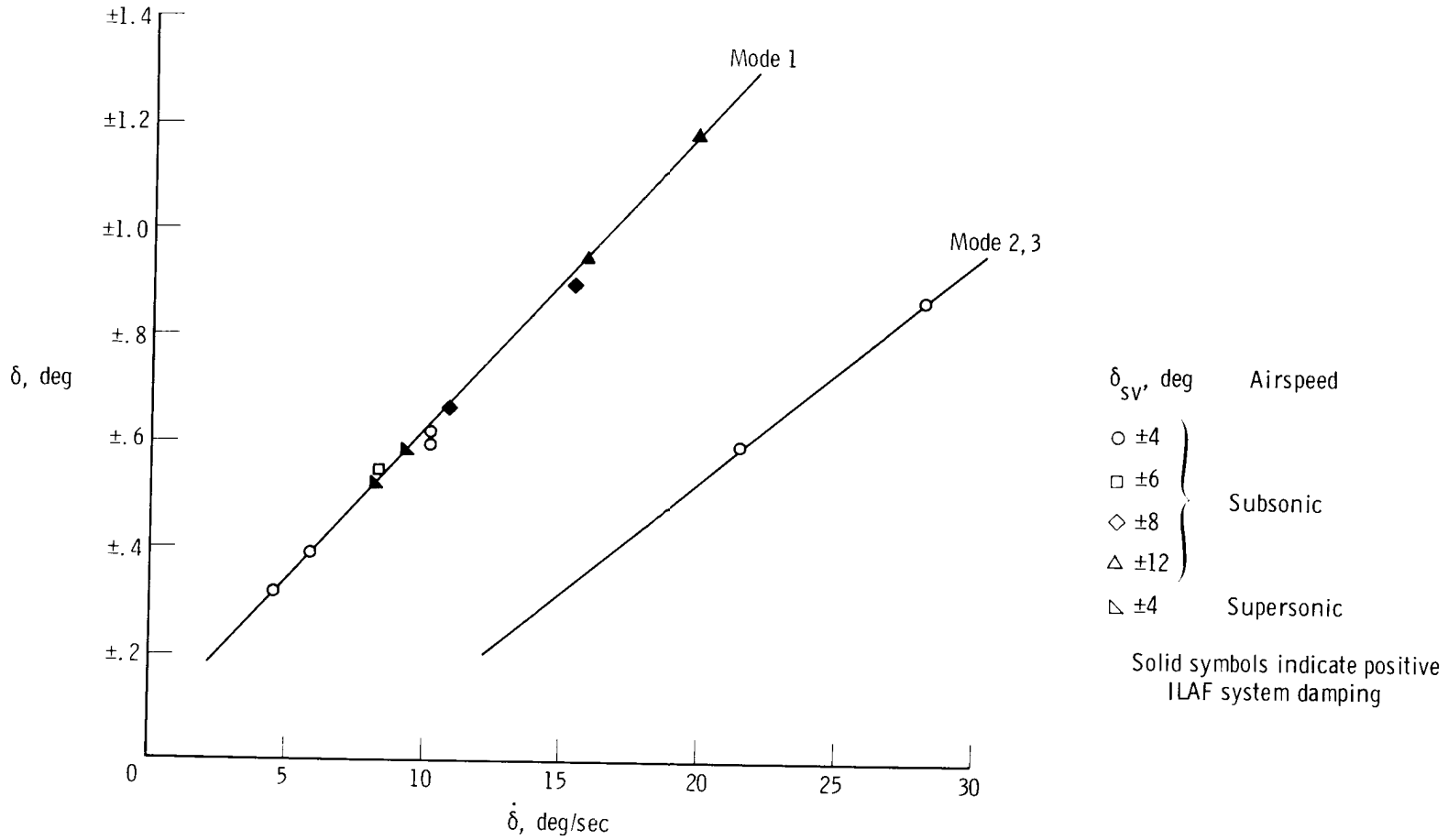

Figure 19. Inboard elevon deflections as a function of elevon rates measured at modal frequencies.

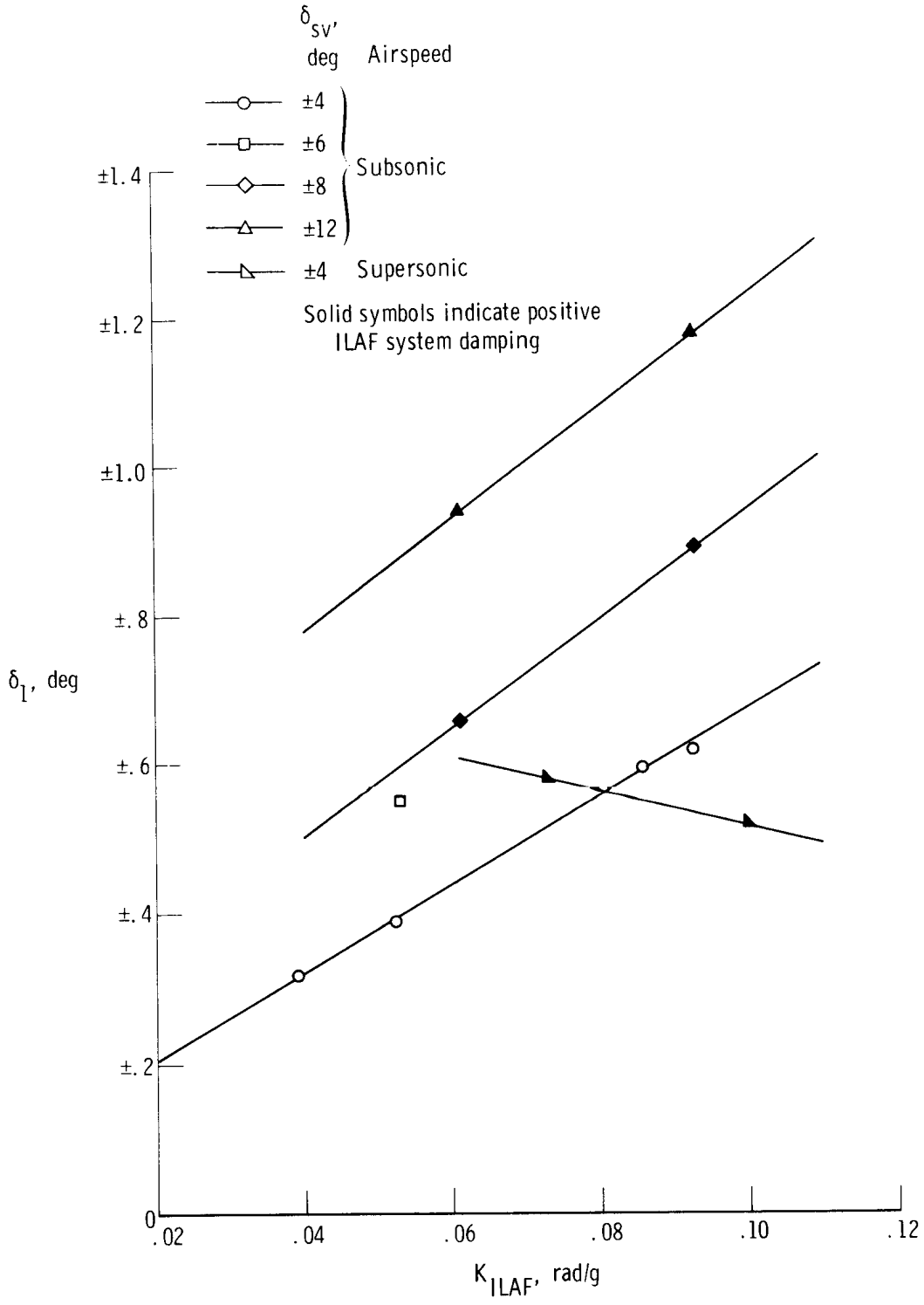

Figure 20. Inboard elevon motion measured at peak vehicle response as a function of ILAF system gain. First mode only.

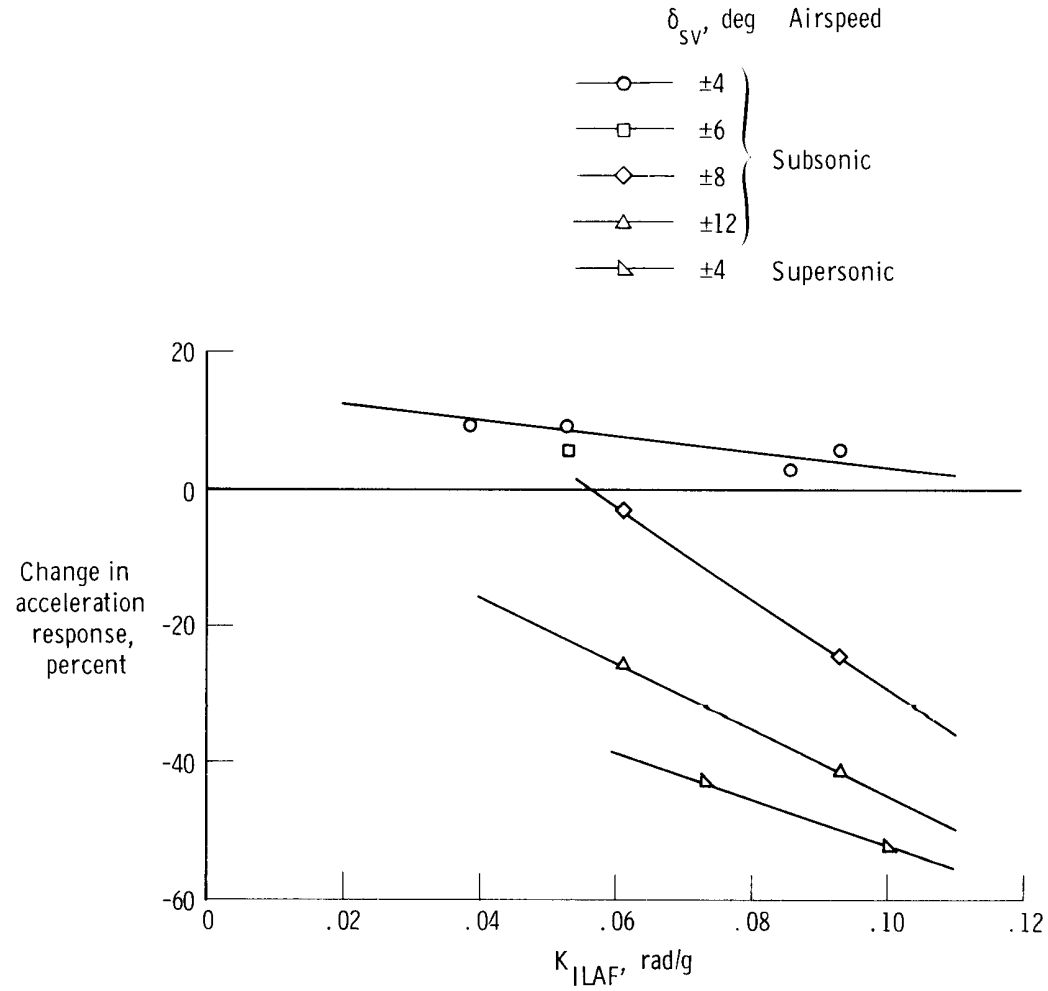

Figure 21. Percentage of change in vehicle acceleration with the ILAF system engaged for the first structural mode as a function of ILAF system gain.

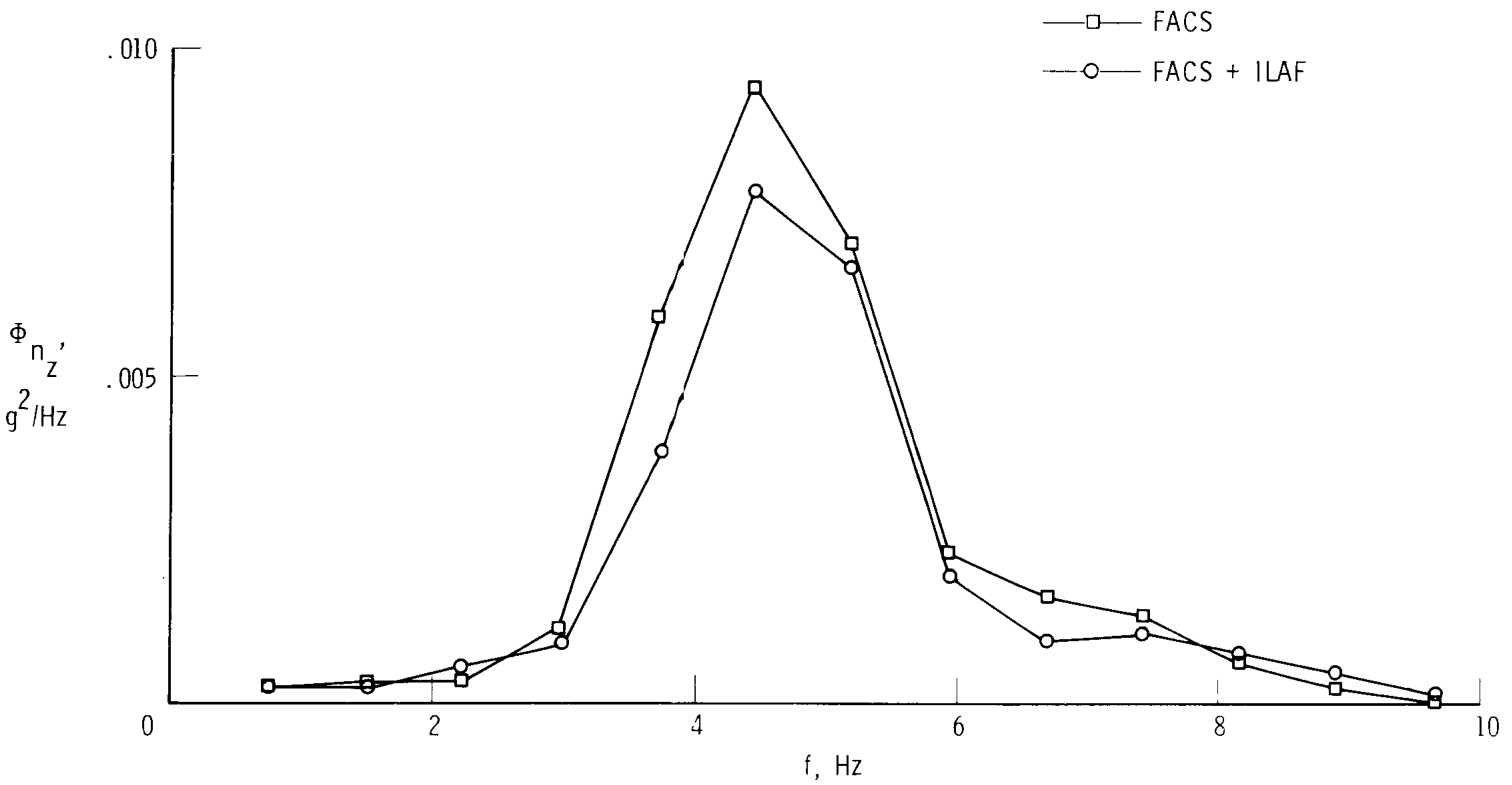

Figure 22. Power spectral density of flight-measured vertical acceleration response at the pilot's station during a turbulence encounter with and without the ILAF system engaged. M = 1.20; h_p = 9754 m (32,000 ft); $\delta_t = 65°$; σ_{ω_g} = 0.30 m/sec (1 ft/sec).

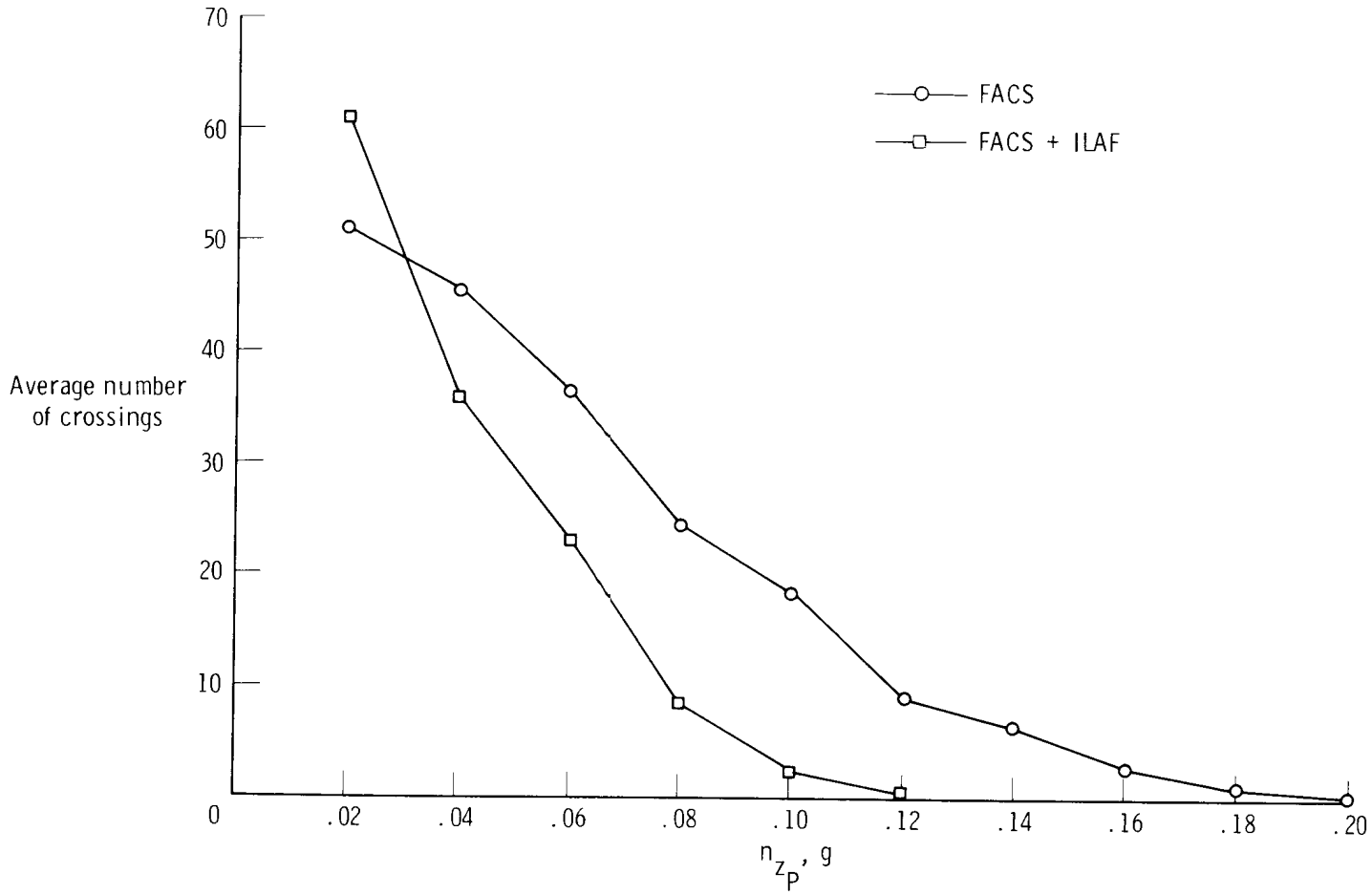

Figure 23. Average number of zero crossings as a function of the flight-measured vertical acceleration response at the pilot's station during a turbulence encounter with and without the ILAF system engaged. M = 1.20; h_p = 9754 m (32,000 ft); δ_t = 65°.

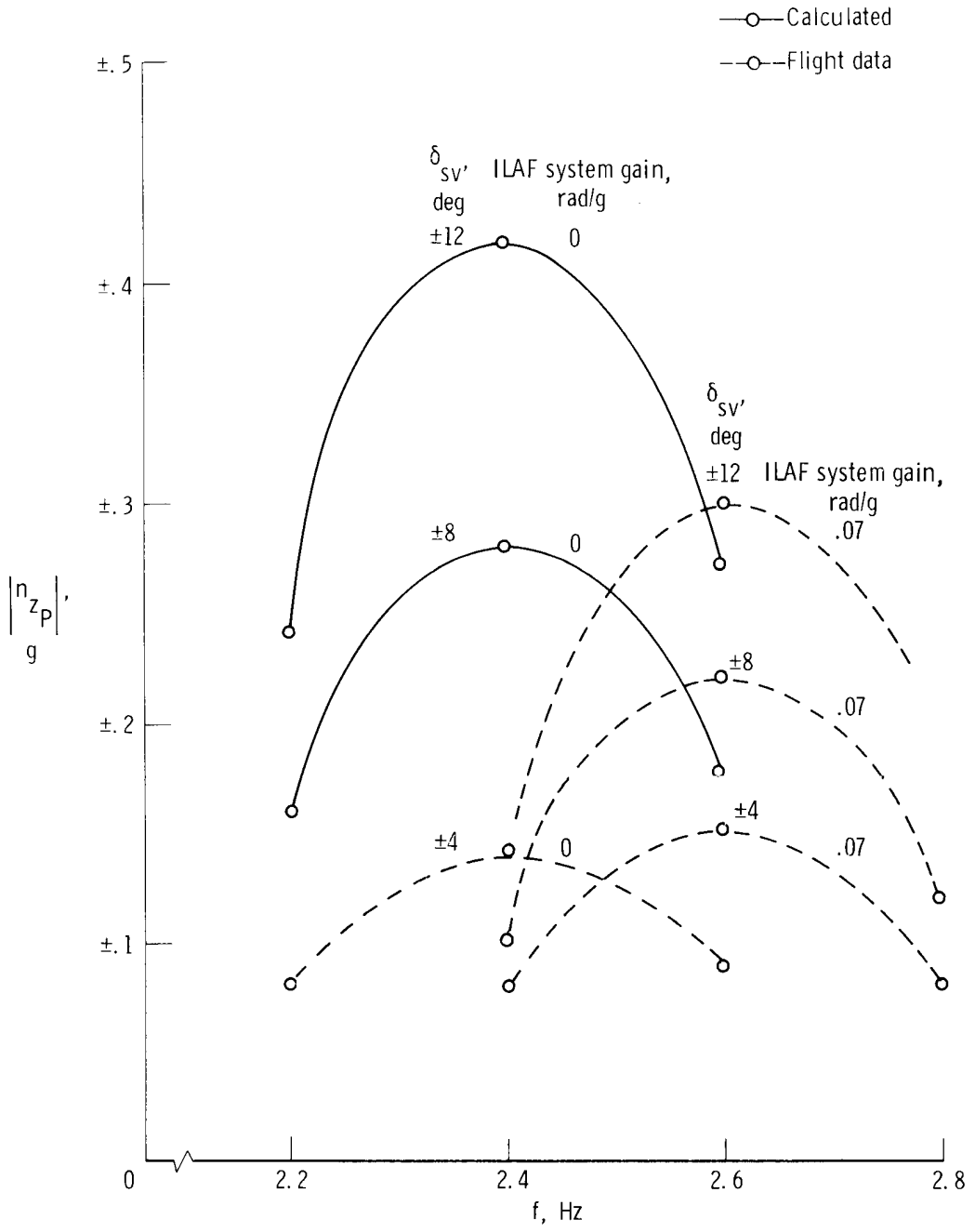

Figure 24. Effects of the nonlinear characteristics of the ILAF system on system performance. First mode; lightweight, M = 0.86; h_p = 7620 m (25,000 ft); $\delta_t = 25°$.

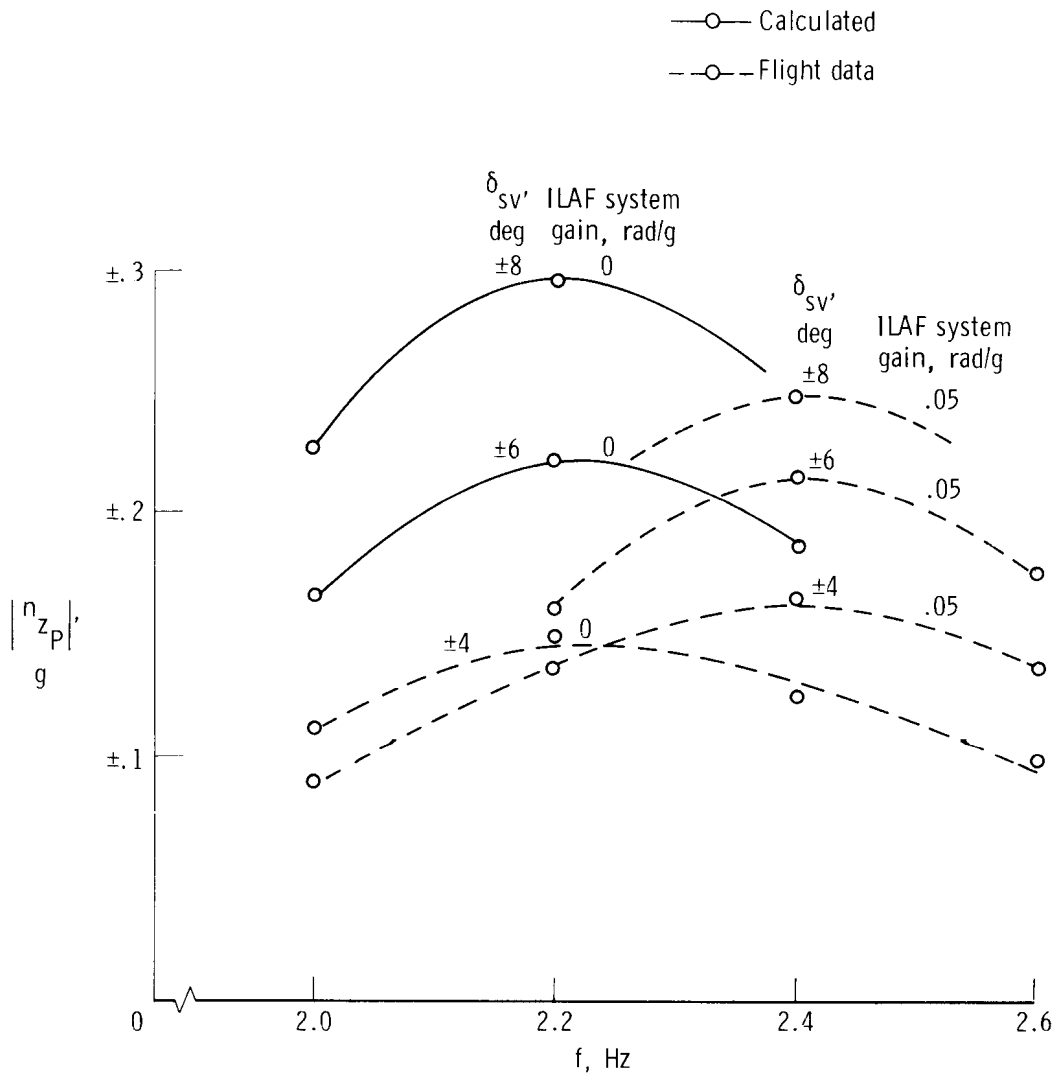

Figure 25. Effects of the nonlinear characteristics of the ILAF system on system performance. First mode; heavyweight, M = 0.87; h_p = 7620 m (25,000 ft); $\delta_t = 25°$.

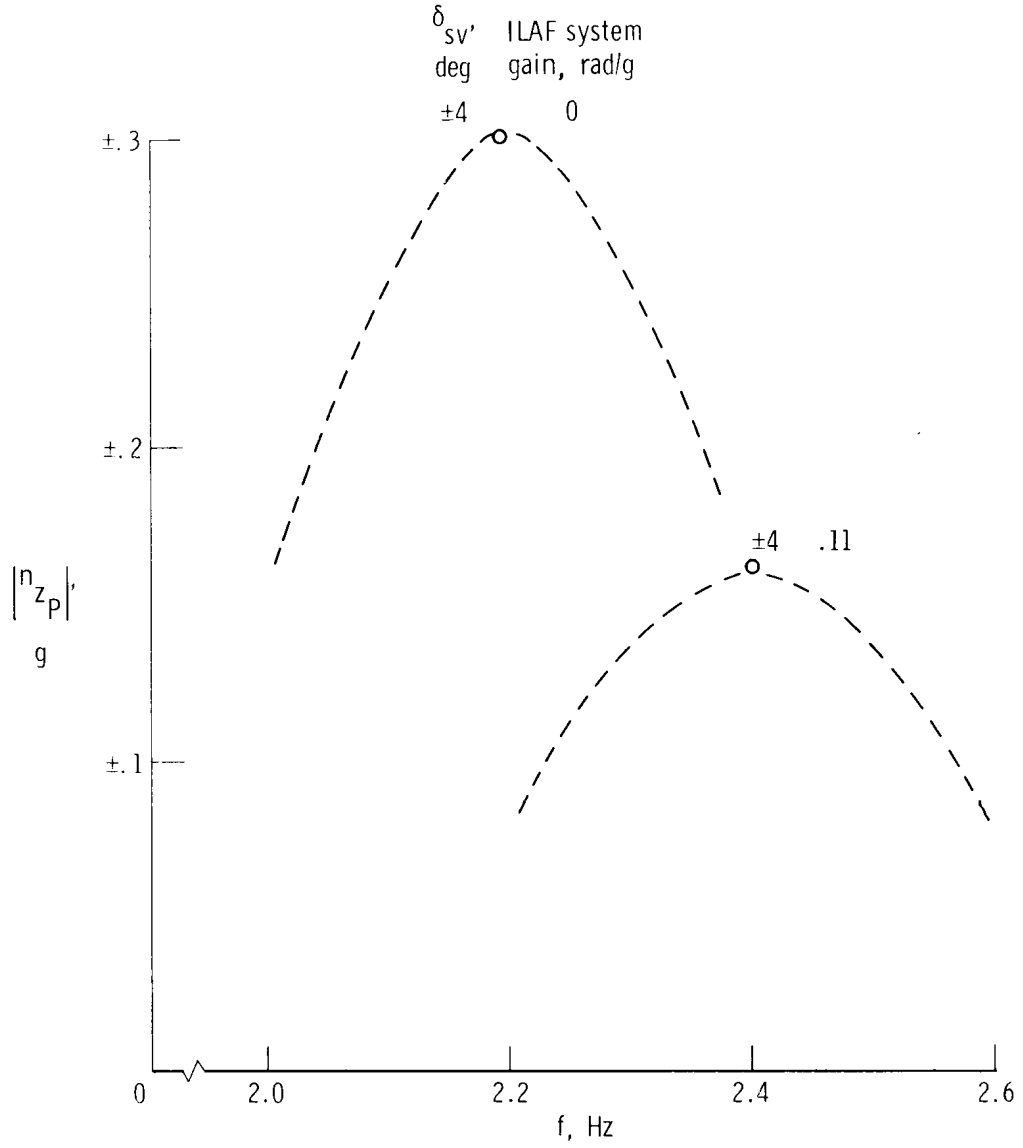

Figure 26. Effects of the nonlinear characteristics of the ILAF system on system performance. First mode; flight-test data; mediumweight, M = 1.59; h_p = 11,918 m (39,100 ft); δ_t = 65°.

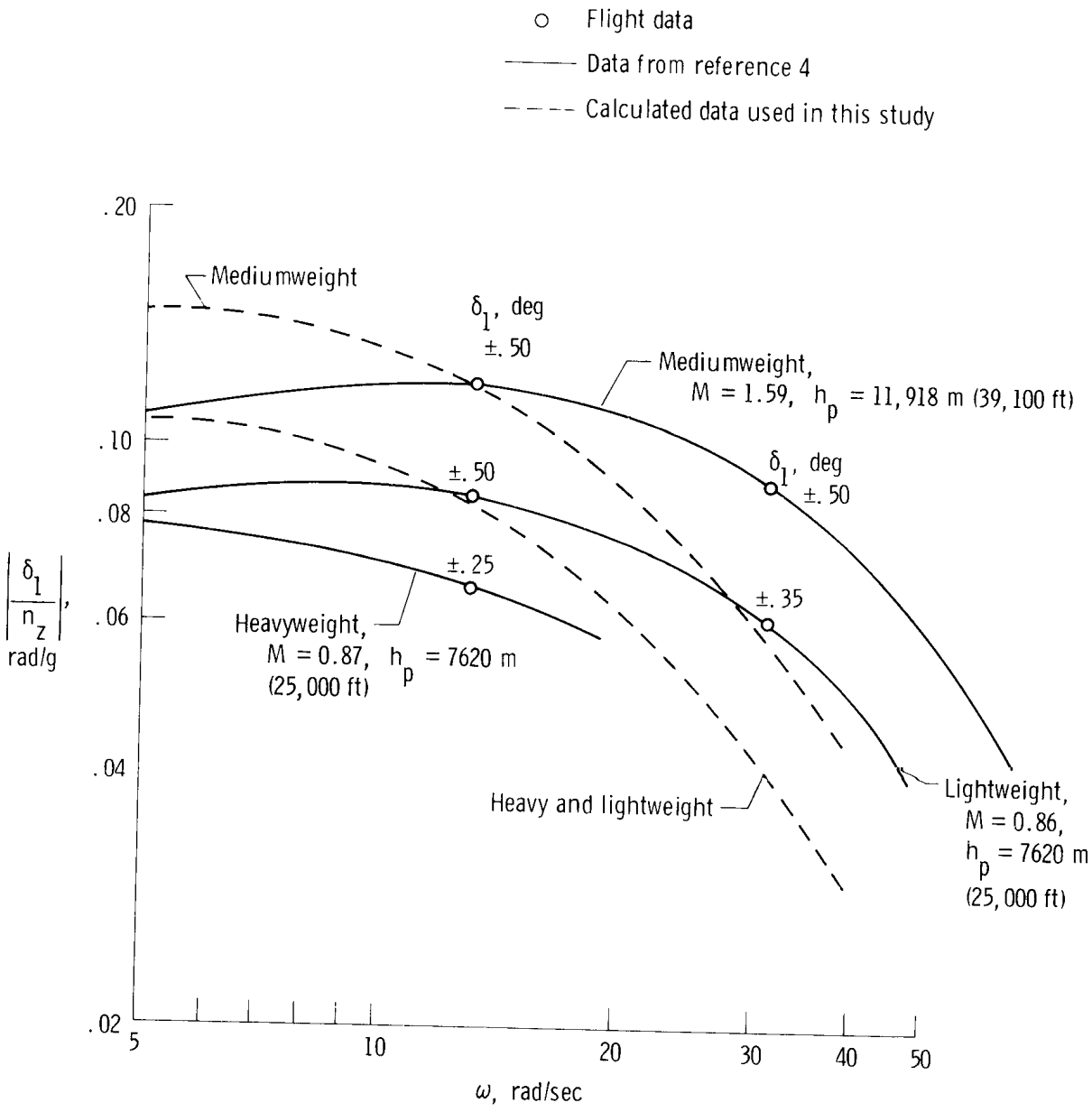

(a) Amplitude.

Figure 27. Frequency response from the blended ILAF system accelerometer input through the inboard elevon output.

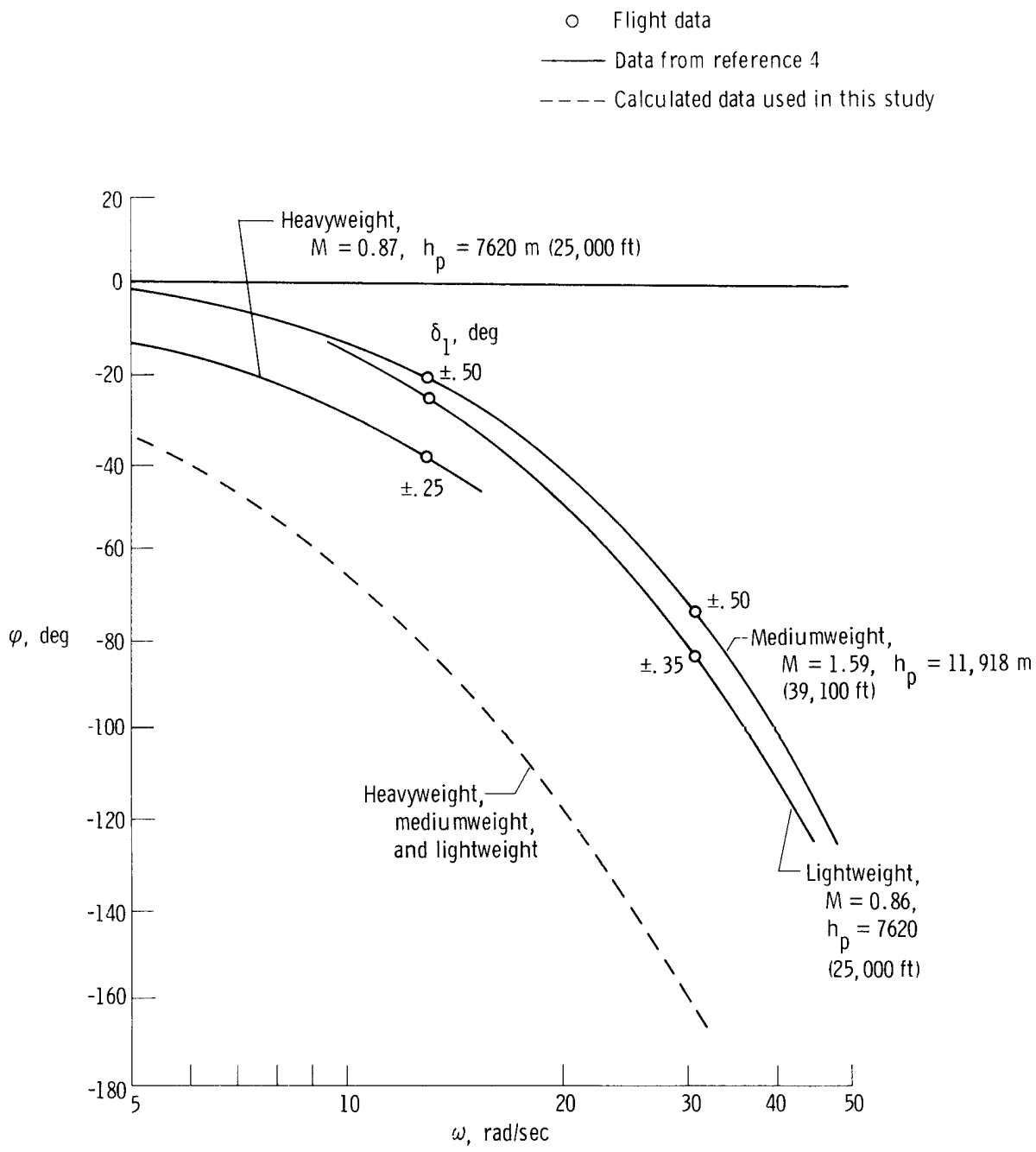

(b) Phase angle.

Figure 27. Concluded.

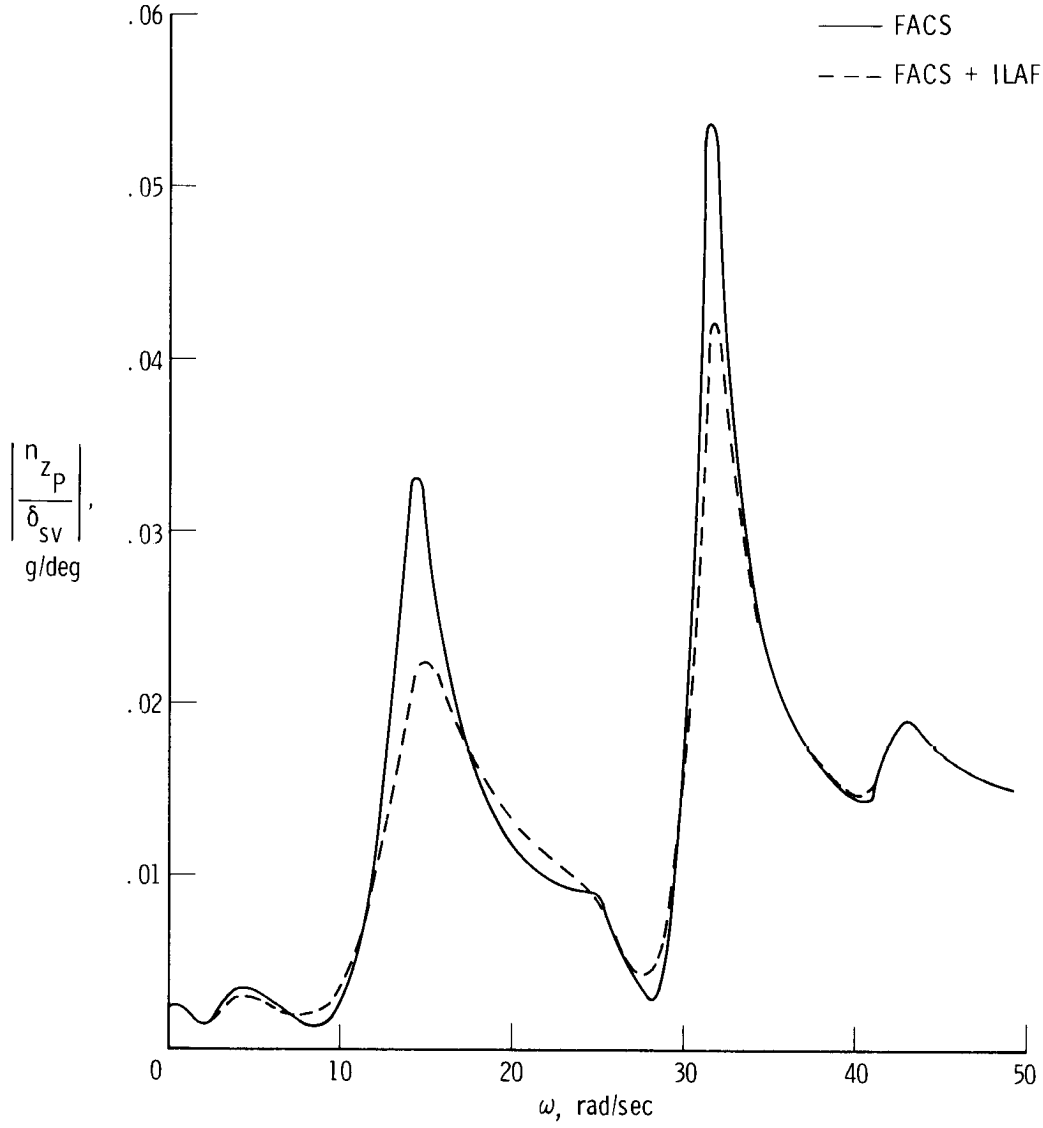

Figure 28. Calculated vertical acceleration response at the pilot's station due to shaker-vane input. Heavyweight, M = 0.87; h_p = 7620 m (25,000 ft); $\delta_t = 25°$.

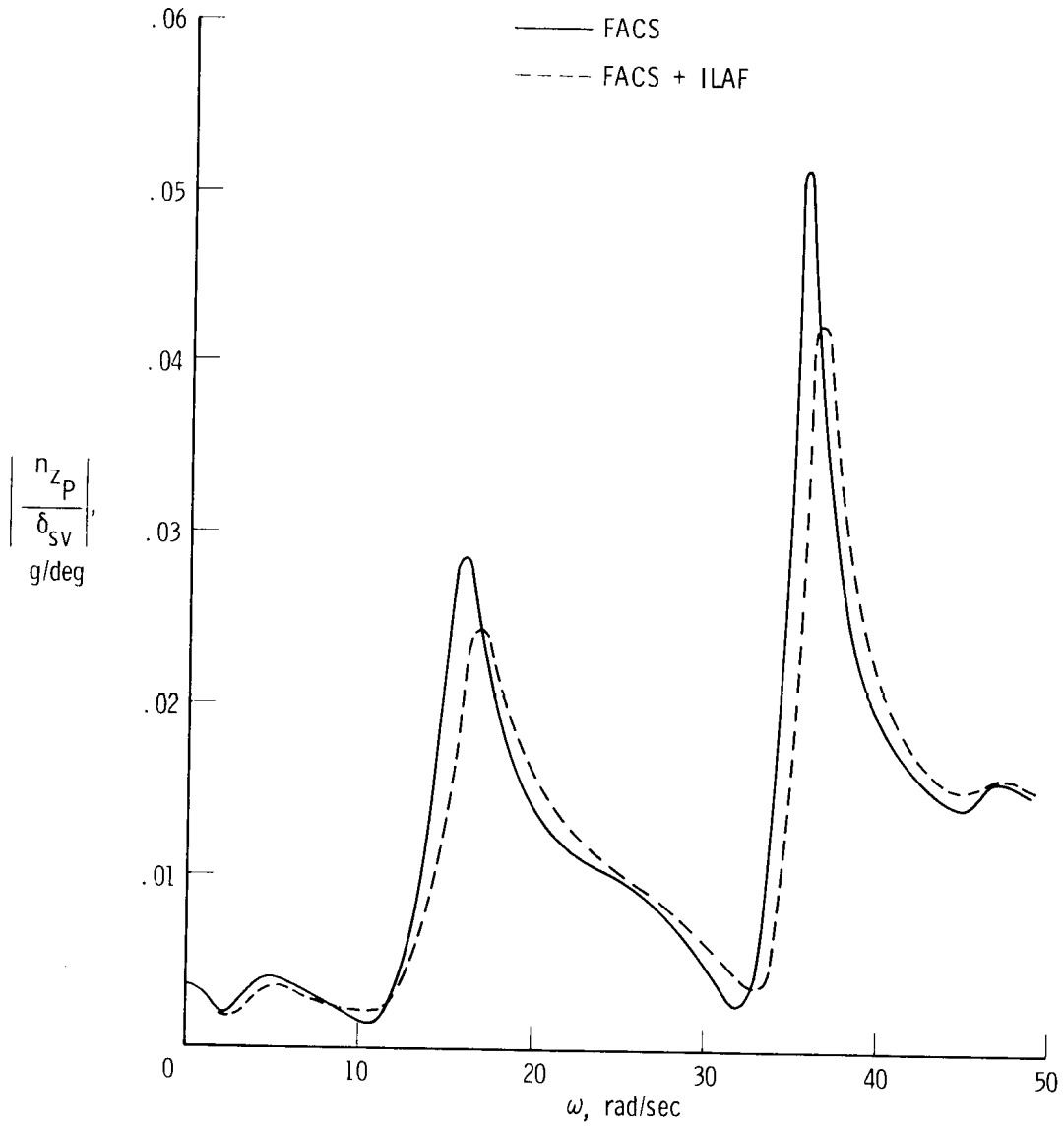

Figure 29. Calculated vertical acceleration response at the pilot's station due to shaker-vane input. Lightweight, M = 0.86; h_p = 7620 m (25,000 ft); $\delta_t = 25°$.

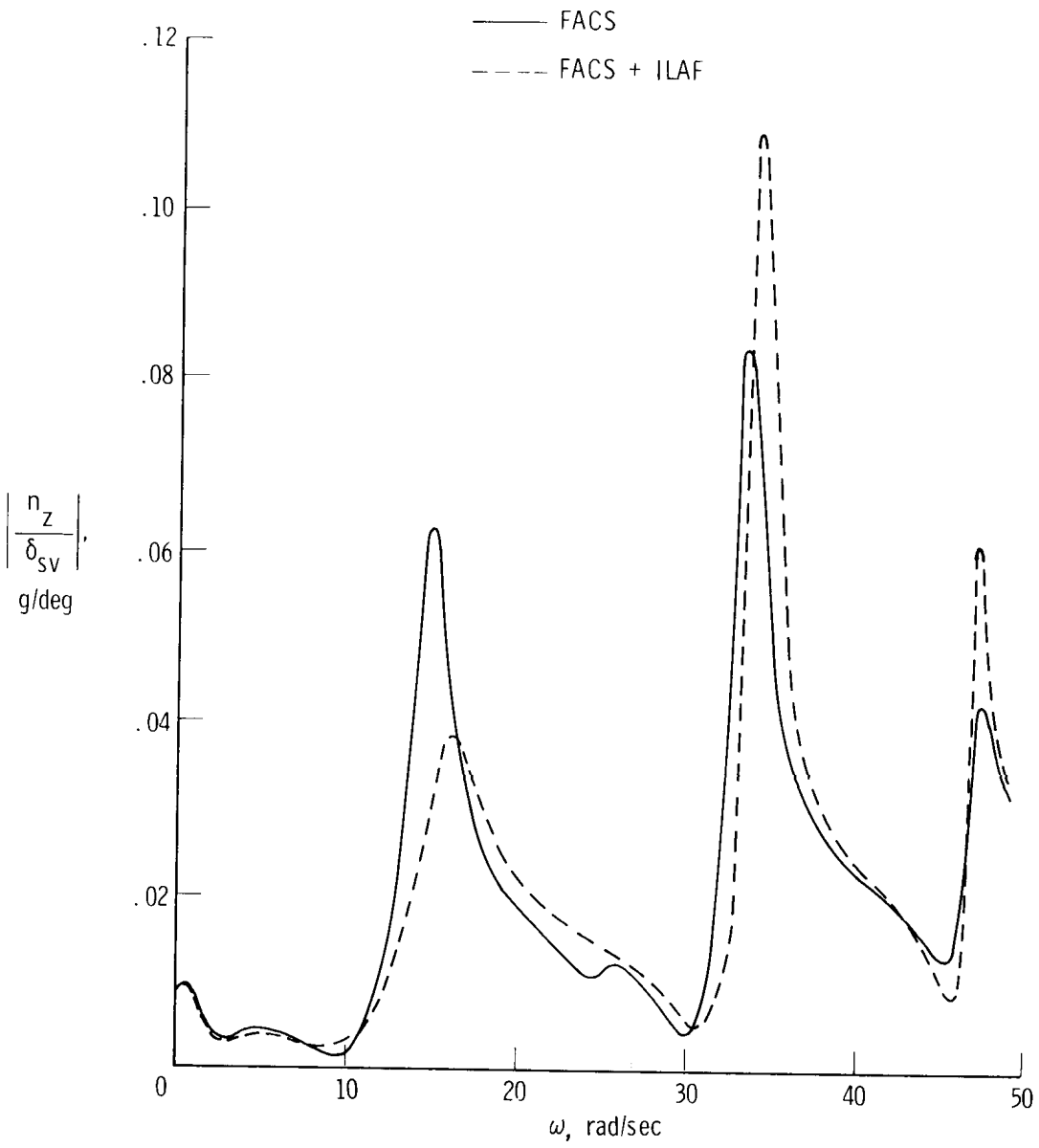

Figure 30. Calculated vertical acceleration response at the pilot's station due to shaker-vane input. Mediumweight, M = 1.59; h_p = 11,918 m (39,100 ft); $\delta_t = 65°$.

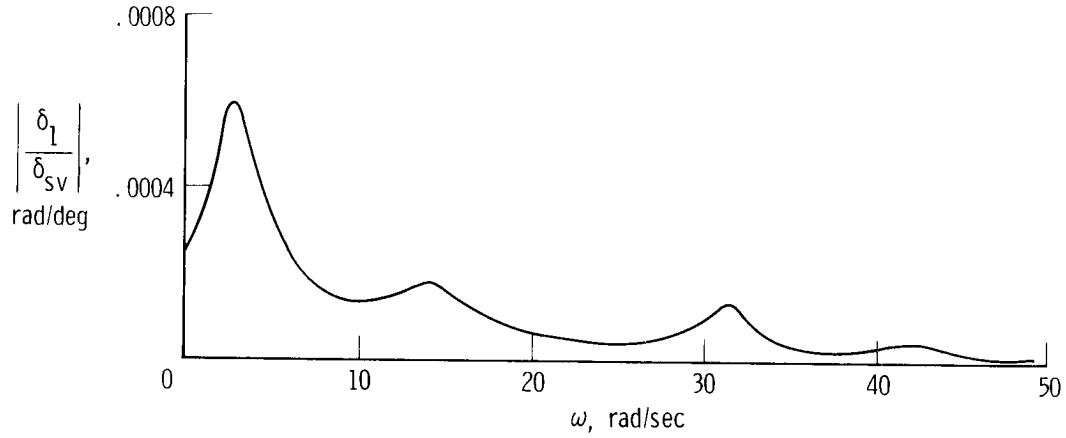

(a) Inboard elevon, FACS.

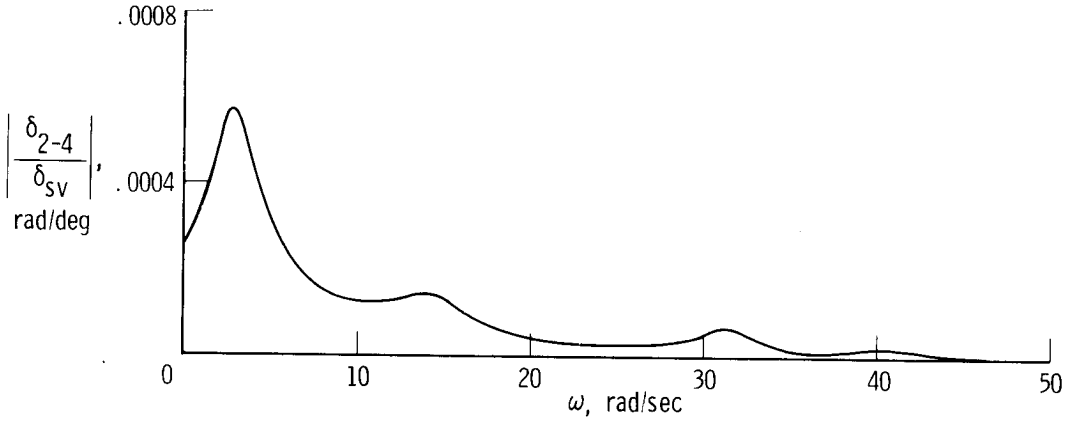

(b) Outboard elevons, FACS.

Figure 31. Calculated elevon deflection due to shaker-vane input with FACS or FACS + ILAF operating. Heavyweight, M = 0.87; h_p = 7620 m (25,000 ft); $\delta_t = 25°$.

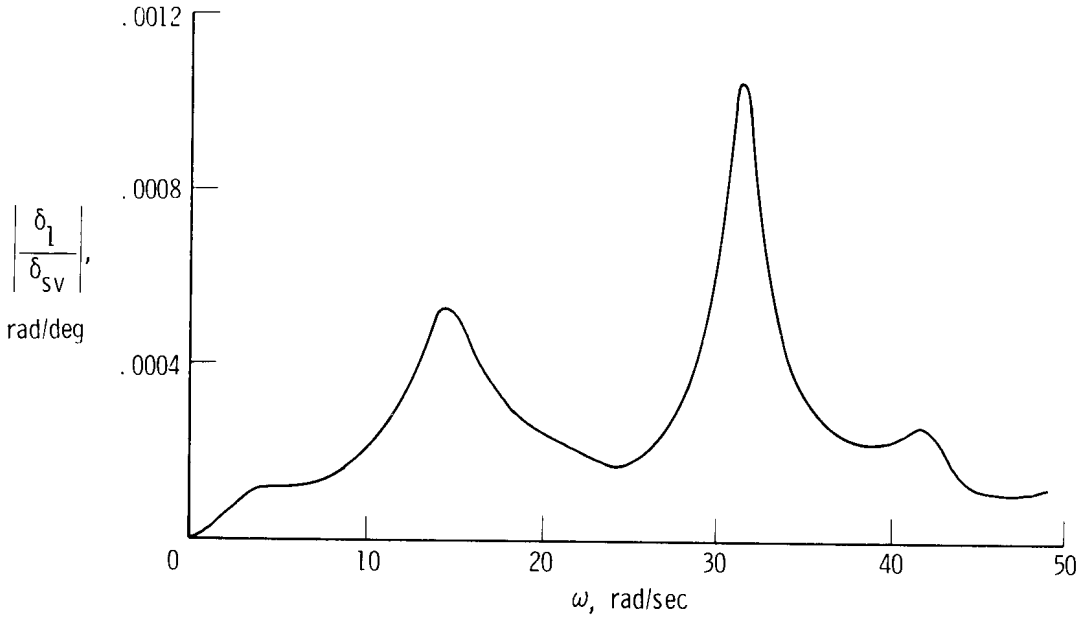

(c) Inboard elevon, FACS + ILAF.

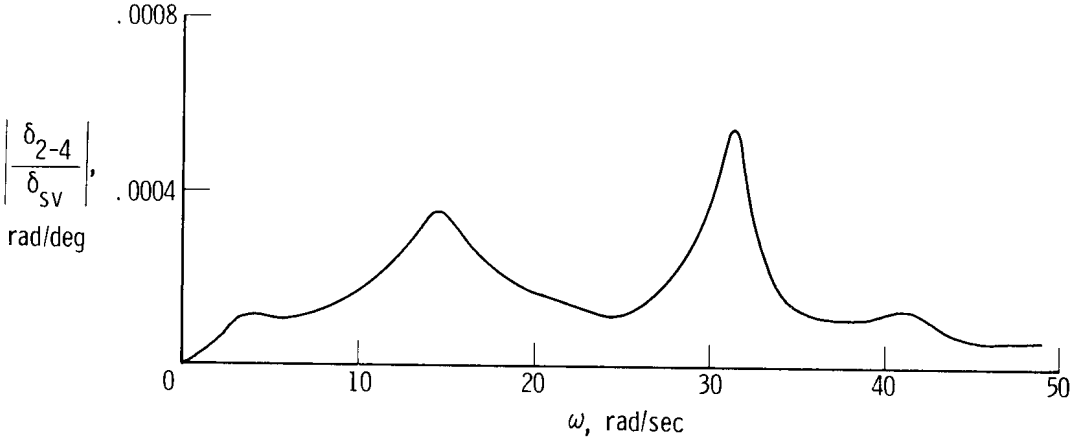

(d) Outboard elevons, FACS + ILAF.

Figure 31. Concluded.

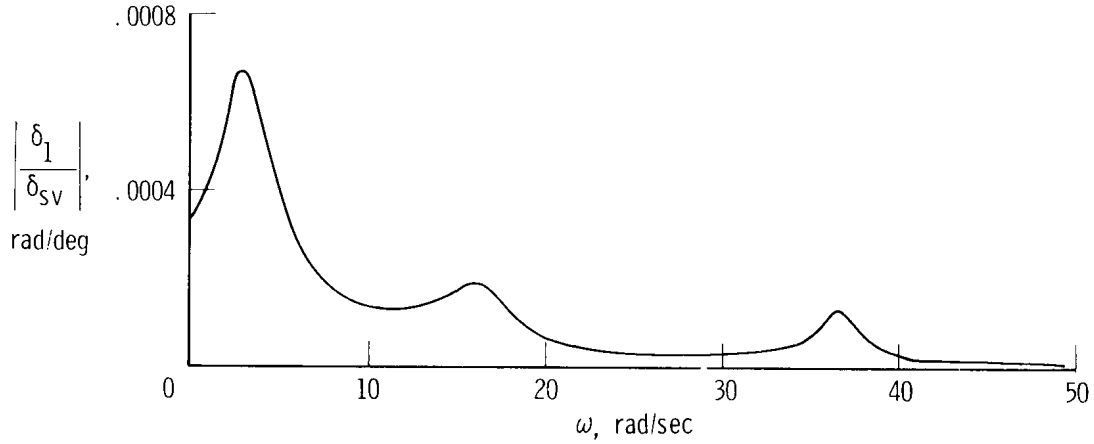

(a) Inboard elevon, FACS.

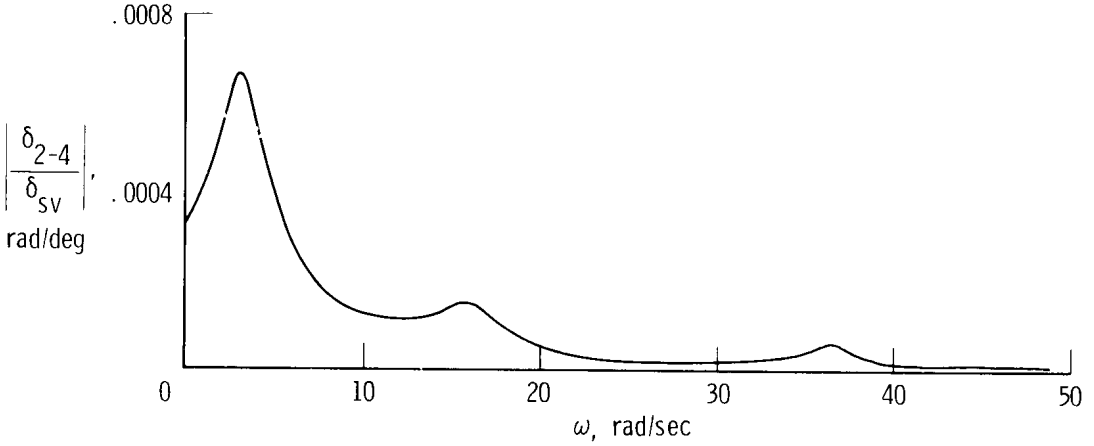

(b) Outboard elevons, FACS.

Figure 32. Calculated elevon deflection due to shaker-vane input with FACS or FACS + ILAF operating. Lightweight, M = 0.86; h_p = 7620 m (25,000 ft); $\delta_t = 25°$.

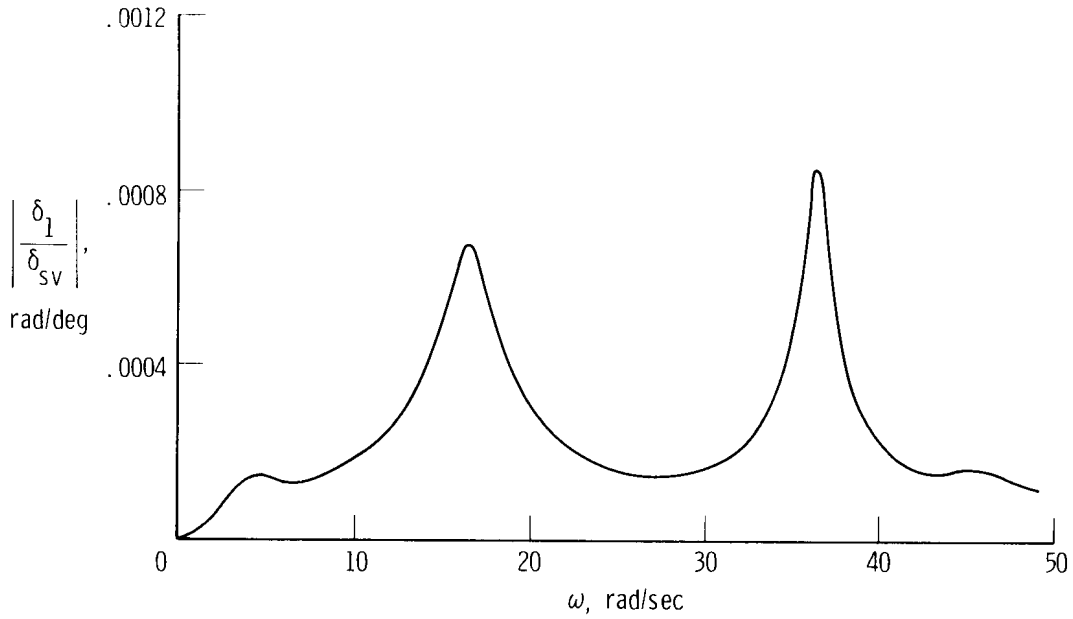

(c) Inboard elevon, FACS + ILAF.

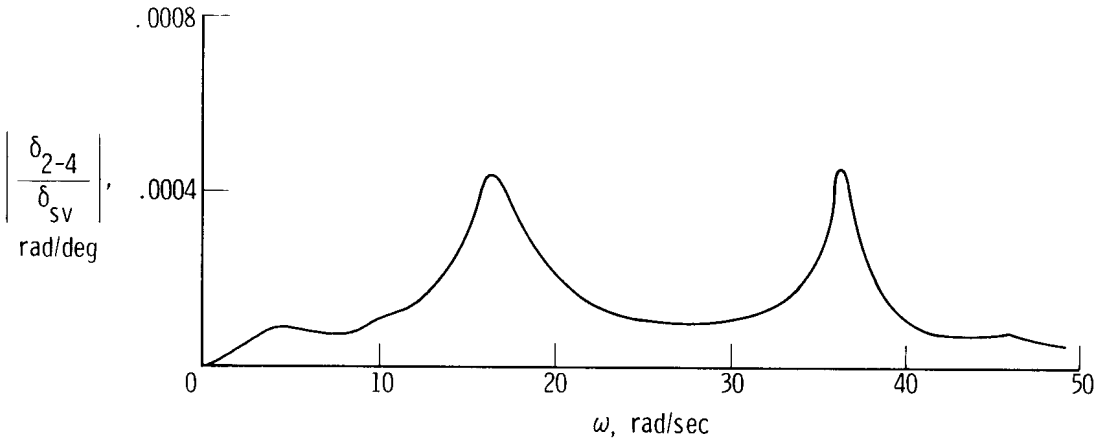

(d) Outboard elevons, FACS + ILAF.

Figure 32. Concluded.

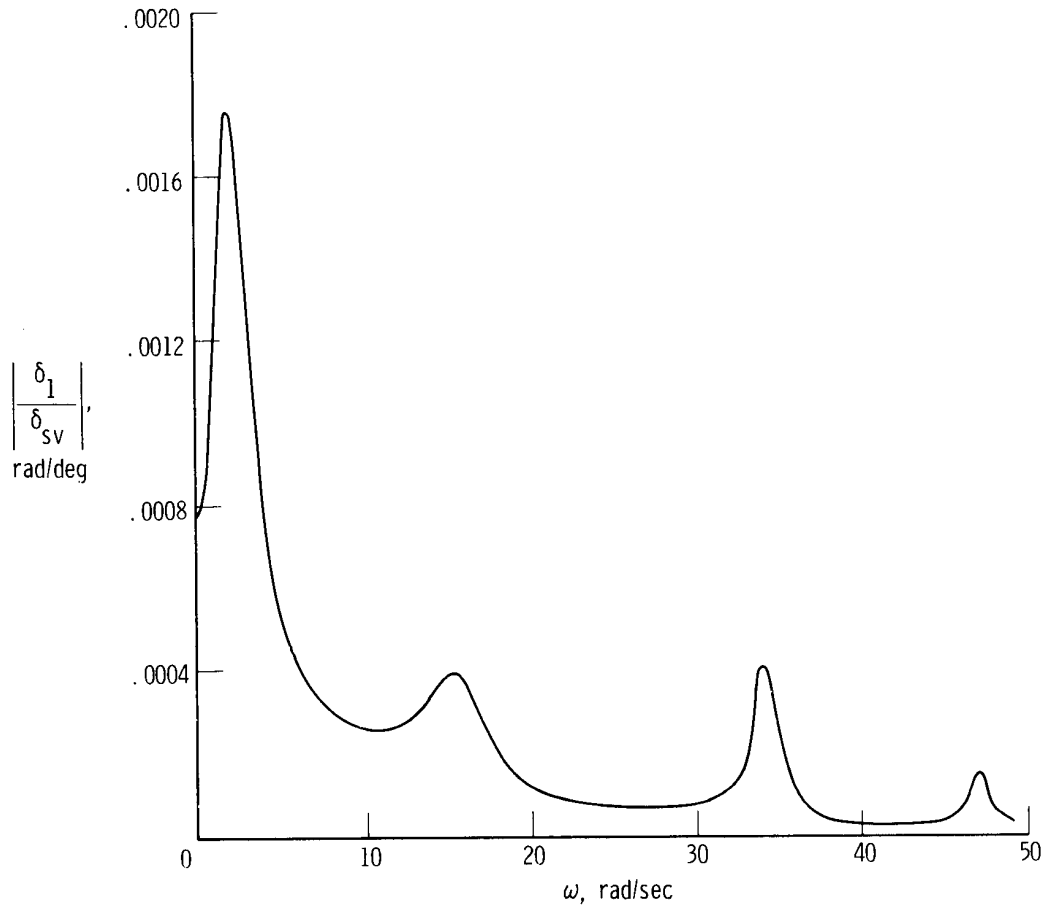

(a) Inboard elevon, FACS.

Figure 33. Calculated elevon deflection due to shaker-vane input with FACS or FACS + ILAF operating. Mediumweight, M = 1.59; h_p = 11,918 m (39,100 ft); $\delta_t = 65°$.

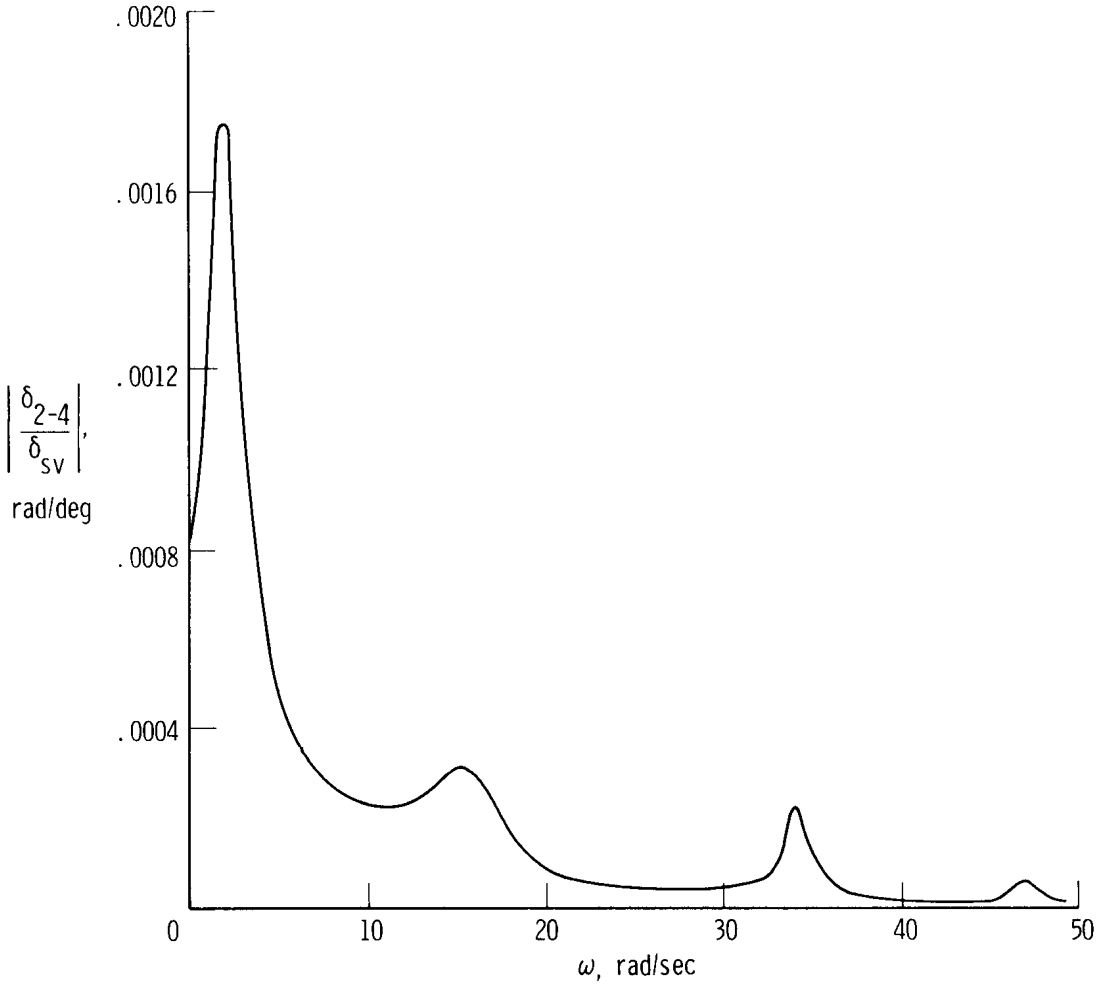

(b) Outboard elevons, FACS.

Figure 33. Continued.

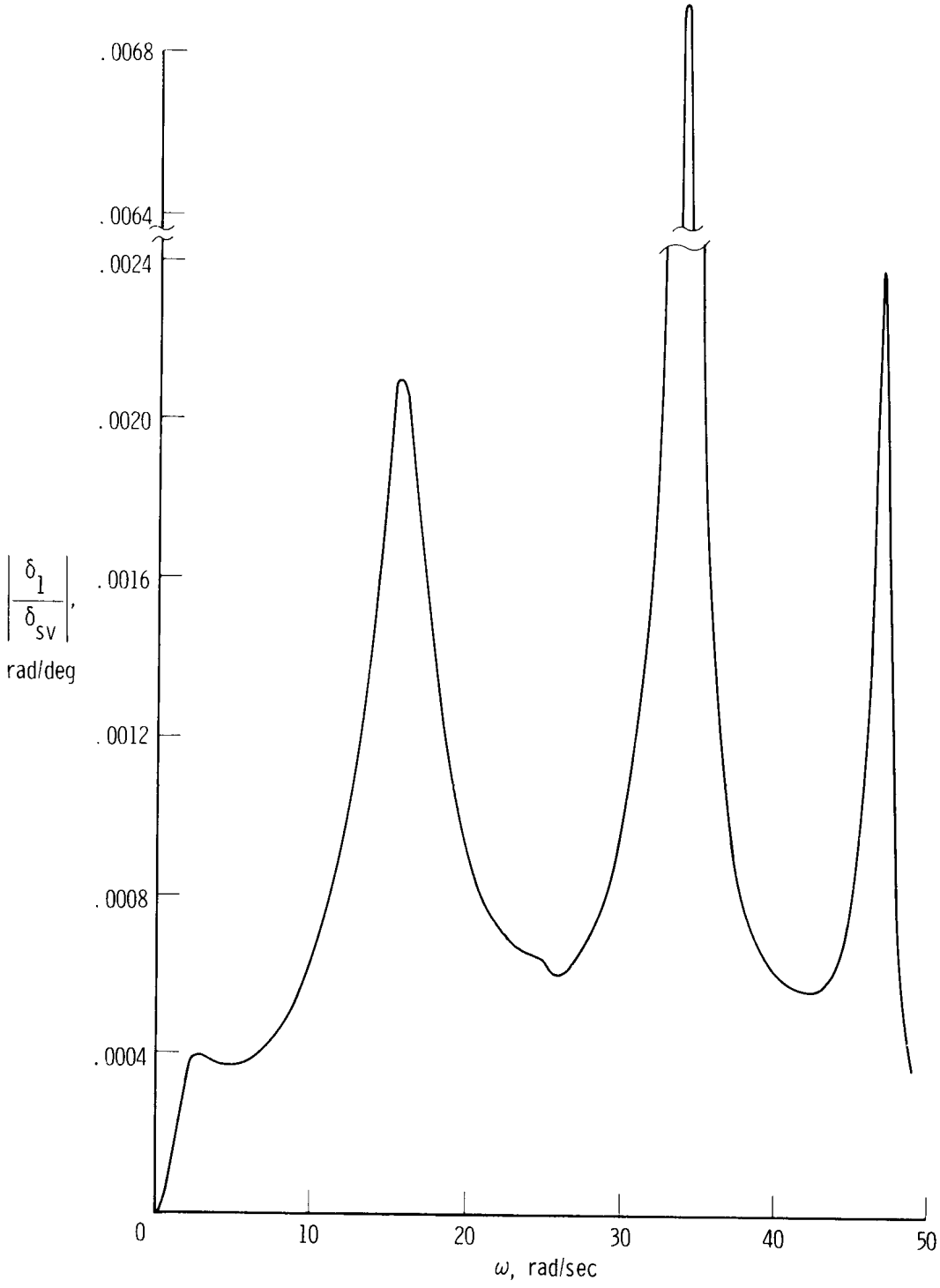

(c) Inboard elevon, FACS + ILAF.

Figure 33. Continued.

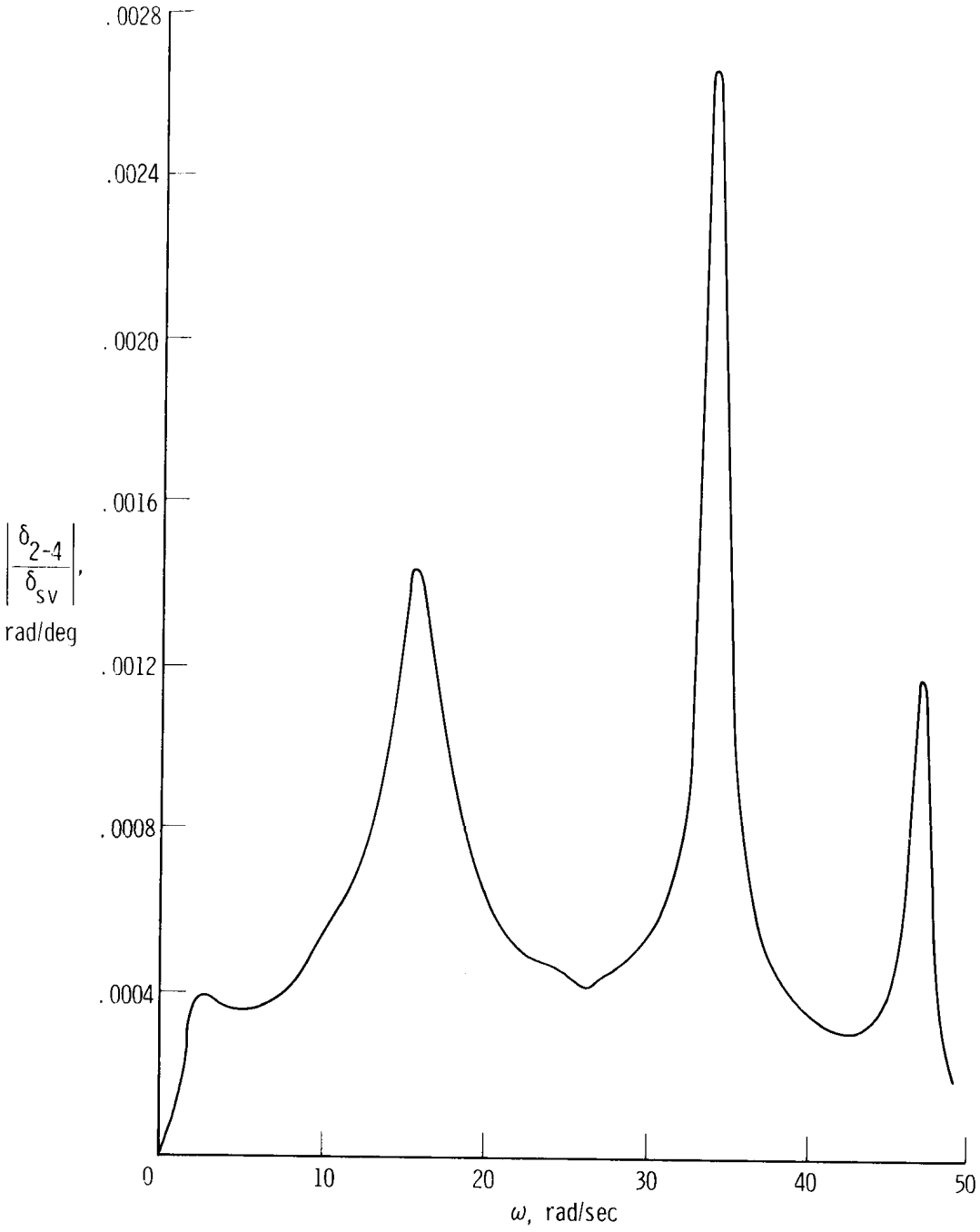

(d) Outboard elevons, FACS + ILAF.

Figure 33. Concluded.

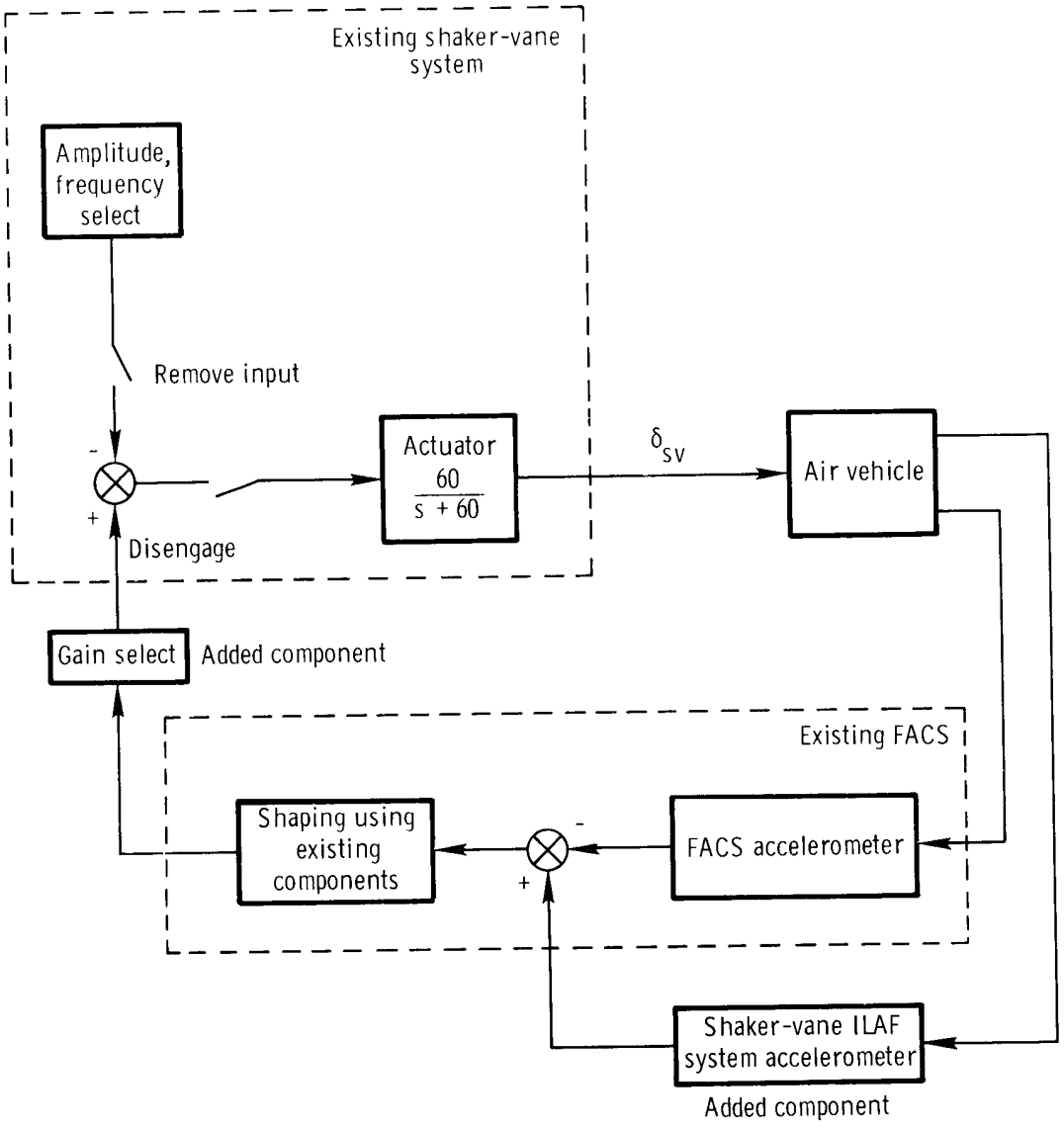

Figure 34. Block diagram showing modification of existing shaker-vane and FACS equipment required to perform structural mode control function.

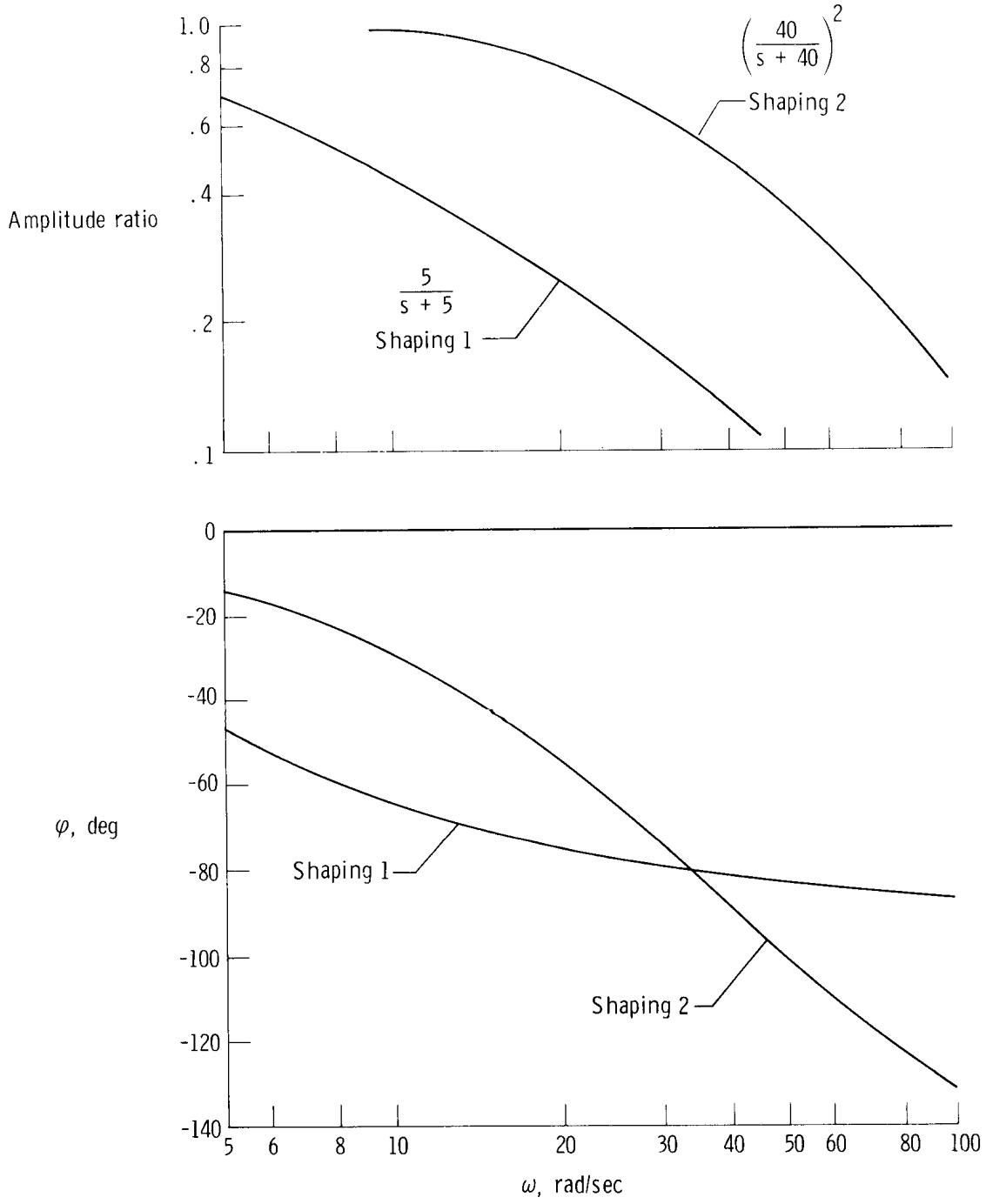

Figure 35. Shaker-vane ILAF system shaping networks. Analytical data.

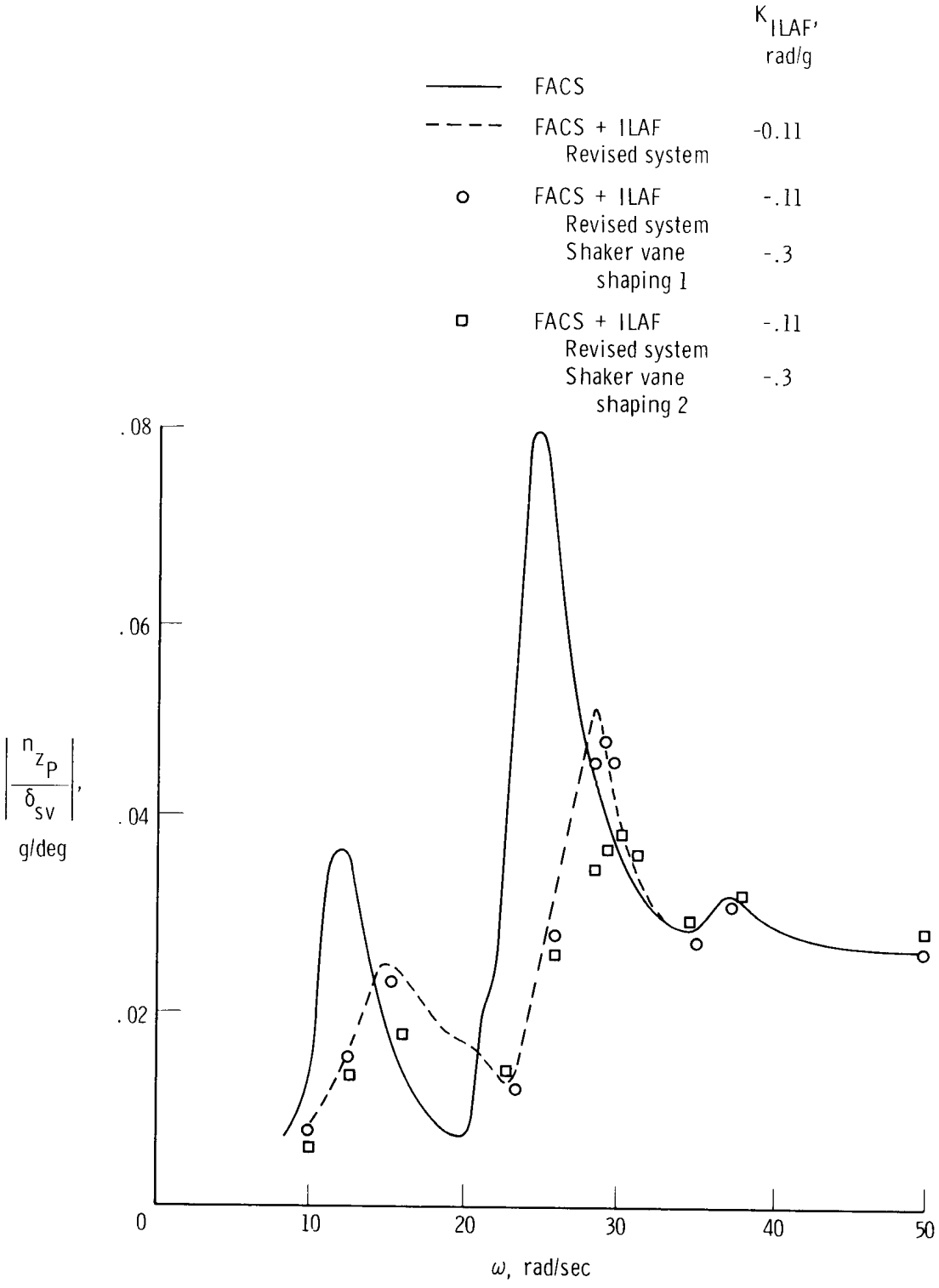

(a) Mediumweight, M = 1.59, h_p = 11,918 m (39,100 ft), δ_t = 65°.

Figure 36. Performance of shaker-vane ILAF system. Shaker-vane excitation based on analytical data.

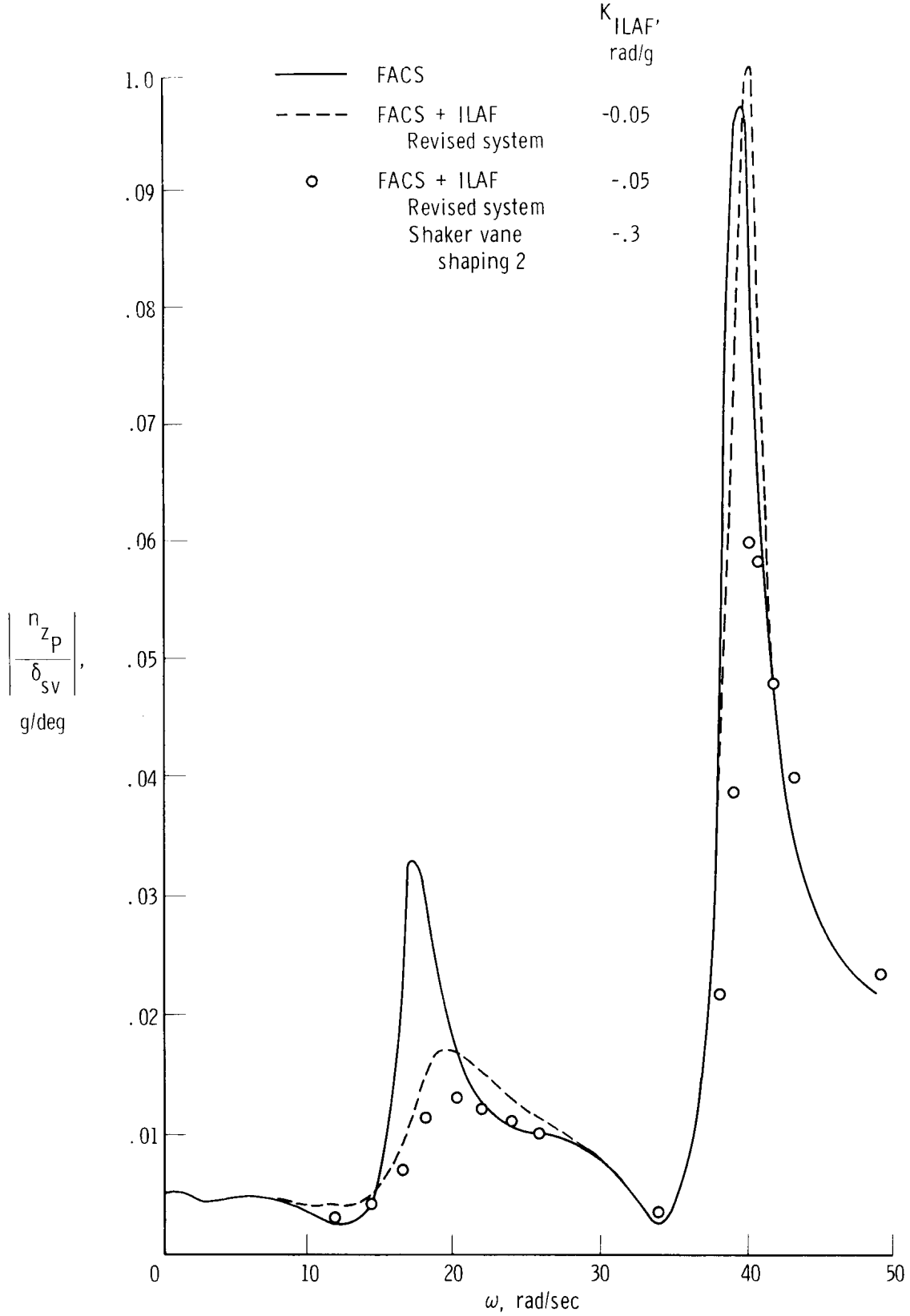

(b) Lightweight, M = 0.86, h_p = 7620 m (25,000 ft), δ_t = 25°.

Figure 36. Concluded.

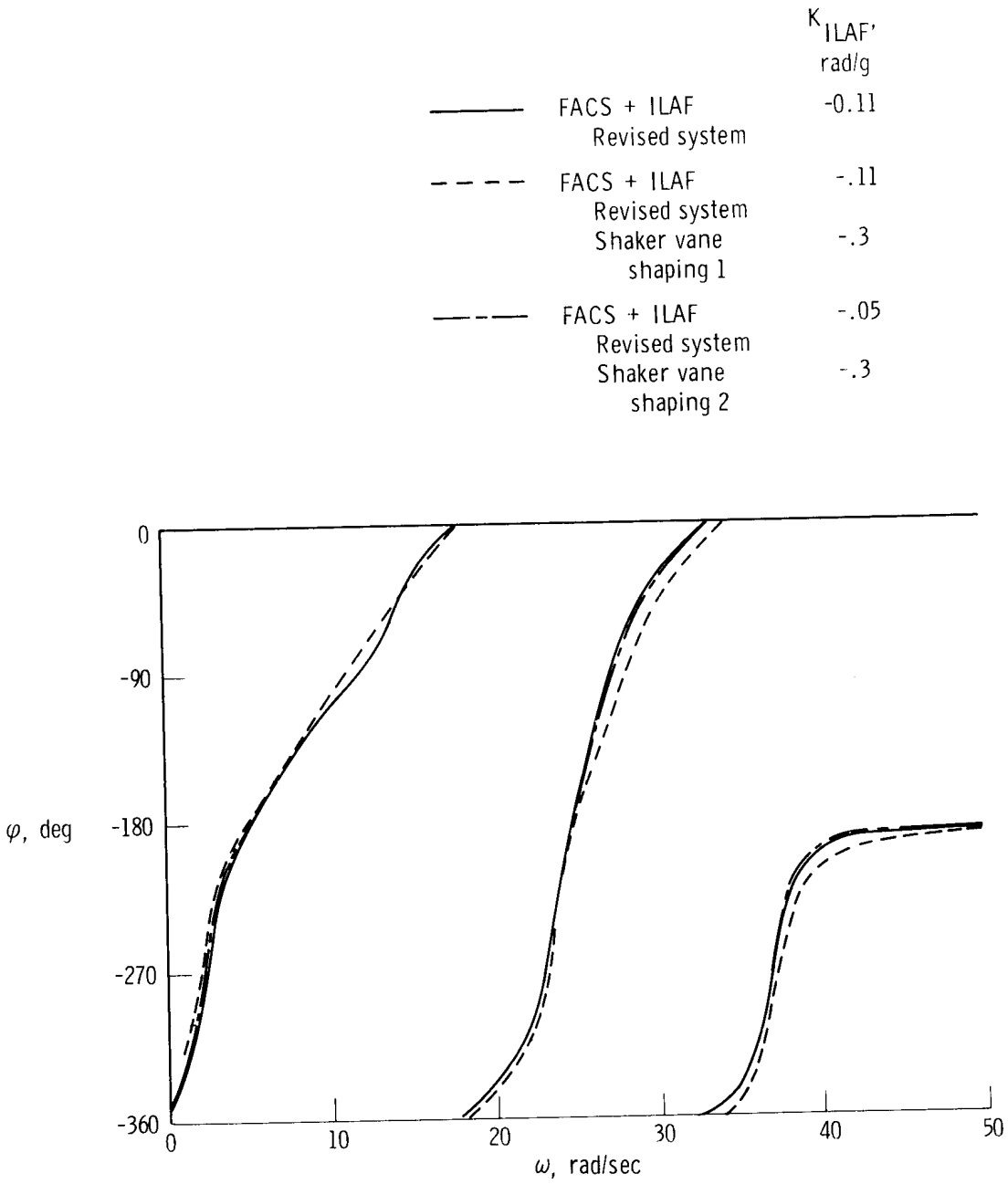

(a) Mediumweight, M = 1.59, h_p = 11,918 m (39,100 ft), $\delta_t = 65°$.

Figure 37. Control system stability analysis, characteristic determinant phase angle. Analytical data.

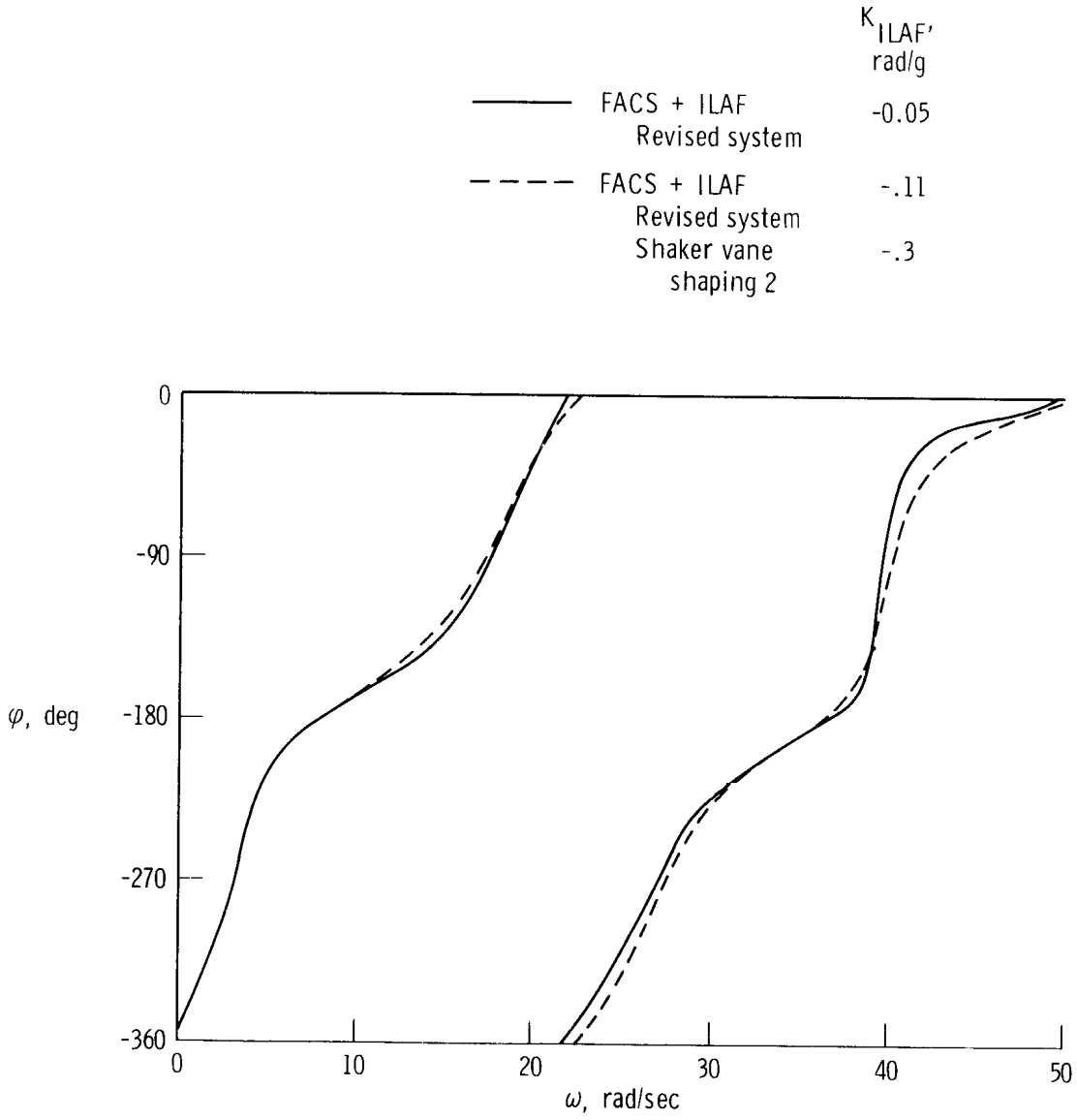

(b) Lightweight, M = 0.86, h_p = 7620 m (25,000 ft), δ_t = 25°.

Figure 37. Concluded.

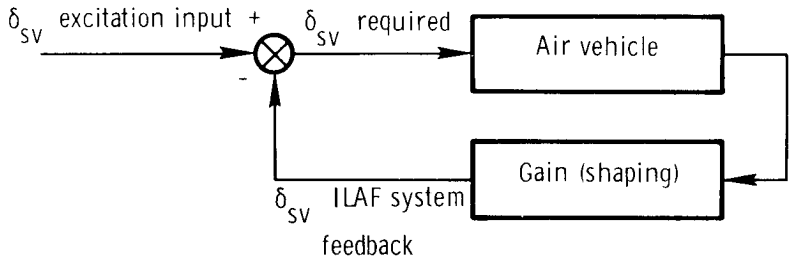

(a) Block diagram of shaker-vane system.

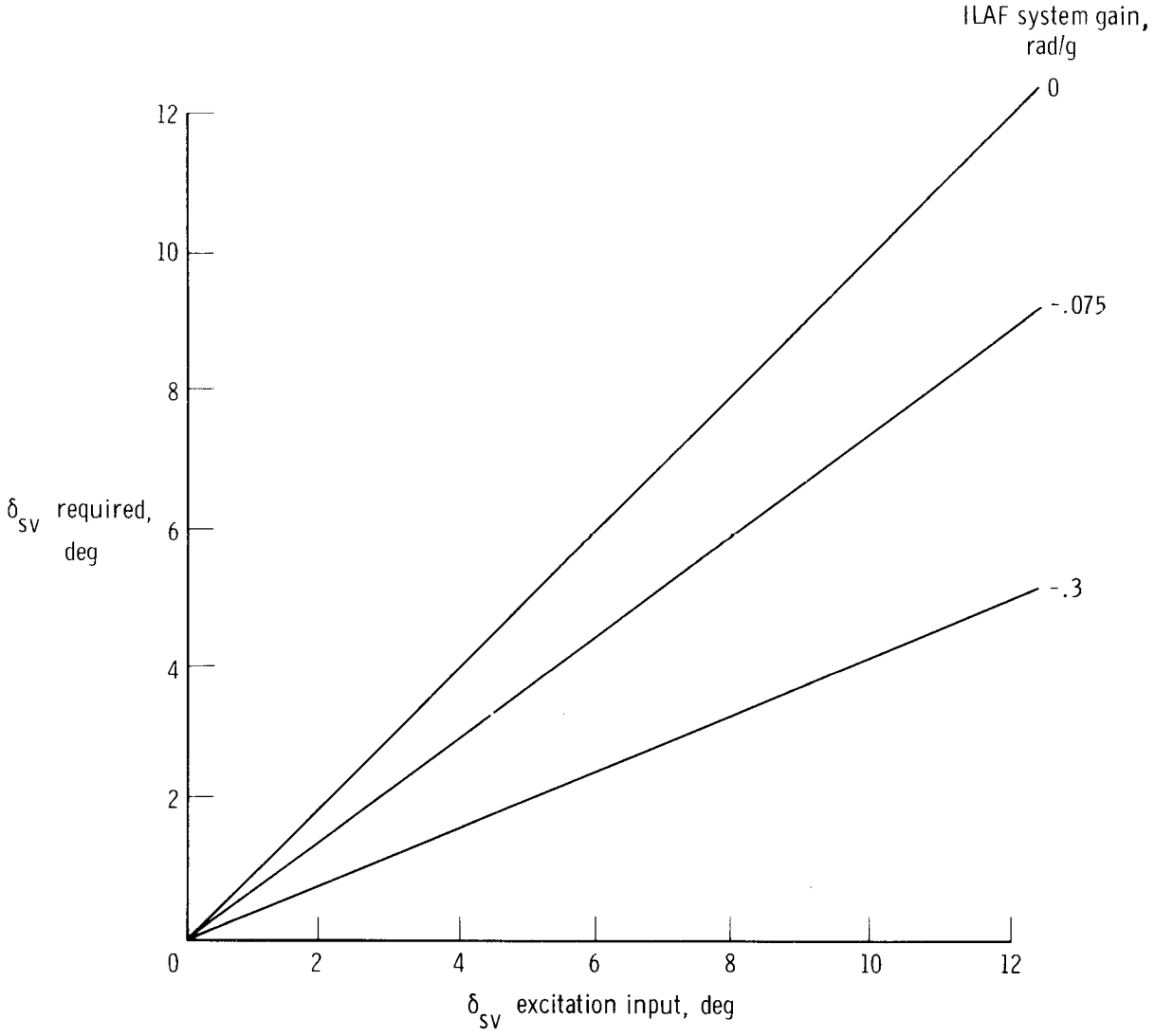

(b) Deflection requirements.

Figure 38. Shaker-vane deflection requirements operating both as an excitation source and a structural mode control.

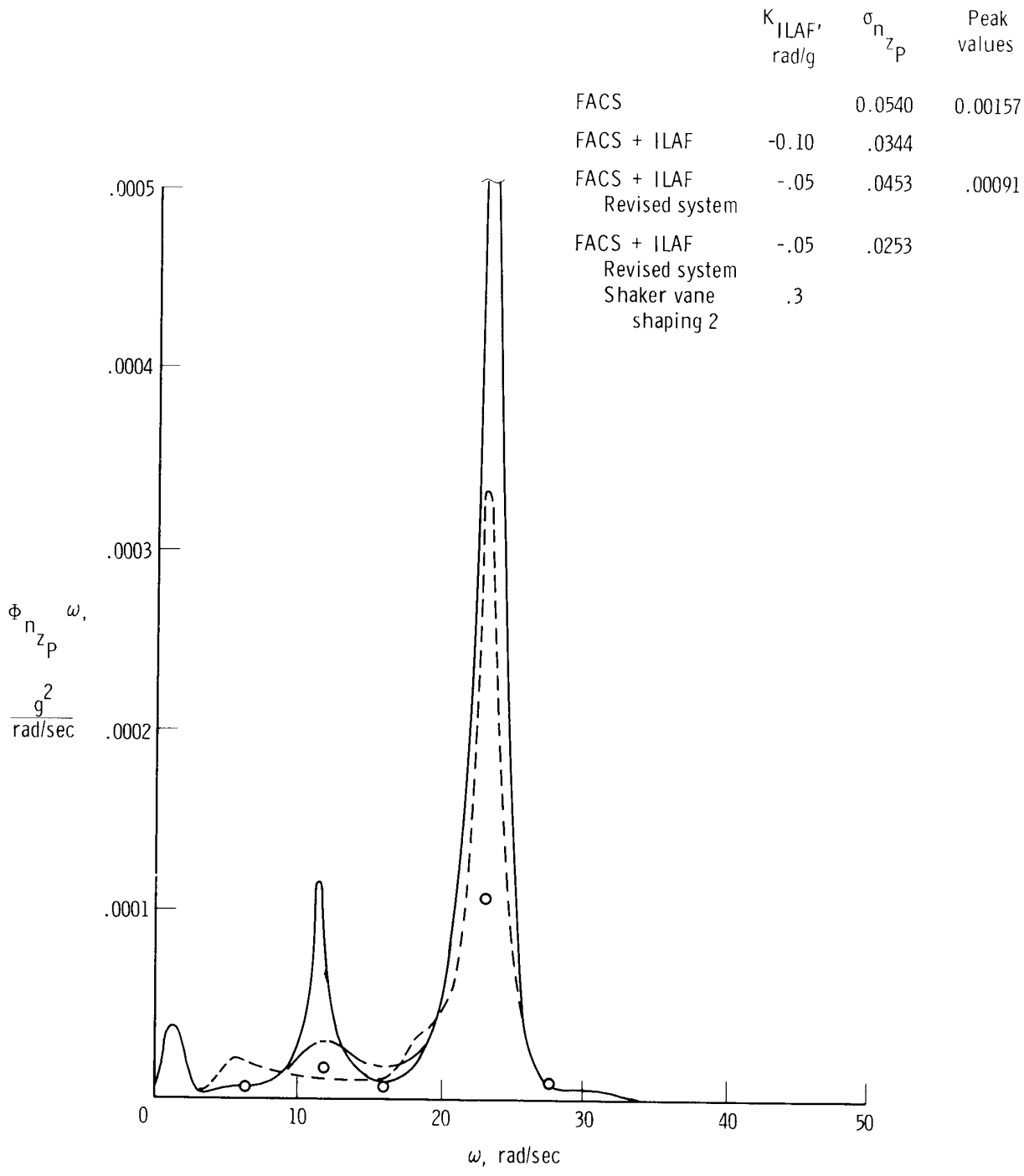

Figure 39. Performance of shaker-vane ILAF system. Gust excitation based on analytical data. Heavyweight, M = 0.87; h_p = 7620 m (25,000 ft); $\delta_t = 25°$; σ_{ω_g} = 1 ft/sec.

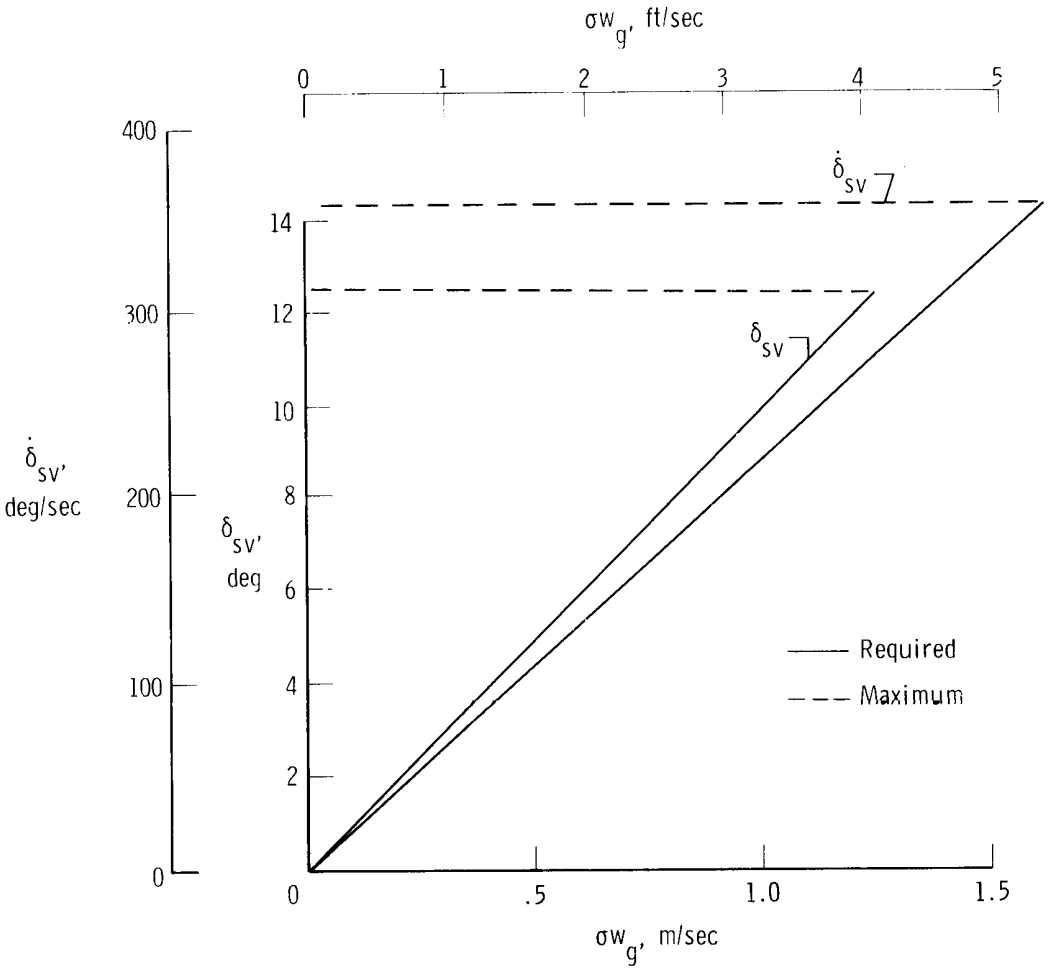

Figure 40. Shaker-vane ILAF system deflection and rate requirements as a function of gust intensity. Analytical data.

NASA-Langley, 1973 — 2 H-732